Formation and functions of the paucimannosidic-rich *N*-glycosylation of human myeloperoxidase

Presented by

Julian Ugonotti

Supervisor: Dr. Morten Thaysen-Andersen

A thesis submitted to Macquarie University for the Master of Research degree

Faculty of Science and Engineering

Department of Molecular Sciences

Macquarie University, Sydney, Australia

MACQUARIE University
SYDNEY·AUSTRALIA

October 2019

Table of Contents

Statement of Originality and Ethics

The research presented within this thesis was conducted between January 2019 and September 2019 for the completion of the Master of Research degree in the department of Molecular Sciences in the Faculty of Science and Engineering at Macquarie University, Sydney, Australia. This thesis is certified to be an original work by the author, unless otherwise referenced in the literature and/or acknowledged in text as a collaboration.

The appropriate human ethics (Reference #5201500813 and #5201500409), Biohazard Risk Assessments (Reference #5201500813 and #NIP041214BHA) and Biosafety approvals were obtained from the Human Research Ethics Committee at Macquarie University prior to the commencement of the research. The use of all samples was strictly for research purposes only.

This thesis entitled "**Formation and functions of the paucimannosidic-rich *N*-glycosylation of human myeloperoxidase**" is formatted according to Master of Research Thesis guidelines prescribed by the Faculty of Science and Engineering and Department of Molecular Sciences. It has not been submitted to any other institution for assessment.

Regards,

Julian Ugonotti

24th October 2019

Student No.: 43712835

Acknowledgements

First and foremost, I would like to offer up my deepest thanks and gratitude to my supervisor Dr. Morten Thaysen-Andersen. This past year has been an immensely enjoyable experience and it would not have been possible without your supervision and guidance. I have learnt a great deal from you this year due to your endless knowledge and wisdom. You have helped me build up my confidence as a researcher and I can't thank you enough for it. I would like to extend this gratitude to Prof. Nicolle Packer. Without the foundations you have built throughout the years, this research would not be possible. Thank you for valuable guidance and suggestions towards my project throughout this year.

Next, I would like to thank my colleagues in the MTA lab group. To Rebeca and Hannes, the proficient post-docs, thank you for your valuable support throughout the year towards my experiments and helping me overcoming the difficulties of research. To Sayantani, thank you for initially spending five weeks during my rotation to train me in the art of glycomics and for offering your support all throughout this year. You are an excellent teacher and a skilful researcher while you're at it. To Anastasia, thank you for your constant words of support as we have experienced this year together. To Kevin, thank you for the chats and discussions throughout the year, I hope I can offer up my experience to you as you move through your research career. Last but not least, I would like to thank you, Harry. We have collaborated extensively this year and I owe much of my training and research outcomes to you. I hope I have not distracted you too much but allowed you to reach your potential through training me.

To the members of the Glyco@MQ group, I would like to extensively thank you for the support throughout the year and listening in to my presentations at group meetings. Particularly, Ed and Tej, your valuable knowledge in analytical techniques is paramount and I am deeply thankful for you bestowing that knowledge to me. To Nick, thank you for all your support and allowing me to vent to you throughout this year, it's been a blast experiencing this MRes with you. To Liisa, thank you for your guidance and training around the lab. To Nima, for your valuable knowledge in the glycochemistry field and discussions throughout the year.

To my wonderful partner, Hayley, I cannot thank you enough for your endless support, encouragement and belief in me, which has allowed me to push through the challenges of the past year. I am forever grateful. To my friends, my beloved Scorps and extended company, thank you for your support and belief in me this year and for always showing interest in what I do, it means a lot.

Lastly, I would like to thank my family. To my sister, Isabel, thank you for your encouragement and support and putting up with me throughout this year. To Mum and Dad, I would like to take this chance to sincerely thank you for always believing in me no matter what I do and for teaching me to work hard and enjoy the experience along the way. You two have been pillars of support throughout my whole life, without which, I would not be where I am today.

Abbreviations

4-MU	4-Methylumbelliferone
ABC	Ammonium bicarbonate
ACN	Acetonitrile
Asn	Asparagine
Asp	Aspartic acid
Az	Azurophilic (granule)
BCA	Bicinchoninic acid assay
BSA	Bovine serum albumin
C/EBPα	CCAAT/enhancer binding Protein α
CID	Collision induced dissociation
CLP	Common lymphoid progenitor
CMP	Common myeloid progenitor
Cp	Ceruloplasmin
CXCR2/4	C-X-C chemokine receptor type 2/4
DNA	Deoxyribonucleic acid
DTT	Dithiothreitol
EIC	Extracted ion chromatogram
ER	Endoplasmic reticulum
ESI	Electrospray ionisation
FA	Formic acid
FBS	Foetal bovine serum
Fuc	Fucose
FWHM	Full width at half maximum
Ge	Gelatinase
GlcNAc	*N*-acetyl-glucosamine
GnT-I	*N*-acetyl-glucosaminyl-transferase
Glu	Glutamic acid
HCD	Higher-energy collision induced dissociation
Hex	*N*-acetyl-β-hexosaminidase
HOCl	Hypochlorous acid
HPLC	High performance liquid chromatography
HSC	Haematopoietic stem cells
IAA	Iodoacetamide
IMDM	Iscove's Modified Dulbecco's Media
kDa	Kilo-Dalton
LC	Liquid chromatography
LPO	Lactoperoxidase
LTQ	Linear ion trap quadrupole
Man	Mannose
MES	2-(*N*-morpholino)-ethanesulfonic acid
MPO	Myeloperoxidase
MS	Mass spectrometry
MS/MS	Tandem mass spectrometry
MUG	4-Methylumbelliferyl-2-acetamido-2-deoxy-β-D-glucopyranoside
MUGS	4-Methylumbelliferyl-2-acetamido-2-deoxy-β-D-glucopyranoside-6-sulfate
NETs	Neutrophil extracellular traps
NeuAc	*N*-acetylneuraminic acid
NGS	Next generation sequencing
PAGE	Polyacrylamide gel electrophoresis
PBS	Phosphate buffered saline
PCR	Polymerase chain reaction
PDB	Protein data bank
PGC	Porous graphitised carbon

PIPES	Piperazine-N, N'bis [2-ethanesulfonic acid]
PMN	Polymorphonuclear
PMP	Paucimannosidic protein
PMSF	Phenyl methyl sulfonyl fluoride
PNGase F	Peptide-*N*-glycosidase-F
Pro	Proline
PVDF	Polyvinylidene fluoride
RBC	Red blood cell
RIPA	Radioimmunoprecipitation Assay
ROS	Reactive oxygen species
RPMI	Roswell Park Memorial Institute Medium
SDF-1	Stromal cell-derived factor 1
SDS	Sodium dodecyl sulfate
Ser	Serine
sgRNA	Single guide ribonucleic acid
Sp	Specific
TFA	Trifluoroacetic acid
Thr	Threonine
TMB	3,3',5,5'-Tetramethylbenzidine
TPO	Thyroid peroxidase
WBC	White blood cell

Abstract

Myeloperoxidase (MPO) is a key neutrophil glycoprotein critically involved in neutrophil-mediated innate immunity. Recently, it was discovered that MPO and other important neutrophil glycoproteins are decorated with paucimannosidic glycans ($Man_{1-3}GlcNAc_2Fuc_{0-1}$), an under-explored *N*-glycan class in human glycobiology. Our knowledge of the formation and functions of these peculiar and heavily truncated glycoproteins expressed by human neutrophils remains incomplete. Firstly, I employed enzyme activity assays and mass spectrometry-based glycomics on a collection of CRISPR-Cas9-edited neutrophil-like (HL-60) mutants displaying impaired *HEXA* and *HEXB* genes in order to provide *in vitro*-based evidence for a *N*-acetyl-β-hexosaminidase (Hex)-driven production of paucimannosidic proteins in human neutrophils. Secondly, solvent accessibility measurements, three-dimensional structural assessments, chlorination activity assays, and glycopeptide analysis of granule-separated and *in vitro*-generated MPO glycoforms were used to characterise the formation and functions of the *N*-glycans carried by MPO. These studies provided mechanistic insight into the site- and granule-specific glycosylation of monomeric and dimeric MPO, and, importantly, demonstrated that MPO exhibits glycoform-dependent chlorination activities and ceruloplasmin-mediated inhibition characteristics. The peculiar *N*-glycans decorating Asn355 and Asn391 were found to be critical in defining the MPO activity and inhibition potential. In conclusion, this thesis has generated novel data that advance our understanding of the fascinating complex neutrophil glycobiology.

Chapter 1: Introduction and Aims

Neutrophils are polymorphonuclear leukocytes, an abundant type of white blood cell widely regarded as essential components of the innate immune system (1-4). Myeloperoxidase (MPO) is a heme-containing dimeric enzyme that is abundantly expressed in neutrophils and to a lesser extent in monocytes, another essential cell type of the innate immune system (3). Under physiological conditions, MPO catalyses the production of hypochlorous acid (HOCl) from hydrogen peroxide (H_2O_2) and chloride ions (Cl^-). It is understood that this MPO-halide-hydrogen peroxide system plays a significant role in the antimicrobial actions performed by neutrophils (5-7). Human MPO is a heavily glycosylated protein containing no less than ten *N*-glycosylation sites per mature dimer i.e. five sites span each of the two identical MPO monomers.

MPO, along with many other proteins residing in specialised granules of neutrophils, are decorated with paucimannosidic *N*-glycans ($Man_{1-3}GlcNAc_2Fuc_{0-1}$), an under-explored class of *N*-glycosylation in human glycobiology (8). Inference from paucimannose-rich lower organisms suggests that the formation of paucimannosidic proteins, i.e. MPO, in human neutrophils is predominantly performed by *N*-acetyl-β-hexosaminidase (Hex), which in humans exists as various isoenzymes formed by the *HEXA* and *HEXB* gene products, the Hex α- and β-subunits, respectively. However, this notion still requires validation. Thus, the principal aim of this thesis was to characterise a number of CRISPR-Cas9-edited *HEXA*$^{-/-}$ and *HEXB*$^{-/-}$ HL-60 (a neutrophil-like precursor cell type often used to study neutrophil biology) cell lines to validate the link between Hex and the formation of paucimannosidic proteins in human neutrophils. Despite the key roles of MPO in human immunology and a growing appreciation that protein glycosylation significantly impacts the human immune system, surprisingly little is known about the structure and function of the MPO *N*-glycans. Thus, as part of a large collaborative effort, a separate but related aim of this thesis was to characterise the structure-function relationship of the understudied peculiar *N*-glycans decorating MPO. Altogether, this thesis aims to extend our understanding of some intricate facets of neutrophil glycoimmunology.

This opening section aims to succinctly introduce key scientific topics and concepts underpinning the thesis. Discipline-specific terminology and background literature useful to understand, interpret and reflect on the data presented in the Result and Discussion sections are introduced. Finally, this section provides a rationale for the research project and outlines the thesis aims.

1.1. Neutrophils, essential components of the innate immune system

1.1.1. Characteristics of neutrophils

Neutrophils are the most abundant class of polymorphonuclear (PMN) granulocytes, an essential type of white blood cells in our innate immune system. Neutrophils are characterised by their segmented nuclei and distinct lipid membrane-enclosed intracellular compartments known as granules. Of note, two other less abundant types of PMN granulocytes known as basophils and eosinophils exist, however, they will not be discussed in this thesis.

Mature neutrophils comprise three distinct subsets of granules including the azurophilic granules (Az, alternatively referred to as "primary" granules), specific granules (Sp, "secondary" granules) and gelatinase granules (Ge, "tertiary" granules) that are classified based on their protein content (9, 10). In addition to these distinct granules, the neutrophils contain another compartment known as the secretory vesicles. The neutrophil granules, which contain a number of antimicrobial proteins, form sequentially during the different stages of neutrophil maturation (discussed below).

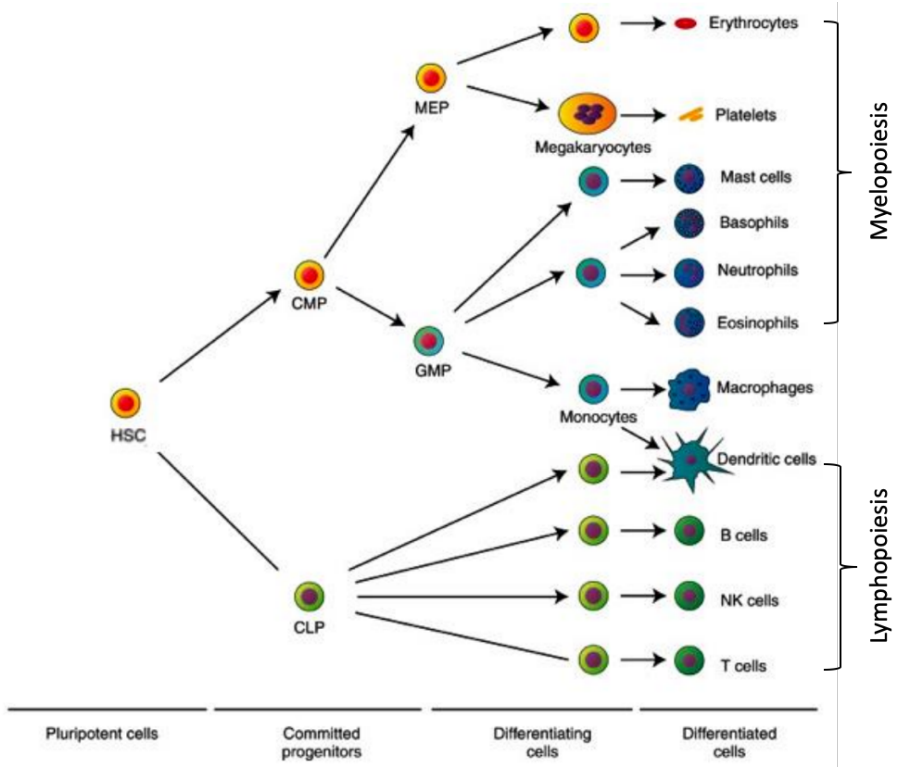

***Figure 1. Human haematopoiesis**. Multipotential haematopoietic stem cells (HSCs) differentiate into common myeloid (CMP) and lymphoid progenitor cells (CLP) forming different blood cell types. Neutrophils are formed via granulopoiesis from granulocyte-macrophage progenitors (GMPs). MEP, megakaryocyte/erythroid progenitor. Modified from (11).*

1.1.2. Origin of neutrophils

All white blood cells originate from haematopoietic stem cells (HSCs), a common progenitor cell type, via a differentiation process known as haematopoiesis (11, 12). HSCs are capable of differentiating into myeloid and lymphoid effector cells via myelopoiesis and lymphopoiesis, respectively, **Fig. 1**. The generation of neutrophils falls under myelopoiesis, more specifically granulopoiesis; other differentiation pathways are outside the scope of this thesis. HSCs reside in niche environments created by osteoblasts in the bone marrow (12)

and typically interact with osteoblasts and the extracellular matrix via β_1-integrins expressed on the surface of HSCs (13-16). In the bone marrow, a number of transcription factors are involved in determining the lineage commitment (17). The transcription factors CCAAT/enhancer binding protein α (C/EBPα) and PU.1 are crucial to commit HSCs to the myeloid lineage (18, 19). It is understood that a balance between C/EBPα and PU.1 determines the commitment of myeloid progenitors to either granulopoiesis or to monocytopoiesis, the formation of monocyte/macrophages (20, 21). C/EBPα is essential for granulopoiesis whilst high expression of PU.1 promotes the monocyte-macrophage lineage utilisation.

1.1.3. Neutrophil maturation

Myeloblasts are the first committed cell type in the process of granulopoiesis. In the bone marrow, several transcription factors including C/EBPα and PU.1 guide the process of neutrophil maturation (22). Myeloblasts are capable of differentiating into neutrophils, basophils, eosinophils and into the monocyte-macrophage lineage (see above). Only when myeloblasts differentiate into neutrophilic promyelocytes, they truly commit to eventually mature into neutrophils and can no longer differentiate into basophils or eosinophils (23).

The cell line HL-60, which was isolated from a female patient with acute promyelocytic leukemia (24), represents a valuable research tool for neutrophil biologists. This cell line, which is a cancerous promyelocytic or a “neutrophil-like” cell type, is frequently utilised for *in vitro* myeloid/neutrophil differentiation and functional studies (25).

Promyelocytes are able to differentiate into myelocytes. Myeloblasts, promyelocytes and myelocytes make up what is known as the “mitotic pool” (26), a population of dividing immature neutrophil precursors. Once myelocytes differentiate into metamyelocytes, this marks the commencement of the “post-mitotic pool”; these immature cells and the more mature granulocytic cells formed downstream can no longer divide. The metamyelocytes differentiate into banded neutrophils, and, finally, into mature neutrophils that may enter circulation. Under physiological conditions, the process of neutrophil maturation is understood to take approximately 14 days. Mature neutrophils are estimated to have a half-life in circulation of five to seven days (27, 28).

1.1.4. Circulation and extravasation of mature neutrophils

Under physiological conditions, the majority of mature neutrophils reside in the bone marrow, known as the bone marrow reserve (29). Upon infection, cytokines are released by affected tissues, macrophages and by other immune cells, which serve as powerful signal molecules that promote

the release of neutrophils from the bone marrow. The release of neutrophils is mediated by the cytokine receptors C-X-C chemokine receptor type 2 (CXCR2) and type 4 (CXCR4) expressed on neutrophil surfaces (30). The CXCR4 receptor and its ligands e.g. stromal cell-derived factor 1 (SDF-1) retain neutrophils in the bone marrow, whilst the ligands C-X-C ligand 1 and 2 (CXCL1 and CXCL2) act on CXCR2 to cause neutrophil release. The cytokine granulocyte colony-stimulating factor (G-CSF), released in response to infection, lowers the expression of SDF-1 and upregulates the expression of CXCL1 and CXCL2, and hence is considered an essential mediator of neutrophil trafficking from the bone marrow into the circulation (31, 32).

Once in the circulation, neutrophils may be mobilised to the site of infection in the peripheral tissue through a process known as the leukocyte adhesion cascade (33). The endothelial cells, which line the blood vessels in the vicinity of the site of infection, increase their expression of P-selectin and E-selectin upon cytokine stimulation (34). These selectins are known to bind P-selectin ligand 1 (PSGL-1), L-selectin and CD44 which are expressed on the surface of neutrophils. The interaction of neutrophils binding and releasing from the endothelial cells is a process commonly referred to as rolling. The firm adhesion of neutrophils to the endothelial cells is mediated by the interactions between β_2-integrins, LAF-1 and Mac-1, that are also expressed on the neutrophil surface and the intercellular adhesion molecule 1 and 2 expressed on surfaces of endothelial cells. Once adhered, neutrophils extravasate via either transcellular migration, where they penetrate through the endothelial cells they just adhered to, or via paracellular migration, where they squeeze through the tight junction existing between endothelial cells. Once neutrophils have passed through the endothelium, they are able to migrate to the site of infection via chemotaxis (not discussed here due to space constraints) where they perform their antimicrobial function.

1.1.5. Antimicrobial functions of neutrophils

At the site of infection, activated neutrophils utilise three distinct killing mechanisms to perform their antimicrobial functions i.e. phagocytosis, degranulation and neutrophil extracellular traps (NETs), **Fig. 2** (2, 18). These protective mechanisms will be briefly described below.

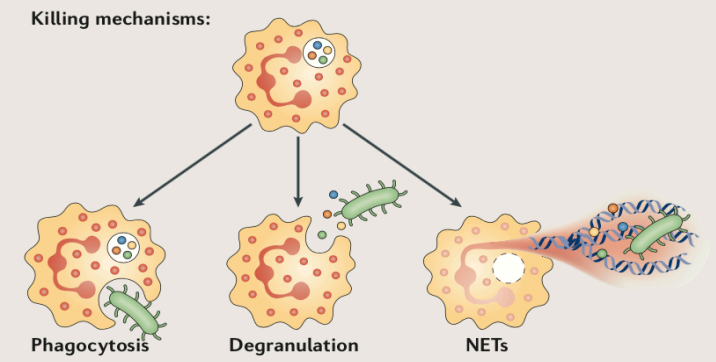

Figure 2. The three proposed killing mechanisms carried out by neutrophils. *The pathogen is in green. From (2).*

1.1.5.1. Phagocytosis

Although not using phagocytosis as much as macrophages, neutrophils are capable of performing phagocytosis to destroy invading microbes (35). In this process, neutrophils engulf the invading microbes, encapsulating them in lipid membrane-enclosed organelles known as phagosomes. The neutrophils kill the microbes by fusing the phagosome with the Az granules that contain a spectrum of antimicrobial proteins including, but certainly not limited to, MPO, which is of principal interest in this thesis. Within this fused compartment, the phagolysosome, MPO generates HOCl and subsequently reactive oxygen species (ROS) that are toxic to the microbes.

1.1.5.2. Degranulation

Whilst the neutrophil granules, in particular the Az granules, are capable of fusing with the phagosome, they are also capable of fusing with the plasma membrane of neutrophils upon stimulation hereby releasing their soluble content into the extracellular environment (36, 37). The neutrophils utilise this mechanism to release antimicrobial proteins into the extracellular environment to destroy invading microbes without the need to necessarily perform phagocytosis.

1.1.5.3. Neutrophil extracellular traps (NETs)

The formation and use of NETs to entrap and destroy invading microbes is a recent and still heavily debated discovery (38). The current literature harbours conflicting results and opinions on this matter (39). NETs are mesh-like structures composed of neutrophil granular proteins, such as neutrophil elastase and MPO, and deoxyribonucleic acid (DNA) that has been released extracellularly by the neutrophil. It is believed that NETs serve the purpose of immobilising pathogens, particularly bacteria, preventing them from spreading and infecting neighbouring tissue while at the same time killing or perhaps just preventing the growth of microbes through the action of antimicrobial proteins dispersed through the NETs.

1.1.6. Granule-specific proteomes and the "targeting-by-timing" hypothesis

As mentioned previously, neutrophils possess three distinct granule types (Az, Sp and Ge granules) and secretory vesicles. These compartments harbour an arsenal of proteins that display antimicrobial functions amongst other critical neutrophil functions. It was originally thought that the granular proteins were sorted to their respective compartments based on specific signal sequences (40). However, the "targeting-by-timing" hypothesis proposed by Borregaard and colleagues (41) has since gained acceptance as the more likely mechanism driving the fascinating protein sorting during granule formation. This hypothesis proposes that the neutrophil granules, and their protein content, form sequentially during the different stages of neutrophil maturation

(discussed above). Hence, each granule subset has its own unique proteome "fingerprint" (42). The Az granules are the first granules to be formed upon myeloblast-to-promyelocyte differentiation and is known to contain ~70% of the MPO carried by neutrophils (42). In addition to MPO, the Az granules contain several other antimicrobial proteins such as neutrophil elastase, cathepsin G and azurocidin. Next, the specific (Sp) granules rich in neutrophil gelatinase-associated lipocalin and lactoferrin are formed at the promyelocyte-to-myelocyte differentiation stage. The gelatinase (Ge) granules, which are formed at the myelocyte-to-metamyelocyte/banded neutrophil stage, are characterised by their high quantities of gelatinase. Finally, the secretory vesicles are primarily formed at the mature neutrophil stage via endocytosis (43), and possibly via pinocytosis, as opposed to the three other endoplasmic reticulum (ER)-Golgi derived granule compartments. Hence, the secretory vesicles are rich in plasma proteins e.g. albumin.

1.2. MPO, a fascinating glycoprotein with key roles in innate immunity

1.2.1. Tissue-expression and functions of MPO

MPO is an animal peroxidase that is categorised in the Chordata peroxidase superfamily alongside eosinophil peroxidase (EPO), lactoperoxidase (LPO) and thyroid peroxidase (TPO) (44). MPO is exclusively expressed in the myeloid lineage at the promyelocyte stage and hence MPO is restricted to neutrophils and monocytes. In neutrophils, MPO catalyses the formation of HOCl from hydrogen peroxide (H_2O_2) and chloride ions (Cl^-) (45). Although MPO mainly resides in the Az granules of resting neutrophils (see above), data suggests that it carries out the peroxidase activity predominantly in the phagolysosome of activated neutrophils. NADPH oxidase assembles in the phagolysosomal membrane and performs what is known as the 'respiratory burst', consuming oxygen and transferring electrons into the phagosome, **Fig. 3** (46). Simultaneously, a voltage-gated proton pump, Hv1, transfers H^+ ions into

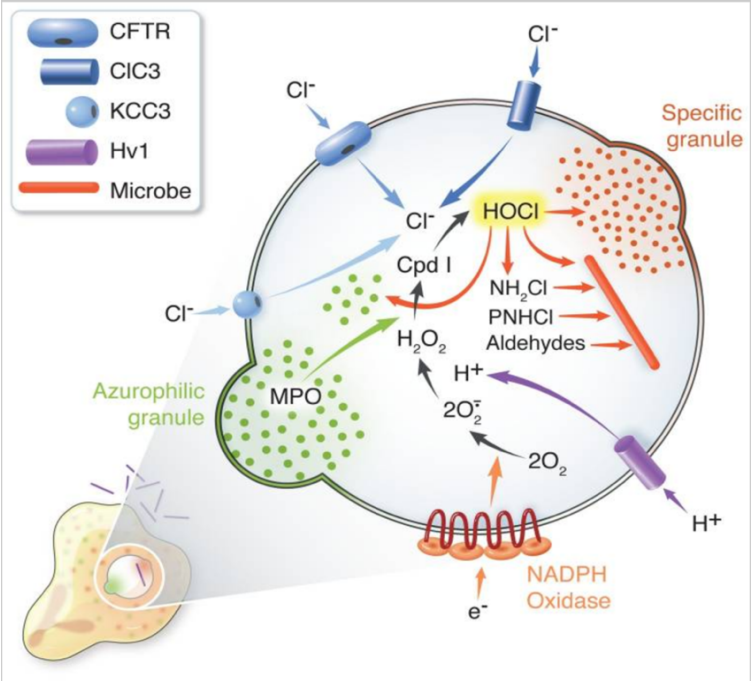

Figure 3. HOCl generation in the phagosome of neutrophils. *Steps involved in the generation of HOCl via MPO in the phagosome, see text for more. Retrieved from (45).*

the phagosome (47). Together this generates superoxide anions ($O_2^{\cdot -}$) that are quickly converted into H_2O_2. The majority of the chloride ions in the phagosome are transported from the cytoplasm via the cystic fibrosis transmembrane conductance regulator (48), however, the K^+-Cl^- co-transporter (KCC) and the CIC-3 anion channel have also been implicated in Cl^- transport into the phagosome (49, 50). Once MPO is delivered to the phagosome via heterotypic fusion by the Az granules, it catalytically consumes H_2O_2 to form compound I (Cpd I, see **Fig. 3**) (51), which, in turn, utilises Cl^- to produce HOCl. Once produced, HOCl reacts rapidly with several functional groups of proteins and peptides to form chloroamines and dichloroamines that readily decompose to aldehydes (52). Furthermore, HOCl is known to react with lipids and DNA (53). This hyper-reactivity of HOCl is a main contributor to the degradation and destruction of the phagocytosed microbes, but, if not appropriately controlled, can also be harmful to proteins and cells of the host.

1.2.2. Measuring MPO activity

Given the key innate immune-related roles of MPO and its biomarker potential of a range of inflammatory conditions e.g. cardiovascular diseases (54), the accurate measurement of the MPO activity has been of interest for a considerable period of time. MPO is a heme-containing peroxidase and hence it is possible to measure MPO activity *in vitro* using typical peroxidase substrates such as 3,3',5,5'-tetramethylbenzidine (TMB), *o*-dianisidine and guaiacol. MPO oxidises these substrates, allowing for its activity to be determined quantitatively by measuring the absorbance of the oxidised substrates. Whilst these assays are simple, and are widely used throughout literature, there is still no consensus on how to assess the MPO activity (55). Additionally, there seems to be some confusion around the specific type of MPO activity that is being assessed. In addition to the above-mentioned assays that measure the peroxidase activity of MPO, it is possible to measure the chlorination activity of MPO (56). Chlorination assays determine the generation of HOCl, or rather the hypochlorite anion (ClO^-), by MPO, using either fluorescent probes that are measured fluorometrically or compounds that once chlorinated can be measured quantitatively by absorbance. The chlorination assays are regarded as more specific towards MPO, as it measures the generation of reactive oxygen species (i.e. HOCl), rather than its peroxidase activity. Determining the peroxidase activity of MPO in tissues or whole blood is challenging as other proteins such as myoglobin and haemoglobin also display peroxidase activity and thus may interfere with the assay (57).

In addition to the above *in vitro* assays, it is possible to measure MPO chlorination activity *in vivo.* One study utilised bioluminescence imaging and a bioluminescent compound known as luminol,

which is oxidised by HOCl produced by MPO and thus allowed quantitation of the MPO chlorination activity *in vivo* in several animal models with inflammatory conditions (58). Whilst not directly assaying the MPO activity, but instead the MPO level, another group demonstrated the presence of extracellular MPO *in vivo* in mice suffering from autoimmune encephalomyelitis, by injecting a synthetic gadolinium-tagged MPO and utilising molecular magnetic resonance imaging (55).

1.2.3. MPO inhibition by ceruloplasmin

Whilst the potent MPO-HOCl system is essential for neutrophil-mediated defence against microbial invasion, it is also a known contributor to several chronic inflammatory diseases including atherosclerosis and cardiovascular disease, chronic kidney disease and rheumatoid arthritis (59). In chronic inflammatory diseases, MPO is excessively released into the extracellular space, due to prolonged activation and degranulation of neutrophils. Consequently, HOCl and the reactive by-products are known to react with the host tissue and cause oxidative damage, contributing to chronic inflammation. Given the potential of MPO to cause oxidative damage and chronic inflammation, natural inhibitors of MPO have evolved to prevent excess oxidative damage in the body. Ceruloplasmin (Cp) is a plasma protein that predominately functions as a copper transporter in blood (60). It was demonstrated that Cp interacts with and inhibits the peroxidase activity of MPO (61). In fact, MPO, lactoferrin (a antimicrobial glycoprotein expressed in the Sp granules of neutrophils) and Cp have the potential of forming large protein complexes (62). It is now established that Cp is a potent endogenous inhibitor of MPO, preventing HOCl production by trapping MPO in the reduced compound II state, averting it from reaching the HOCl-producing Cpd I (63). It was proposed that Cp, an anionic protein (pI ~4), interacts with the cationic MPO (pI ~10) through electrostatic forces (61). Based on the crystal structure of Cp in complex with MPO (Protein Data Bank, PDB: 4EJX), it was suggested that a flexible loop of Cp (amino acid residues 881-892) obstructs the heme cavity of MPO, thus preventing catalytic activity, **Fig. 4** (also discussed

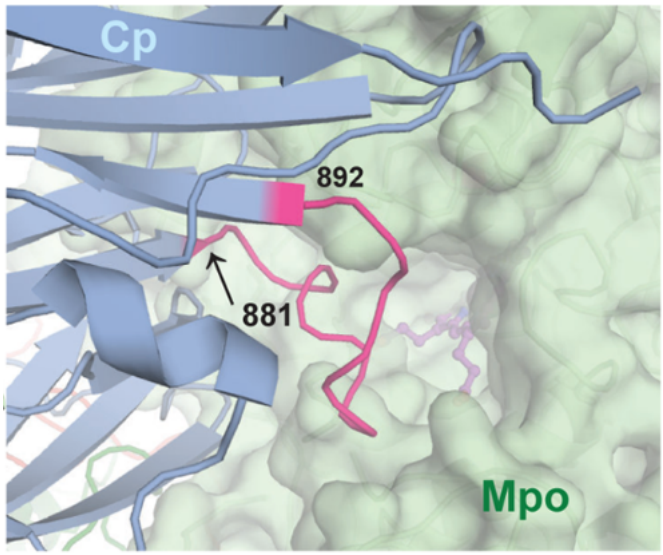

Figure 4. The loop region of ceruloplasmin (Cp) obstructing the heme cavity of MPO. *Cp is in pale blue, MPO is in pale green. PDB: 4EJX. From (64).*

further below) (64). Synthetic peptides mimicking this loop region of Cp demonstrated a dose-dependent inhibition of MPO, further supporting this inhibitory mechanism (64).

1.2.4. The structure of mature MPO

Several crystal structures of human MPO have been deposited into the Protein Data Bank (PDB). Thus, many structural facets of the α-helix-rich MPO have been extensively characterised, **Fig. 5** (65, 66). Mature MPO is a ~150 kDa homodimer, consisting of two identical ~12.5 kDa light (α-) chains and two heavy (β-) chains. The β-chains are extensively glycosylated (five potential glycosylation sites per chain), and hence span a molecular mass of ~60-65 kDa. MPO glycosylation will be discussed below. The MPO monomers are covalently linked through the two β-chains via a single disulfide bridge at Cys^{319}. The heme group, which is the catalytic core of MPO, is a derivative of the protoporphyrin IX class and is covalently linked via ester bonds to Glu^{242} and Asp^{94}, and additionally to Met^{243} via a sulfonium ion linkage. The heme gives MPO its green colour and usually accounts for the pale green colour of pus, a sign of neutrophil secretion. The chloride-binding site is formed by residues 324-327 (β-chain), residues 30-33 (α-chain) and Trp^{436} (β-chain). Calcium is a co-factor of MPO; the calcium-binding site displays the typical bipyramidal coordination to Ca^{2+} via Asp^{96}, Thr^{168}, Phe^{170}, Asp^{172}, and Ser^{174} of the MPO α-chain.

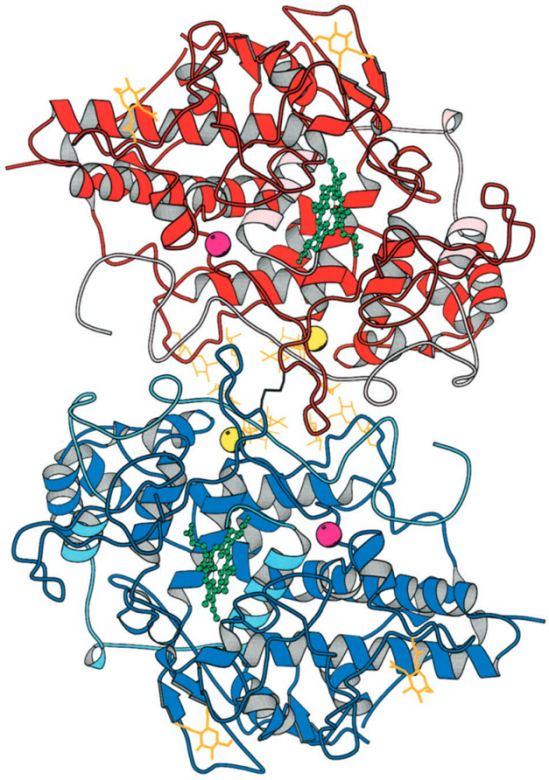

***Figure 5. The structure of mature MPO**. The heavy (β-) chains of each monomer of MPO are in dark red and blue, whilst the light (α-) chains are in light red and blue. The heme groups (green), chloride (yellow) and calcium (magenta) are shown. The Cys^{319} disulfide bond is at the dimer interface (black). The β-chains of MPO are extensively glycosylated (GlcNAcβ-Asn, orange). PDB:1D2V. From (65).*

1.2.5. Homology of MPO to other peroxidases

As mentioned above, MPO belongs to the Chordata peroxidase superfamily, alongside EPO, LPO and TPO. Only the 3D structure of MPO has been characterised. EPO is a ~70 kDa monomeric glycoprotein, consisting of a 58 kDa β-chain and a 12 kDa α-chain that resembles monomeric MPO. The slightly larger LPO and TPO are also single chain glycoproteins of ~80 kDa and 100 kDa,

respectively. Several features are shared between these human peroxidases. MPO, EPO and LPO are all encoded by single genes located on chromosome 17 in humans that share a similar intron-exon arrangement (67). This suggests that these peroxidases have evolved from a common ancestral gene via gene duplication. TPO has a intron-exon arrangement that is dissimilar to the other peroxidases (68), and is believed to have evolved independently from the other peroxidases. This is supported by the fact that TPO is the only transmembrane protein of the four peroxidases (69, 70). Based on amino acid sequence alignment, important catalytic residues and residues involved in the linkage of the heme group, as well as some glycosylation sites, are conserved amongst all four peroxidases (71). Of note here, MPO shares two glycosylation sites with the other peroxidases i.e. Asn355 and Asn391, two glycosylation sites of particular interest in this thesis (discussed below).

1.2.6. Biosynthesis of MPO

The biosynthesis of MPO is complex as it involves many processing steps. The primary translational product, the "pre-MPO" (80 kDa), is co-translationally glycosylated in the endoplasmic reticulum (ER) forming the "apopro-MPO" (90 kDa), **Fig. 6** (72). *N*-glycan processing is discussed below. In the ER, the glycans conjugated to apopro-MPO interact with the ER-resident molecular chaperone proteins ERp57, calnexin and calreticulin (73, 74). These chaperones assist the folding of MPO and other proteins in the ER, preventing aberrantly folded proteins from continuing in the secretory pathway. MPO also acquires the heme in the ER as demonstrated by the observation that when heme synthesis is arrested, it halts MPO biosynthesis at the apopro-MPO stage (75-77). Additionally, when a Golgi-disruptor known as Brefeldin A is utilised in cell culture, MPO biosynthesis is halted at the heme-containing "pro-MPO" stage (77). Pro-MPO undergoes several processing

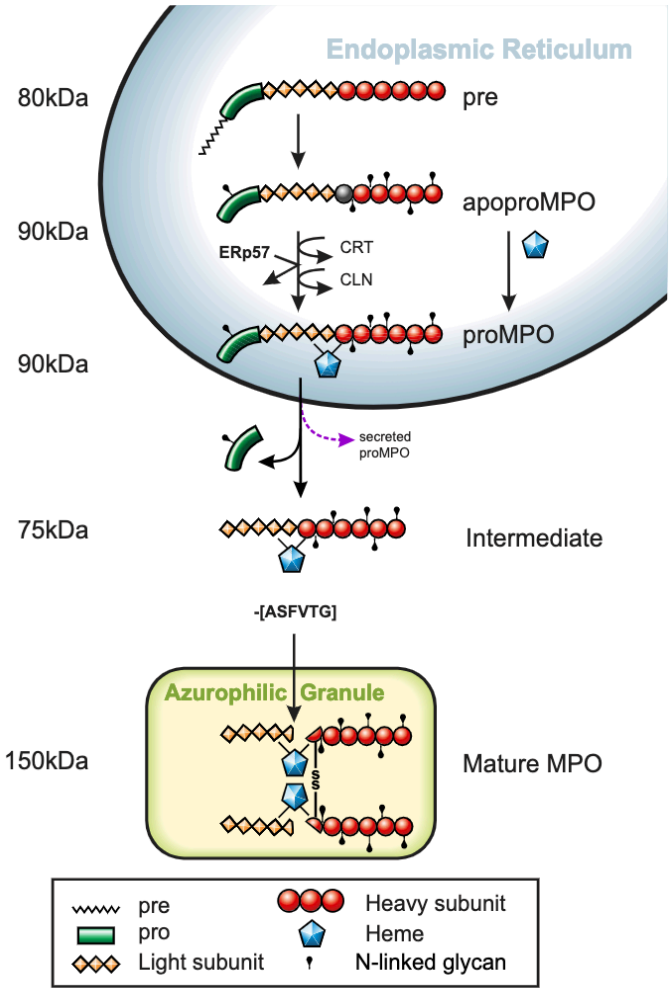

Figure 6. Overview of the biosynthesis of human MPO. *See text for details. From (72).*

steps before the mature MPO is being packaged in the Az granules of neutrophils, however, the order of events is still unclear. Brefeldin A-based evidence indicates that the cleavage of the propeptide on pro-MPO occurs after the ER, as MPO biosynthesis is arrested in the propeptide form. Removal of the 116 amino acid propeptide, yielding a 75 kDa intermediate, is necessary for the generation of mature dimeric MPO residing predominantly in the Az granules, a step catalysed by a putative proprotein convertase. When the peptide CMK-RVKR, a known inhibitor of proprotein convertases, is added to cell cultures producing MPO, the biosynthesis of MPO is arrested at the pro-MPO stage (78), supporting the notion of a proprotein convertase mediating the cleavage of the propeptide. Whilst the majority of the pro-MPO leaving the ER is destined for maturation in the Az (or other) granules, a small portion (~10%) of pro-MPO is secreted from the neutrophil as observed from cultures of human bone marrow (79), myeloid cell lines e.g. HL-60 (80, 81) and heterologous expression systems of MPO (82). Both the intracellular and secreted pro-MPO types are enzymatically active, and, intriguingly, the activity of these pro-forms is indistinguishable from "mature MPO" (83). Prior to MPO reaching maturity, an internal hexapeptide i.e. ASFVTG is cleaved from the protein sequence, resulting in the formation of the α- and β-chains of MPO that remain joined through covalent ester linkages between conserved Asp and Glu residues and the heme group. The identity of the (endo)protease(s) performing this cleavage is unknown. It is also unclear whether the hexapeptide elimination occurs before or after MPO dimerisation. The crystal structure of pro-MPO containing the hexapeptide demonstrates that the hexapeptide is surface-exposed and hence may be cleaved after MPO dimerisation (84), which was previously suggested to occur in the granules (85). Surprisingly, when treating mature MPO in mild reductive conditions to break the S-S bonds, the resulting "hemi-MPO" has a catalytic activity that is indistinguishable to that of mature MPO (86). Thus, the functional advantage of dimeric MPO, if any, over the monomeric form is unknown.

1.3. Protein glycosylation, a complex and understudied feature of MPO

1.3.1. Protein glycosylation

Protein glycosylation is a co- and post-translational modification that involves the conjugation of complex carbohydrates (hereafter referred to as glycans) to proteins, resulting in the formation of glycoproteins. Found in all domains of life, it is no surprise that protein glycosylation is implicated in very diverse biological processes essential for life, including, but certainly not limited to, mediating protein folding (as exemplified above by calnexin and calreticulin), involvement in biological recognition events e.g. cell-cell and cell-extracellular matrix communication and

contributing to protein stability and solubility (87, 88). Whilst there are many types of protein glycosylation, the focus of this thesis is on asparagine-linked (*N*-linked) glycosylation.

1.3.2. N-linked glycosylation

N-linked glycosylation, or *N*-glycosylation, is the attachment of glycans to the nitrogen atom of the side-chain of asparagine (Asn) residues located in the conserved sequence Asn-X-Ser/Thr (NXS/T), where X ≠ Pro. Literature commonly describes three conventional classes of *N*-glycans in humans: oligomannosidic-, complex- and hybrid-type glycans, which all share a trimannosylated chitobiose core comprising two *N*-acetylglucosamine (GlcNAc) and three mannose (Man) residues that can exist with or without core fucosylation, **Fig. 7**. Of particular relevance to this thesis, two non-conventional *N*-glycan types, the chitobiose core- and paucimannosidic-type, also exists (discussed below). Galactose (Gal) and the acidic *N*-acetylneuraminic acid (NeuAc) often referred to as sialic acid are common building blocks found in the antenna region of the complex- and hybrid-type *N*-glycans. The synthesis of *N*-glycoproteins requires numerous glycoside hydrolases and glycosyltransferases that are located throughout the ER and Golgi apparatus, **Fig. 8**. The glycoside hydrolases enzymatically remove terminal monosaccharide residues whilst the glycosyltransferases transfer monosaccharides to glycoproteins in discrete trimming and elongation processes. The addition of sugar building blocks requires sugar nucleotide donors such as uridine diphosphate-GlcNAc, guanine diphosphate-Fuc and cytidine monophosphate-NeuAc.

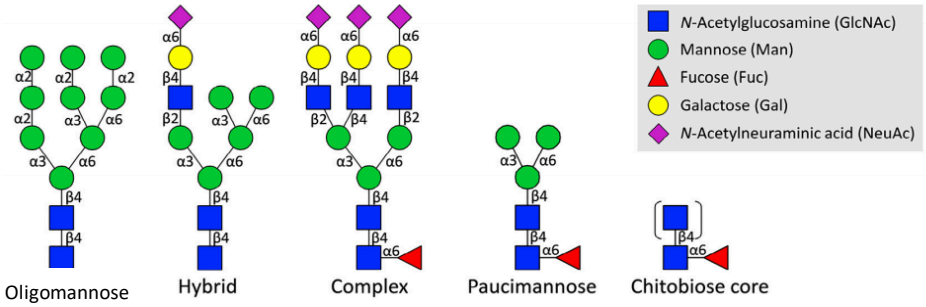

Figure 7. Conventional and non-conventional classes of N-glycans of human proteins.

The *N*-glycosylation is initiated in the ER, with the transfer of a common *N*-glycan precursor, $Glc_3Man_9GlcNAc_2$, onto the Asn residue of the nascent polypeptide chain (89). This precursor is trimmed in the ER by ER glucosidase I and II (Glc I and Glc II) and multiple ER-resident mannosidases before the glycoprotein is transported to the *cis*-Golgi for further processing. As glycoproteins traffic the *cis*-, *medial*-, and *trans*-Golgi, they encounter several glycosidase hydrolases and glycosyltransferases, many competing for the same glycoprotein substrates, that serve to process the *N*-glycoproteins to maturation. The maturing glycoproteins may leave this enzymatic pathway

at any point and hence, create a vast heterogeneity of structurally related *N*-glycoprotein structures known as glycoforms.

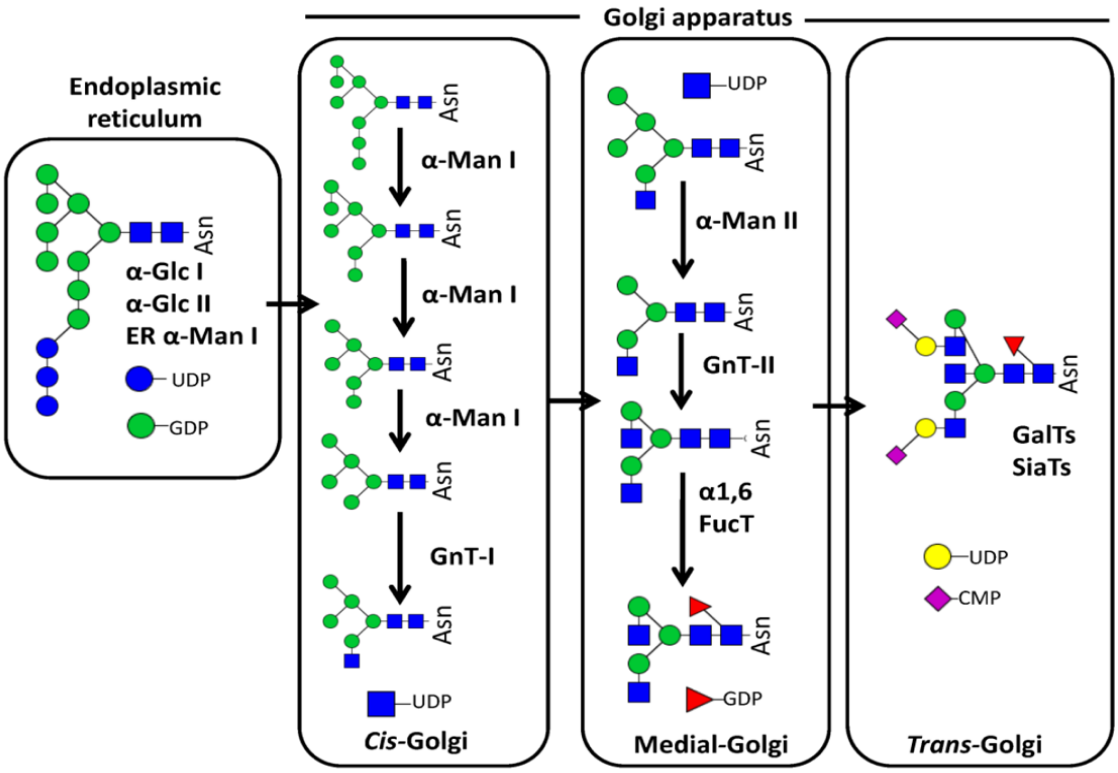

Figure 8. The "conventional" N-glycosylation pathway. *Initiated by the transfer of a common glycan precursor to nascent polypeptides in the ER, the subsequent processing of N-glycoproteins is an intricate and complex process involving many glycoside hydrolases, glycosyltransferases and sugar nucleotide donors. This enzymatic process, which is highly dynamic and physiology-dependent, generates a vast heterogeneity of the resulting glycoproteins (glycoforms). This pathway does not explain the existence of the non-conventional N-glycan types including protein paucimannosylation observed in neutrophil biology (8), see Figure 22 in the Discussion for a proposed route.*

1.3.3. MPO glycosylation

MPO is an extensively glycosylated protein. As correctly reported by Nauseef and colleagues, the monomeric proMPO contains five *N*-glycosylation sites (90). However, it was later found that there are in fact six *N*-glycosylation sites in the MPO precursor, proMPO, namely Asn139, Asn323, Asn355, Asn391, Asn483 and Asn729 (84, 91). Asn139 is located in the propeptide region of proMPO and hence is removed before maturation. The other five *N*-glycosylation sites are all located in the β-chain of mature MPO. Although there are many available crystal structures of human MPO, these resources are not particularly informative when it comes to the decorating glycans due to the inherent limitations of forming and visualising protein crystals with the flexible glycans using x-ray crystallography.

In fact, the glycosylation of human MPO remain severely understudied. To the best of my knowledge, only two biochemical studies have directly reported on the detailed glycosylation features of human neutrophil-derived mature MPO (91, 92). Both of these studies reported on the site-specific macro- and micro-heterogeneity of MPO *N*-glycans as characterised using mass spectrometry. In short, they found that MPO carries a range of oligomannosidic-, complex- and hybrid-type *N*-glycans, but unfortunately, neither documented the fine structures of MPO glycosylation nor accurately covered the entire *N*-glycan repertoire and occupancy of all MPO glycosylation sites.

In 2015, Thaysen-Andersen and colleagues surveyed the *N*-glycome of sputum from pathogen-infected individuals and discovered an abundance of paucimannosidic-type *N*-glycans (93), a glycan type still rather controversial and less reported in human glycobiology. Paucimannosidic *N*-glycans (*pauci-* = few or little in Latin) may be defined as *N*-glycan structures that contain one, two or three mannose residues on a chitobiose core, structures that can appear with or without core fucosylation, **Fig. 9**. Additionally, it was previously found that these paucimannosidic *N*-glycans are abundantly decorating neutrophil proteins residing in the Az granule, including MPO, which were being secreted into pathogen-infected sputum (94). Recently, another study identified even further truncated *N*-glycan types (of the so-called chitobiose core-type i.e. $GlcNAc_{1\text{-}2}Fuc_{0\text{-}1}$) on neutrophil proteins including cathepsin G (95). These findings raise several interesting questions, for example, what is the biosynthetic route of these non-conventional truncated *N*-glycans in human neutrophils and what are their functional roles, particularly on MPO?

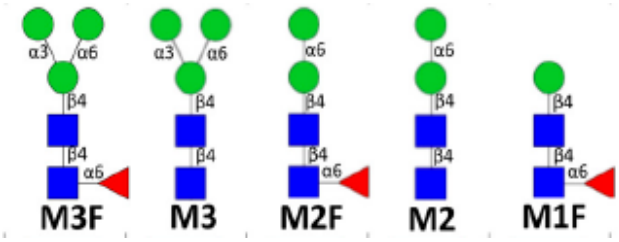

Figure 9. Examples of paucimannosidic N-glycans and their short-hand nomenclature.

1.3.4. Formation of paucimannosidic N-glycans in neutrophils

The biosynthesis of paucimannosidic proteins across the eukaryotic kingdom has recently been extensively reviewed (8). In paucimannose-rich organisms, such as in insect e.g. *Drosophila melanogaster* (96) and in plants e.g. *Lotus japonicus* (97), the generation of paucimannosidic proteins is attributed to the enzymatic activity of *N*-acetyl-β-hexosaminidase (Hex). In these species, Hex is known to cleave terminal non-reducing end GlcNAc residues of glycoprotein intermediates at a critical point in the biosynthetic machinery to generate paucimannosidic proteins. The human Hex isoenzyme is found in either a homodimeric (αα, "Hex S" and ββ, "Hex B") or heterodimeric (αβ, "Hex A") forms. The Hex α- and β-subunits forming these three isoenzymes are encoded by *HEXA*

and *HEXB*, respectively. The two human Hex subunits were found to have a high protein sequence similarity (~53%) to the Hex of the paucimannose-rich lower organisms (94). In addition, immunofluorescence for paucimannosidic epitopes using a paucimannose-recognising antibody (Mannitou) displayed co-localisation with human Hex in the Az granules of immature neutrophil-like HL-60 cells (94). Furthermore, proteomics profiling of isolated granules demonstrated evidence of Hex being expressed in the Az granules of neutrophils (42). Collectively, this strongly suggest that Hex is the likely glycoside hydrolase catalysing the generation of paucimannosidic proteins in human neutrophils, however, concrete evidence is required to establish this proposed pathway.

1.3.5. Functions of MPO glycosylation

Given the extensive glycosylation of human MPO, it is highly likely that the *N*-glycans decorating MPO carry out or modulate important functions. This was supported by the observation that when MPO is partially deglycosylated, the enzyme activity is compromised (91). The contribution of the *N*-glycans to the enzymatic activity of MPO is yet to be elucidated. Based on the crystal structure of human MPO, the *N*-glycans situated at Asn323 and Asn483 are located directly at the dimeric interface of MPO (65), potentially impacting the dimer formation and/or stability. Structural and functional *N*-glycan characterisation studies of the paucimannose-rich cathepsin G and neutrophil elastase from Az granules of neutrophils have revealed novel insights into the potential immune-modulating functions of paucimannosidic *N*-glycans (95, 98). In analogy, it is plausible that the paucimannosylation of MPO may play immune-modulatory roles in neutrophil glycobiology and in the innate immune system.

1.4. Aims of Research

Many biochemical aspects of MPO have been established over the years using classical techniques in molecular and cellular biology. This has demonstrated beyond doubt the importance of MPO in the innate immune system. However, much is yet to be uncovered in regard to MPO glycobiology. The complex *N*-glycan moieties decorating human MPO are immensely understudied and little remains known of their site-specific structure and function, warranting further investigation using modern technologies in glycobiology and glycoimmunology. In addition, the proposed Hex-mediated formation of the paucimannosidic *N*-glycans carried by MPO and other neutrophil Az granule proteins requires evidence to validate this formation pathway. To this end, this thesis comprises two major aims:

1. To characterise *HEXA*$^{-/-}$ and *HEXB*$^{-/-}$ CRISPR-Cas9 edited HL-60 cell lines to solidify the involvement of the Hex isoenzymes in the formation of paucimannosidic proteins, including MPO, in human neutrophils.

2. To characterise the structure and function of the *N*-glycans decorating MPO residing in the various granules of resting neutrophils.

These two aims will be targeted using a variety of techniques and contemporary methods in cell and molecular biology in order to yield new insight into the biosynthesis and functional roles of the fascinating glycosylation features embellishing human MPO, see **Fig. 10** for overview of the experimental design. The overarching goal with this thesis was to advance our knowledge of MPO and neutrophil glycobiology and its immediate relevance to fundamental and applied areas of human glycoimmunology.

Chapter 2: Materials and Methods

2.1 Materials

2.1.1. Chemicals and reagents

All chemicals, reagents and materials used in this research were purchased from Sigma-Aldrich or Thermo Scientific (Sydney, Australia) unless otherwise stated.

2.2 Methods

Diverse analytical workflows and methods were utilised to address the aims of this thesis. An overview of the experimental design is provided in **Fig. 10**.

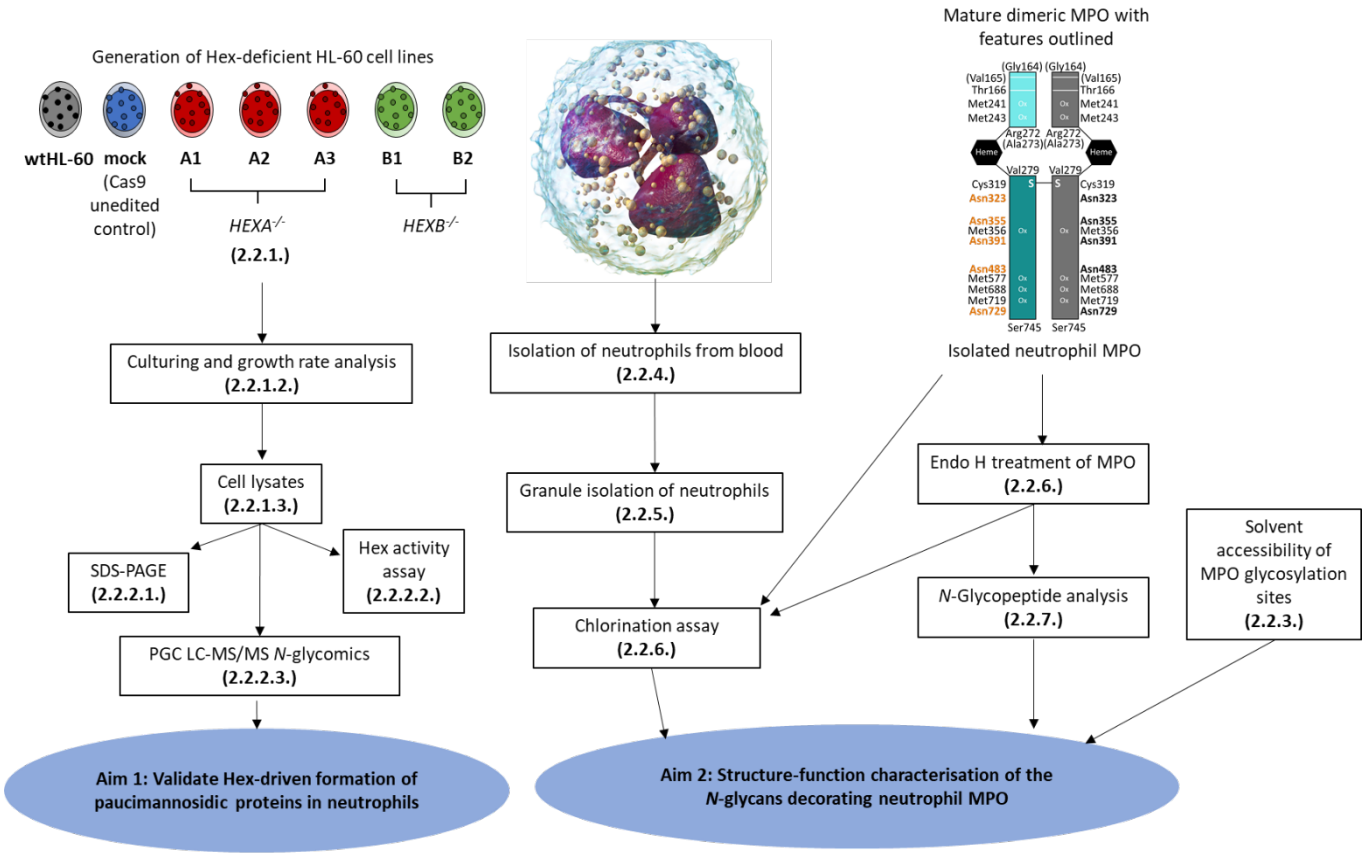

Figure 10. Overview of the aims, biological samples, experiments and methods of this thesis.

2.2.1. Generation and culturing of Hex-deficient HL-60 cell lines

Biosafety approval for the handling, culturing and the subsequent processing of the genetically edited HL-60 cells was obtained from the Human Research Ethics Committee (Reference #5201500813, BioHazard Risk Assessment, Exempt Dealings, Reference #5201500813) at Macquarie University, Sydney, Australia.

2.2.1.1. CRISPR-Cas9-mediated gene editing of HL-60 cells

The CRISPR-Cas9 gene editing of HL-60 cells was kindly performed by Prof. Neelamegham and Yuqi Zhu at University at Buffalo, NY, U.S. In brief, the targets of Hex genes were picked from a previously published CRISPR-Library (99). Single guide ribonucleic acid (sgRNA) was synthesised using polymerase chain reaction (PCR) amplification and *in vitro* transcription using EnGen® sgRNA Synthesis Kit (New England Biolabs, Ipswich, MA) following the manufacturer's protocol. A customised DNA oligo was synthesised with the target gene after a T7 promoter, followed by the first 17 bases of the sgRNA scaffold. The sgRNA was made by mixing the synthesised DNA with the sgRNA scaffold, T7 enzyme and reaction mix with incubation at 37°C for 2 h. Next, prior to transfection, wild-type HL-60 (wtHL-60) cells were passaged into fresh complete Iscove's Modified Dulbecco's Media (IMDM) (Gibco™ IMDM 1640 Medium, HEPES) with 10% (v/v) foetal bovine serum

(FBS), 1% arachidonic acid (AA) and 1% glutamax. On the day of electroporation, 1 μg sgRNA was premixed with 1 μg Cas9 (EnGen® Cas9 NLS, *Streptococcus pyogenes*, New England Biolabs, Ipswich, MA), room temperature, 25-30 min to form the ribonucleoprotein particles. The cells (0.15-0.25 million) were then resuspended in 10 μl Resuspension Buffer R provided by the Neon Transfection Kit (Thermo Scientific). The cells were then mixed with the ribonucleoprotein particles and electroporated using the Neon Transfection System (Thermo Scientific) at an optimised condition: 1600 V, 10 ms, 3 pulses (100). After electroporation, the cells were transferred to a 24-well plate containing 500 μL conditioned IMDM medium. To validate the genetic editing, next generation sequencing (NGS) was used. Genomic DNA was isolated from sorted single clones and a PCR was performed with gene specific primers to amplify the edited region. PCR purification was performed by gel extraction and the products were sent for NGS off-site.

2.2.1.2. Culturing, monitoring and growth profiling of HL-60 cells

The HL-60 cell lines, which were received in a frozen condition, were thawed and cultured in Roswell Park Memorial Institute Medium (RPMI)-1640 media (ATCC, Manassas, U.S.) supplemented with 10% (v/v) FBS in Corning T25 cell culture flasks. Stable growth conditions were maintained by an incubator set to 37°C and 5% carbon dioxide levels. Once confluency was reached, indicated by the colour change of the media and the presence of cellular debris (every 48-72 h), the media was collected and centrifuged at 150-200 g for 5-10 min. The pellet containing the live HL-60 cells was resuspended in 1-3 mL of pre-warmed (37°C) fresh media whilst the supernatant containing the dead cells and cellular debris was discarded. To monitor the live cell counts and viabilities, 20 μL of the cell suspensions were mixed with 20 μL 0.4% (w/v) trypan blue, 10 μL of which was loaded onto cell counting slides (BioRad) and counted using an automated TC20™ Cell Counter (Bio-Rad). Based on the cell counts, the appropriate amount of fresh pre-warmed media was added to each flask to ensure the density was ~1-2 x 10^5 cells/mL. The cell morphology was visualised at 10-40X magnification under an inverted light microscope. To monitor the growth rate of each cell line, 1 million cells from each line was seeded into 10 mL of fresh media. After 24 h, the cells were centrifuged and counted as mentioned above and the total number of live cells was recorded. This was repeated every 24 h for 72 h.

2.2.1.3. Harvesting and lysis of HL-60 cells

The cells were harvested by centrifuging the media at 150-200 g for 10 min. The supernatant was discarded while the cell pellet containing the live cells was washed twice in phosphate-buffered saline (PBS) and then resuspended in 500 μL radioimmunoprecipitation assay (RIPA) buffer

containing a protease inhibitor cocktail (cOmplete™, Roche). The cells were then lysed via two rounds of probe sonication (Sonifier 450, Branson) on ice at 26 A for 10 s. The tubes containing the frothy suspension were then centrifuged at 10,000 g for 10 min and the resulting cell lysate (supernatant) was stored at 4°C whilst the pellet containing cell debris and nuclei was discarded. The concentration of the cell lysates was determined using a bicinchoninic acid assay (BCA) on a 96-well-plate according to manufacturer's instructions (101). Various concentrations (0-2 mg/mL) of bovine serum albumin (BSA) were used to establish a protein standard curve.

2.2.2. Processing of HL-60 cell lysates

2.2.2.1. Sodium Dodecyl Sulfate-Polyacrylamide Gel Electrophoresis (SDS-PAGE) and staining of cell lysates

Cell lysate (10 μg) was treated with 500 mM dithiothreitol (DTT, 10X) and Nu-PAGE™ sample loading buffer (4X) and incubated at 70°C for 10 min to reduce the disulfide bonds of the proteins. Each sample was then loaded on a Nu-PAGE™ 4-12% Bis-Tris protein gel (1.5 mm, 12-well, 20 μL/well loading volume) and run in 2-(*N*-morpholino)ethanesulfonic acid (MES) buffer at 200 V for 35 min. A Novex™ sharp pre-stained protein standard was run alongside the lysates. Following gel electrophoresis, the gel was washed in MilliQ water and stained overnight in a Coomassie Blue solution in a closed container incubating at room temperature on a shaker (102). The next day, the stain was poured off and the gel was de-stained in 20% (v/v) aqueous methanol and washed with MilliQ water. The gel was imaged on a Gel Doc EZ System (BioRad).

2.2.2.2. Hexosaminidase activity assay

The enzymatic activity of the *N*-acetyl-β-hexosaminidase (Hex) of the HL-60 cell lysates was measured using a published protocol with minor modifications (103). In brief, 1.5 μg cell lysate (0.1 μg/μL) and 1.5 ng recombinant human Hex A and Hex B (RnD Systems, 0.1 ng/μL, positive controls) were incubated with 30 μL pre-warmed 3 mM 4-methylumbelliferyl-2-acetamido-2-deoxy-β-D-glucopyranoside (MUG) or 4-methylumbelliferyl-2-acetamido-2-deoxy-β-D-glucopyranoside-6-sulfate (MUGS) substrate (Merck Millipore) in a phosphate-citrate buffer (pH 5.0) at 37°C for 30 min in the dark. The reaction was stopped by the addition of 0.25 M glycine-carbonate stop buffer (pH 10.0). Upon Hex-mediated MUG and MUGS hydrolysis the fluorogenic product 4-methylumbelliferone (4-MU) is released allowing fluorometric quantitation of the reaction using a plate reader (FLUOstar Optima, BMG Technologies) with an excitation of 360 nm and an emission of 450 nm. The absolute quantity of released 4-MU was determined from a pre-made standard curve created using known concentrations of 4-MU.

2.2.2.3. N-glycomics of HL-60 cell lysates

2.2.2.3.1. N-glycan release and clean up

The *N*-glycan release and subsequent handling steps were performed as previously reported (104). Briefly, 20 μg protein extracts from the cell lysates (n = 3) were reduced with dithiothreitol (DTT), alkylated with iodoacetamide (IAA) and immobilised onto an ethanol-activated polyvinylidene fluoride (PVDF) membrane. After drying and washing the membrane, the protein spots were visualised using 0.1% (w/v) Direct-Blue Stock 71 staining, excised with a scalpel and transferred into a 96-well plate. The wells were blocked to avoid non-specific binding by 1% (w/v) polyvinylpyrrolidone solution, which was subsequently removed. The *N*-glycans were released by the addition of 2 U *N*-glycosidase F (PNGase F, *Elizabethkingia miricola*, Promega) in 10 μL MilliQ water and left to incubate overnight at 37°C. The released *N*-glycans were collected and incubated in 100 mM ammonium acetate buffer ($NH_4CH_3CO_2$, pH 5.0) at room temperature for 1 h, dried in a vacuum centrifuge and then reduced with 0.5 M sodium borohydride ($NaBH_4$) in 50 mM potassium hydroxide at 50°C for 3 h. Next, 2 μL glacial acetic acid was added to quench the reactions. The glycans were desalted using solid-phase extraction (SPE) micro-columns packed with AG 50W X8 strong cation exchange resin (200-400 mesh) (30 μL bed volume) (Bio-Rad) packed into C18 stage tips (Merck Millipore). After equilibration, the *N*-glycan samples were loaded onto the micro-columns, followed by two rounds of washing with 50 μL MilliQ water. The flow-through fractions (containing the *N*-glycans) were dried in a vacuum centrifuge, dissolved in 100 μL methanol and re-dried twice to remove any residual borate by evaporating off the volatile methyl borate. As a final clean-up step, the *N*-glycans were resuspended in 10 μL MilliQ water and passed through an equilibrated porous graphitised carbon (PGC) (BioRad) SPE micro-column packed onto a C18 stage tip (Merck Millipore). The column was washed twice with MilliQ water and the *N*-glycans were eluted with 25 μL 40% acetonitrile (ACN)/0.05% trifluoroacetic acid (TFA) followed by 25 μL 60% ACN/0.05% TFA. The eluted *N*-glycans were dried in a vacuum centrifuge and stored at -20°C until liquid chromatography electrospray ionisation tandem mass spectrometry (LC-ESI-MS/MS) analysis. Bovine fetuin was used as a standard to check the *N*-glycan release and handling protocol and ensure LC-ESI-MS/MS performance.

2.2.2.3.2 PGC-LC-ESI-MS/MS-based N-glycan profiling

The dried *N*-glycans were resuspended in 10 μL MilliQ water, centrifuged at 14,000 g for 10 min and the supernatant transferred into mass spectrometry glass vials (Thermo Scientific) for LC-ESI-MS/MS analysis. The *N*-glycans were separated by capillary PGC-LC (Hypercarb KAPPA capillary column, 180

µm internal diameter x 100 mm length, 5 µm particle size, 200 Å pore size, Thermo Scientific) using an Ultimate 3000 high performance liquid chromatography (HPLC) system (Dionex). The two solvents utilised for separation were solvent A i.e. 10 mM aqueous ammonium bicarbonate (ABC) and solvent B i.e. 10 mM ABC in 70% ACN (v/v). A linear gradient was utilised for the glycan separation starting at 2.6% (v/v) B and increasing to 45% (v/v) B over 80 min and finally equilibrating back to 2.6% (v/v) B. A post-column make-up flow was integrated into the LC-ESI-MS/MS configuration by the supplement of 98% (v/v) ACN at a 3 µL/min flow rate post column to enhance the glycomics performance (105). The separated *N*-glycans were introduced directly into a VelosPro linear ion trap (LTQ) mass spectrometer (Thermo Scientific) operated in negative ion polarity mode. The full scan acquisition range (*m/z* 200-2,200) was kept constant. Utilising data-dependent acquisition, the five most abundant precursor ions were selected for resonance-activation (ion trap) collision-induced dissociation (CID) MS/MS fragmentation. Dynamic exclusion was disabled.

2.2.2.3.3. Data analysis of N-glycans

The PGC-LC-ESI-MS/MS raw data was browsed and handled using the Xcalibur™ Qual Browser v2.2 (Thermo Scientific). The *N*-glycan fine structures were manually characterised based on their monoisotopic precursor mass, CID-MS/MS(-) fragmentation pattern (106, 107) and absolute and relative PGC-LC elution time (108-110). GlycoMod (111) and GlycoWorkbench v2.1 (112) aided the structural characterisation.

2.2.3. 3D structure representation and solvent accessibility of the MPO glycosylation sites

The 3D structure of MPO was visualised using PyMOL Molecular Graphic System v1.74 (Schrodinger). A high-resolution x-ray crystallography entry of human MPO in the Protein Data Bank (PDB) was chosen (PDB: 1D2V). The most abundant *N*-glycans were modelled *in silico* on Asn323, Asn355, Asn391, Asn483 and Asn729 of each MPO monomer (PDB: 1D2V) with the default torsion angles provided by the Glycoprotein builder feature of GLYCAM web (http://glycam.org).

To determine the site-solvent accessibility, NACCESS (113) was applied to five high-resolution x-ray crystallography 3D structures of human MPO deposited in the PDB (1D2V, 1CXP, 1DNU, 1DNW, 5FIW). Both the monomeric and dimeric forms of MPO stripped for any pre-existing Asn-linked glycans were assessed for solvent accessibility. In short, NACCESS allows an assessment of the atomic interactions (Van der Waal's interactions) between the Asn of the *N*-glycosylation site(s) of interest and a spherical probe (radius: 5 Å). The software outputs an arbitrary but comparable value which can be used to determine the relative solvent accessibility of each site.

2.2.4. Isolation of neutrophils from whole blood

2.2.4.1. Drawing of blood

Peripheral blood (187.5 mL/donation) was drawn and collected into a sterile cylinder containing acid-citrate-dextrose by a trained phlebotomist from the medial cubital vein of a healthy adult male donor after obtaining informed consent. The collection of blood and the subsequent isolation of resting neutrophils was approved by the Human Research Ethics Committee (Reference #5201500409) in addition to the completion of the BioHazard Risk Assessment (Non-GMO, #NIP041214BHA) at Macquarie University, Sydney, Australia.

2.2.4.2. Neutrophil isolation

All solutions were sterilised prior to commencing this procedure. The freshly drawn blood (187.5 mL) was added to 62.5 mL acid-citrate-dextrose (1:4) and mixed with 250 mL 2% (w/v) dextran in 0.9% (w/v) sodium chloride (NaCl) solution (1:1). The tube was mixed by repeated inversion (10 times) and incubated at room temperature for 30 min to allow efficient sedimentation of the red blood cells (RBCs). The supernatant (light yellow plasma-rich layer containing peripheral mononuclear and polymorphonuclear cells) was collected and centrifuged at 200 g for 10 min at 4°C whilst the lower layer of RBCs was discarded. The pelleted white blood cells (WBCs) were resuspended in 30 mL 0.9% (w/v) NaCl, and 15 mL Lymphoprep™ (STEMCELL Technologies, Vancouver, Canada) was injected below the WBC suspension layer. The tubes were then centrifuged in a swing bucket rotor at 400 g for 30 min at 4°C with maximum acceleration and no deceleration. As a result, an upper layer of saline and plasma, an interface band containing the mononuclear cells, basophils and platelets, a layer of Lymphoprep™, a band of granulocytes, and a layer of sedimented RBCs were formed. The upper layers were removed by careful aspiration in a circular motion to avoid the adhesion of monocytes to the side of the tube and to avoid activation of neutrophils. For hypotonic lysis of the RBCs, the granulocyte band and the RBC pellet were resuspended in 10 mL sterile water, vortexed for 30 s. The tonicity was restored by the addition of 10 mL 1.8% (w/v) NaCl solution. After centrifugation at 200 g for 6 min at 4°C, the supernatant containing the lysed RBCs was removed. This lysis step was repeated once. The granulocyte pellet containing the neutrophils of interest (114) was resuspended in 5 mL 0.9% (w/v) NaCl to determine the cell count, viability and purity of the isolated neutrophils.

2.2.4.3. Cell count, viability and purity of neutrophils

The granulocyte count and viability of the resuspended granulocyte pellet was determined at different dilutions using a TC20™ Cell Counter (Bio-Rad). The purity of the isolated neutrophils was

measured by depositing and fixing the cell mixtures on a glass slide using the cytospin technique on a cell fixing centrifuge (Orbital 300, Clements), followed by Wright-Giemsa staining with Sorensen's buffer for 15 min (115). The slides were then visualised using a bright field microscope (Olympus Life Science) at 10X, 20X and 40X magnification. The purity was determined by counting approximately 100 cells in a given field and determining the cell type based on morphology.

2.2.5. Subcellular fractionation of isolated neutrophils

2.2.5.1. Disruption of neutrophils by nitrogen cavitation

The subcellular fractionation of isolated blood neutrophils was performed according to an established protocol (116). In brief, the neutrophils were resuspended in a protease inhibitor (PI) solution consisting of two PI mini-tablets (cOmplete™, Roche) dissolved in 5 mL 0.9% (w/v) NaCl and incubated on ice for 10 min. The cells were then centrifuged at 200 g for 6 min at 4°C and the supernatant was discarded. Subsequently, the cells were resuspended in 7.5 mL 1X disruption buffer (100 mM KCl, 3 mM NaCl, 3.5 mM $MgCl_2$, 1.5mM ethylene glycol-bis (β-aminoethyl ether)-N, N, N', N'-tetraacetic acid (EGTA), 10 mM piperazine-N, N'bis [2-ethanesulfonic acid] (PIPES)), 1 mM ATP $(Na)_2$ and 0.5 mM phenylmethylsulfonyl fluoride (PMSF) – all stated as final concentrations. This buffer is designed to mimic the intracellular fluid of neutrophils to ensure that the granules do not lyse upon neutrophil cavitation. Plasma membrane disruption of the neutrophil was performed by nitrogen cavitation via a Parr cavitation bomb (Parr instruments). The sample tube was placed inside a container of ice within a pre-chilled (4°C) Parr bomb that was filled with nitrogen gas (>99.9% purity) and left for 15 min. The valve was slowly released allowing the cell suspension to pass through, and the disrupted material (known as the "cavitate") was collected in a drop-wise fashion into a parafilm-covered 50 mL Falcon tube until the cell suspension was diminished. Prior to this, a volume of EGTA resulting in a final concentration of 100 mM was added to the parafilm-covered tube. The cavitate was then centrifuged at 400 g for 15 min at 4°C. The granule-containing supernatant was collected and mixed with 50 mM ATP $(Na)_2$ and 100 mM PMSF.

2.2.5.2. Granules separation

Percoll (1.129 g/mL) was mixed with 10X disruption buffer and MilliQ water in separate tubes to create four densities of 1.03 g/mL, 1.09 g/mL, 1.11 g/mL, and 1.12 g/mL. The cavitate was mixed in a 1:1 (v/v) ratio with the 1.11 g/mL Percoll solution. Using a 14G x $3^{1/4}$-inch needle, 9 mL of the 1.03 g/mL solution was added to the bottom of a polycarbonate centrifuge tube (Beckmann Coulter, 50 mL), followed by 10 mL of the cavitate 1.11 g/mL mixture, 9 mL of the 1.09 g/mL solution and finally 9 mL of the 1.12 g/mL solution. Importantly, the same volume of each density solution was added

to two or more tubes to balance the centrifuge. The tubes were centrifuged at 37,000 g for 30 min at 4°C in a fixed angle rotor centrifuge (Beckmann Coulter). This separated the less dense plasma membrane on the surface, followed by the denser secretory vesicles, gelatinase (Ge) granules, specific (Sp) granules and lastly the azurophilic (Az) granules; the densest granule type containing the most MPO (42). In total, 37 fractions (1 mL) were collected from the bottom of the Percoll-layered tube into Eppendorf tubes utilising a peristaltic pump (Amersham) and an automated fraction collector (FRAC-200, Amersham).

2.2.5.3. Identification of the MPO-rich granule fractions using a 3,3' ,5,5'-tetramethylbenzidine assay

To determine the MPO-rich fractions, a 3,3' ,5,5'-tetramethylbenzidine (TMB) assay was employed. TMB is a known substrate for peroxidases (117), such as MPO. In brief, 5 μL of each of the 37 fractions was added to a 96-well plate with 150 μL ready-to-use TMB liquid substrate (Sigma) with shaking for 10 min. Subsequently, 100 μL 1 M sulfuric acid was added to quench the reaction, and the absorbance recorded using a plate reader (SPECTROstar Nano, BMG LABTECH) at 450 nm. To remove the LC-MS/MS-incompatible Percoll, the MPO-rich fractions were pooled, transferred to new tubes and ultracentrifuged at 100,000 g for 90 min at 4°C (Optima X, Beckmann Coulter). The isolated granules were collected in the supernatant. The Percoll pellet was discarded.

2.2.6. MPO activity using a chlorination assay

Human MPO purified from isolated neutrophils (5 nM final concentration, Lee Biosolutions, Maryland Heights, U.S.) was incubated with or without 1 μL endoglycosidase H (Endo H, *Streptomyces plicatus*, Promega, Australia) (500 U/μL) overnight at 37°C. The MPO activity was assayed by the formation of HOCl captured via taurine as described (118). Briefly, a HOCl standard curve was constructed by adding known concentrations of HOCl to taurine (5 mM final concentration dissolved in PBS), which were kept on ice for 30 min prior to assay. The concentration of HOCl was determined by measuring its absorbance at 292 nm at pH 12 (ε_{292} 350 M^{-1} cm^{-1}) and subsequently neutralised before use. Protein extracts from each granule fraction (2 μg) and the Endo H-treated and non-treated MPO was combined with taurine (5 mM final concentration) in separate Eppendorf tubes and was incubated in the presence or absence of human ceruloplasmin (100 nM final concentration, Lee Biosolutions, Maryland Heights, U.S) for 30 min at room temperature. The reaction commenced upon the addition of H_2O_2 (20 μM final concentration) and was allowed to run for 20 min at room temperature. The reaction was stopped by the addition of bovine catalase (20 μg/mL, Sigma). 200 μL of each reaction and the HOCl standards were mixed with

50 μL developing reagent (2 mM TMB in 400 mM acetate buffer, 10% dimethylformamide and 100 μM sodium iodide, pH 5.4) in a 96-well plate with mixing. The absorbance was measured in a plate reader (SPECTROstar Nano, BMG LABTECH) at 650 nm and the amount of HOCl produced was determined based on a standard curve.

2.2.7. N-Glycopeptide analysis

2.2.7.1 Generation of MPO (glyco)peptides

To site-specifically determine the MPO *N*-glycoforms after Endo H treatment, Endo H-treated and untreated MPO was subjected to *N*-glycopeptide analysis (119). Briefly, Endo H-treated and untreated MPO was first separated by SDS-PAGE and stained with Coomassie Blue (as performed in **Section 2.2.2.1**). Bovine ribonuclease B with and without Endo H treatment was used as a control. The protein bands containing the MPO β-chains of interest were excised from the SDS-PAGE gel, cut into small pieces, and de-stained with ACN. The protein was then reduced with DTT and alkylated with IAA and digested with porcine trypsin (1:30 enzyme/protein, w/w ratio) in 25 mM ABC (pH 8.0) at 37°C for 18-20 h. The resulting (glyco)peptides were extracted with ACN and formic acid (FA), dried in a vacuum centrifuge and resuspended in 1% (v/v) FA for clean-up via reversed-phase SPE micro-columns. Here, a C18 disc was injected into a small pipette tip, primed with washes of 60% ACN/0.1% FA and then equilibrated with 0.1% FA. The (glyco)peptides were passed through the column, the column washed with 0.1% FA and the (glyco)peptides were eluted with 50 μL 60% ACN/0.1% FA and then 50 μL 90% ACN/0.1% FA. The eluent was dried in a vacuum centrifuge and stored at -20°C until LC-ESI-MS/MS analysis (120).

2.2.7.2. LC-ESI-MS/MS analysis of (glyco)peptides

The (glyco)peptides were reconstituted in 15 μL 0.1% (v/v) FA and centrifuged at 14,000 g for 10 min. The supernatants were transferred into mass spectrometry glass vials (Thermo Scientific) and analysed via LC-ESI-MS/MS on a Q-Exactive™ HF-X Hybrid Quadrupole-Orbitrap™ mass spectrometer (Thermo Scientific) coupled to an Ultimate 3000 HPLC (Dionex) that were operated in positive polarity mode and reversed-phase chromatography mode, respectively. The (glyco)peptides were separated at a flow rate of 600 nL/min on an analytical column (25 cm x 75 μm, 3 μm inner diameter) that was packed in-house with Reprosil-Pur C18-Aq resin (Dr. Maisch, Ammerbuch-Entringen, Germany). The mobile phases were 99.9% ACN in 0.1% (both v/v) aqueous FA (solvent B) and aqueous 0.1% (v/v) FA (solvent A). The concentration of solvent A followed an increasing linear gradient from 2% to 30% over 66 min, 30% to 50% over 5 min, 50% to 95% over 1 min and finally 95% of solvent B for 7 min. The column was then equilibrated with 98% solvent B for

10 min before the next sample was loaded. Using data-dependent acquisition, the Orbitrap acquired a full MS scan at high-resolution 60,000 full width at half maximum (FWHM, measured at *m/z* 200) in the *m/z* range 350-1,800. The 20 most abundant precursor ions were selected from each MS full scan utilising higher-energy collision-induced dissociation (HCD) fragmentation with a normalised collision energy of 28% utilising only precursors that were at least doubly charged. Fragmentation was performed at high resolution (45,000 FWHM) using a precursor isolation window of *m/z* 1.0 and a dynamic exclusion of 30 s after a single isolation and fragmentation of a given precursor.

2.2.7.3. Data analysis of (glyco)peptides

The (glyco)peptide raw data was browsed and handled using Xcalibur™ Qual Browser v2.2 (Thermo Scientific). The MPO glycopeptides were either identified using Byonic™ v.3.4 (Protein Metrics) (121) with a protein FDR of 1% or via manual identification using accurate monoisotopic precursor mass, the HCD-MS/MS fragmentation pattern and the relative LC elution time. GPMAW v9.5 (Lighthouse, Odense, Denmark) (122) was utilised to assist the manual identification. The canonical protein sequence of human MPO was obtained from UniProtKB (P05164) and used for the identification.

Chapter 3: Results

The principal aim of this thesis was to provide evidence for the involvement of the *N*-acetyl-β-hexosaminidase (Hex) isoenzymes in the formation of paucimannosidic proteins in human neutrophils. To this end, a number of CRISPR-Cas9-edited *HEXA*$^{-/-}$ and *HEXB*$^{-/-}$ HL-60 cell lines (called A1-3 and B1-2, respectively) were explored using different biochemical techniques and compared to a CRISPR-Cas9-infected but unedited HL-60 cell line (called mockHL-60) and a wild-type HL-60 cell line (wtHL-60), **Table 1**. HL-60 is a neutrophil-like precursor cell type often used in neutrophil biology. An additional aim of the thesis was to characterise the structure-function of the paucimannose-rich *N*-glycosylation features decorating myeloperoxidase (MPO), a key innate immune-related glycoprotein expressed in human neutrophils.

Table 1. Overview of the investigated HL-60 cell types. *HEXA* and *HEXB* encode the α- and β-subunit of the dimeric Hex, respectively. Hex A (αβ), Hex B (ββ), Hex S (αα). *Theoretical expression. The actual expression of the Hex isoenzymes was not measured.

Name	*HEXA* genotype	*HEXB* genotype	Hex isoform(s) disrupted	Hex isoform(s) still expressed*	Description
wt HL-60	*wt/wt*	*wt/wt*	-	Hex A, Hex B, Hex S	Wild-type HL-60
mock HL-60	*wt/wt*	*wt/wt*	-	Hex A, Hex B, Hex S	CRISPR-Cas9-infected but unedited HL-60
A1	*-/-*	*wt/wt*	Hex A, Hex S	Hex B	*HEXA*-disrupted HL-60 mutants
A2	*-/-*	*wt/wt*	Hex A, Hex S	Hex B	
A3	*-/-*	*wt/wt*	Hex A, Hex S	Hex B	
B1	*wt/wt*	*-/-*	Hex A, Hex B	Hex S	*HEXB*-disrupted HL-60 mutants
B2	*wt/wt*	*-/-*	Hex A, Hex B	Hex S	

3.1. Characterisation of the generated CRISPR-Cas9-edited Hex-deficient HL-60 mutants

3.1.1. Next generation sequencing (NGS)

To validate the CRISPR-Cas9 editing of the HL-60 mutants produced by our collaborators (Prof. Neelamegham, Buffalo Univ, NY), genomic DNA was isolated from sorted clones, and PCR was performed to amplify the putatively edited region. In short, the PCR products were separated on gels, extracted and sequenced via NGS by the collaborators, **Appendix Fig. S1**. NGS confirmed that all mutants contained no wild-type DNA in the target region. Various edits spanning insertions, mutations and deletions were identified around the PAM sequence in the *HEXA*$^{-/-}$ and *HEXB*$^{-/-}$ clones. The smallest gene edit, a single base deletion, occurred in A3.

3.1.2. Morphology and growth profiles of the Hex-deficient HL-60 mutants

HL-60 is a suspension cell type. To investigate the morphology of the Hex-deficient mutants relative to wtHL-60 and mockHL-60, the cells were fixed onto glass slides via the cytospin technique, stained with Wright-Giemsa stain, and visualised under a light microscope (**Appendix Fig. S2**). Neither the *HEXA*$^{-/-}$ (**Fig. S2C-E**) nor the *HEXB*$^{-/-}$ (**Fig. S2F-G**) HL-60 mutants showed major morphological or size

differences relative to wtHL-60 (**Fig. S2A**) and mockHL-60 (**Fig. S2B**). All cells displayed the round promyelocytic morphology of approximately 10-20 µm in diameter, known cellular characteristics of undifferentiated HL-60 cells. The Hex-deficient HL-60 mutants, excluding A2, exhibited decreased viability when compared to wtHL-60 and mockHL-60 (**Appendix Fig. S2H**). Suppressed growth was observed for B2 and, in part, also for A3. However, all HL-60 mutants were clearly viable and thus used for biochemical characterisation following multiple rounds of passaging to achieve sufficient biological material for the various assays.

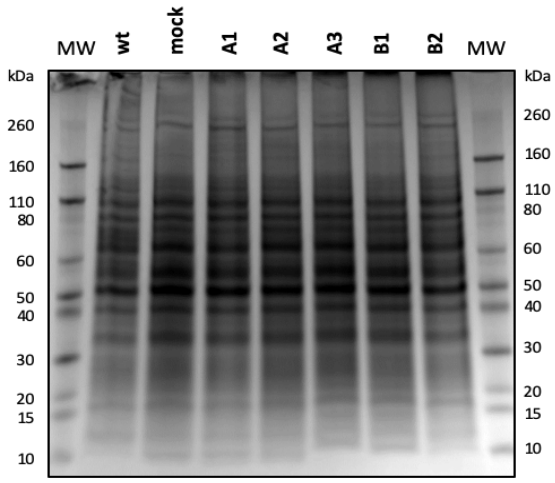

Figure 11. Unaltered protein expression of the Hex-deficient HL-60 mutants. *wtHL-60, wild-type HL-60. mock, unedited control. A1-A3, HEXA$^{-/-}$. B1-B2, HEXB$^{-/-}$ mutants. MW, molecular weight ladder.*

3.1.3. SDS-PAGE of HL-60 protein extracts

After cell harvest and lysis, protein extracts (all adjusted to 10 µg) of the HL-60 variants were analysed by SDS-PAGE to visualise and compare their protein expression patterns (**Fig. 11**). Similar protein band patterns were observed across the HL-60 mutants and the mock and wtHL60, which demonstrated that the Hex disruption did not significantly affect the general protein expression machinery of the HL-60 mutants.

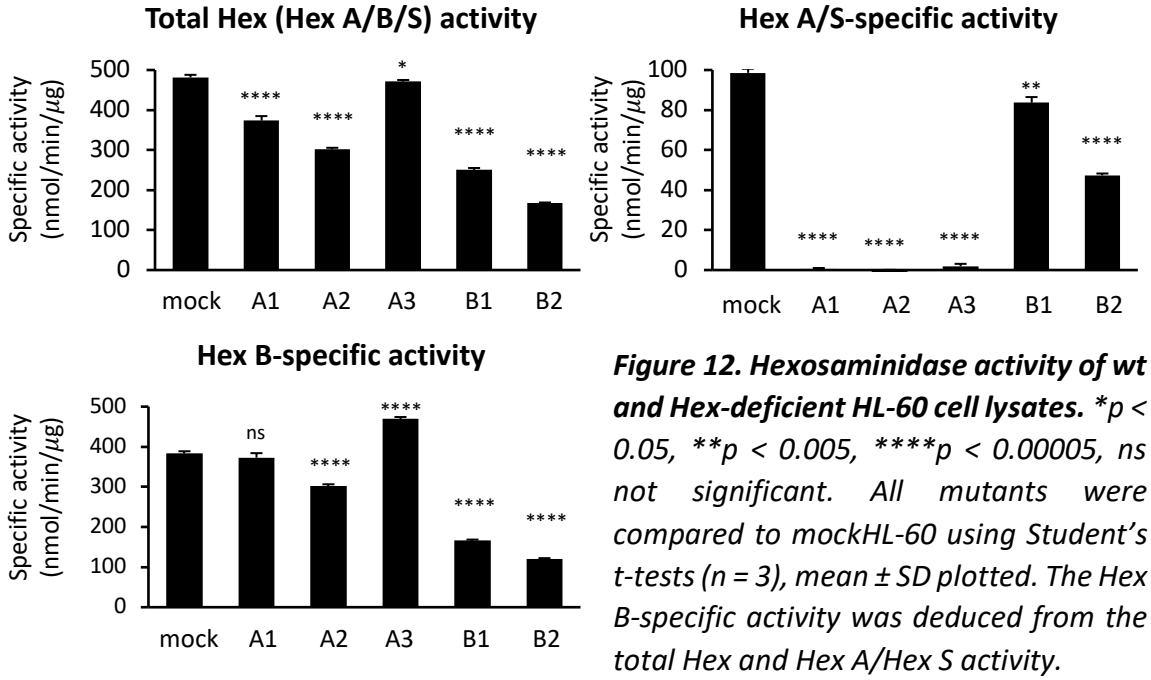

Figure 12. Hexosaminidase activity of wt and Hex-deficient HL-60 cell lysates. **p < 0.05, **p < 0.005, ****p < 0.00005, ns not significant. All mutants were compared to mockHL-60 using Student's t-tests (n = 3), mean ± SD plotted. The Hex B-specific activity was deduced from the total Hex and Hex A/Hex S activity.*

3.1.4. Hexosaminidase activity of Hex-deficient HL-60 mutants

To validate the functional disruption of Hex in the HL-60 mutants, the hexosaminidase activity of the HL-60 variants were measured using two related fluorescence-based enzyme assays (**Fig. 12**). The total hexosaminidase assay measuring the activity of all Hex isoenzymes (Hex A, Hex B and Hex S) was determined by the hydrolysis of 4-methylumbelliferyl-2-acetamido-2-deoxy-β-D-glucopyranoside (MUG) to the fluorescent 4-MU compounds over time whilst the hexosaminidase activity of Hex A and Hex S was measured by the 4-MU production rate from the negatively charged 4-methylumbelliferyl-6-sulfo-*N*-acetyl-β-D-glucosaminide (MUGS) substrate (123, 124). The Hex B-specific activity was deduced from the Hex A/Hex S-specific activity relative to the total Hex activity.

As expected, the Hex-deficient HL-60 cell lines demonstrated a significant reduction of the total hexosaminidase activity relative to mockHL-60. MockHL-60 rather than wtHL-60 was here used as the appropriate comparison control since the CRISPR-Cas9 infection procedure itself may impact the expression and/or activity level of Hex. The two *HEXB*$^{-/-}$ cell lines (B1-B2) displayed a greater reduction in the total hexosaminidase activity compared to the *HEXA*$^{-/-}$ cell lines (A1-A3) possibly reflecting the notion that Hex S (αα) contributes only little, if at all, to the Hex isoenzymatic activity of human cells (125). With regard to the Hex A/Hex S-specific activity, the A1-A3 mutants displayed an almost complete absence of hexosaminidase activity whilst the B1-B2 mutants displayed a significantly reduced but still clearly measurable activity most likely due to some formation and activity of Hex S and/or compensation mechanisms or the presence of nucleocytoplasmic forms of Hex encoded by different genes than *HEXA* and *HEXB* (discussed below). Possibly adding support for the existence of compensation mechanisms, it is interesting to note that the A3 mutant had a significantly higher Hex B-specific activity than wtHL-60 albeit this was only indirectly assayed. Interestingly, the total Hex (Hex A/B/S) activity of mockHL-60 was twice as high as wtHL-60 (data not shown). Taken together, the two hexosaminidase activity assays demonstrated that functional disruption of the *HEXA* and *HEXB* gene products was successfully achieved in all five HL-60 clones, but at the same time also showed that the Hex-disrupted mutants still displayed some residual hexosaminidase enzyme activities.

3.1.5. N-glycan profiling of the Hex-deficient and wtHL-60

LC-ESI-MS/MS-based glycomics was then used to investigate the involvement of the Hex isoenzymes in the formation of paucimannosidic proteins. In short, the *N*-glycans were enzymatically released by PNGase F from the protein extracts of the HL-60 variants and profiled in their reduced form by PGC-LC-ESI-MS/MS. Examples of the resulting MS profiles of mockHL-60, *HEXA*$^{-/-}$ (A1) HL-60 and

HEXB$^{-/-}$(B2) HL-60, are displayed in **Fig. 13** (see all profiles in **Appendix Fig. S3**). Again, mockHL-60 rather than wtHL-60 was here used as the appropriate comparison control since the CRISPR-Cas9 infection procedure itself may impact the glycome expression pattern.

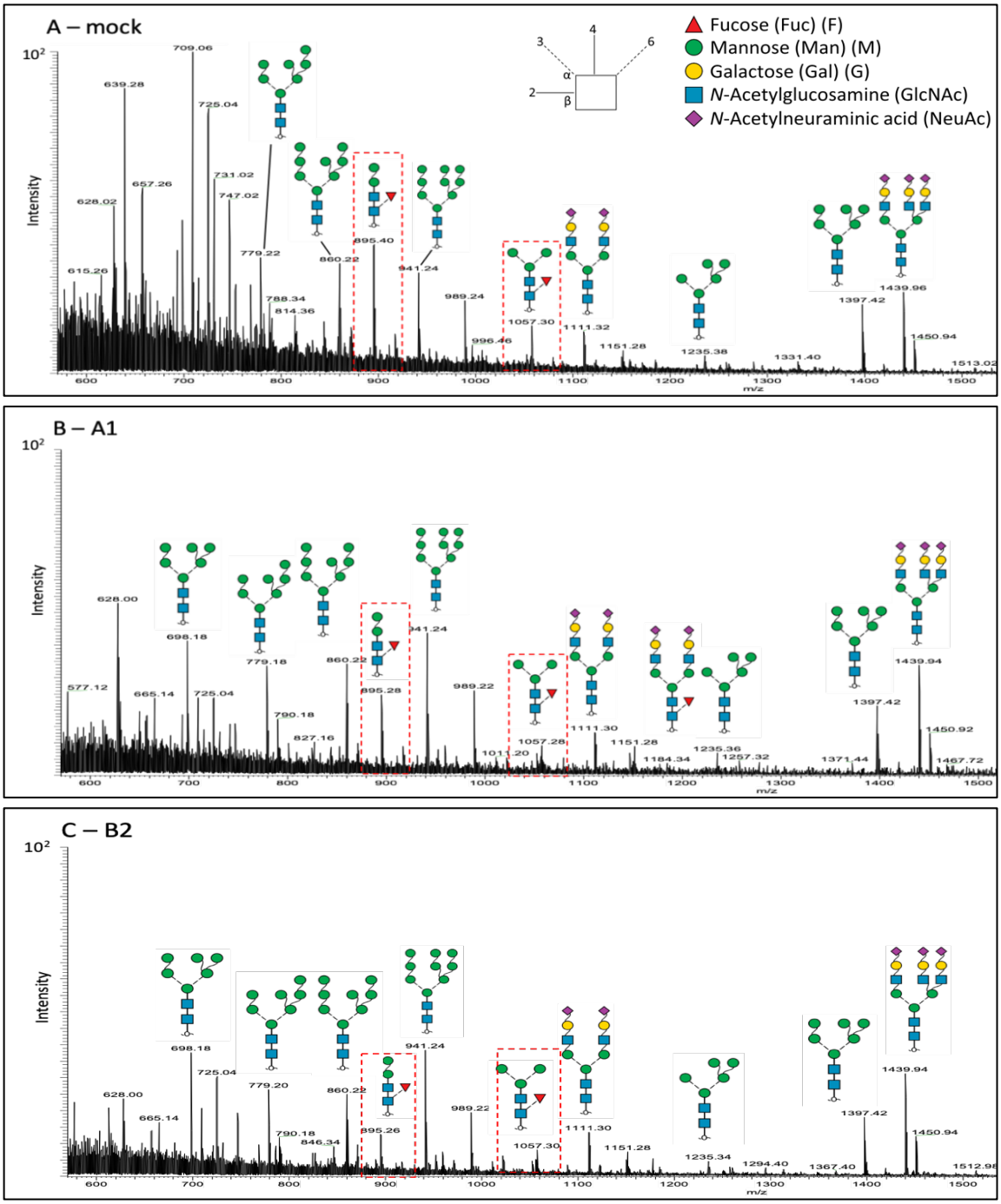

Figure 13. PGC-LC-MS profiles of N-glycans expressed by HL-60 variants. *(A) wt, (B) HEXA*$^{-/-}$ *A1, (C) HEXB*$^{-/-}$ *B2. The MS profiles were summed from 18-65 min to allow for visual comparison of the most abundant N-glycans expressed by the HL-60 variants. Structures as solved by manual annotation are depicted. The two paucimannosidic species* $Man_2GlcNAc_2Fuc_1$ *(M2F, m/z 895.3) and* $Man_3GlcNAc_2Fuc_1$ *(M3F, m/z 1057.3) are boxed in red. See key for glycan symbol nomenclature and the utilised linkage representation (110).*

The initial qualitative comparison of the summed mass spectra indicated that all HL-60 variants expressed similar *N*-glycome profiles including the presence of paucimannosidic-, oligomannosidic- and complex-type *N*-glycans. The glycan fine structures were manually solved using the glycan monoisotopic precursor mass, CID-MS/MS fragmentation pattern and PGC-LC elution time (106, 108, 109). PGC-LC-ESI-MS/MS is advantageous over other *N*-glycan profiling methods e.g. matrix-assisted laser desorption/ionisation-time of flight-MS profiling by allowing for detailed structural characterisation at the glycome-wide level while also providing quantitative data to establish the relative glycan abundances. The glycan structures are still most accurately solved by manual annotation of the CID-MS/MS data (**Appendix Fig. S4**) although assisting software is available. Inspection of the MS profiles indicated that the key paucimannosidic *N*-glycans i.e. $Man_2GlcNAc_2Fuc_1$ (M2F, *m/z* 895.3) and $Man_3GlcNAc_2Fuc_1$ (M3F, *m/z* 1057.3) were noticeably lower in A1 (**Fig. 13B**) and B2 (**Fig. 13C**) than in mockHL-60 (**Fig. 13A**). Concomitantly, the Hex-deficient mutant A2 showed, as expected, a higher expression of the GlcNAc-capped *N*-glycans (i.e. $GlcNAc_2Man_3GlcNAc_2Fuc_1$), putative Hex substrates, **Fig. S3.**

To further investigate these qualitative observations, extracted ion chromatogram (EIC)-based quantitation of the PGC-LC-ESI-MS/MS data was performed (**Fig. 14**). All Hex-deficient clones demonstrated a minor but still significant reduction in the total paucimannose level (10.4% ± 0.4% - 17.1% ± 1.0%, all $p < 0.05$, $n = 3$) when compared to mockHL-60 (20.0% ± 1.0%). This observation excitingly created support for a link between Hex and the formation of paucimannosidic proteins.

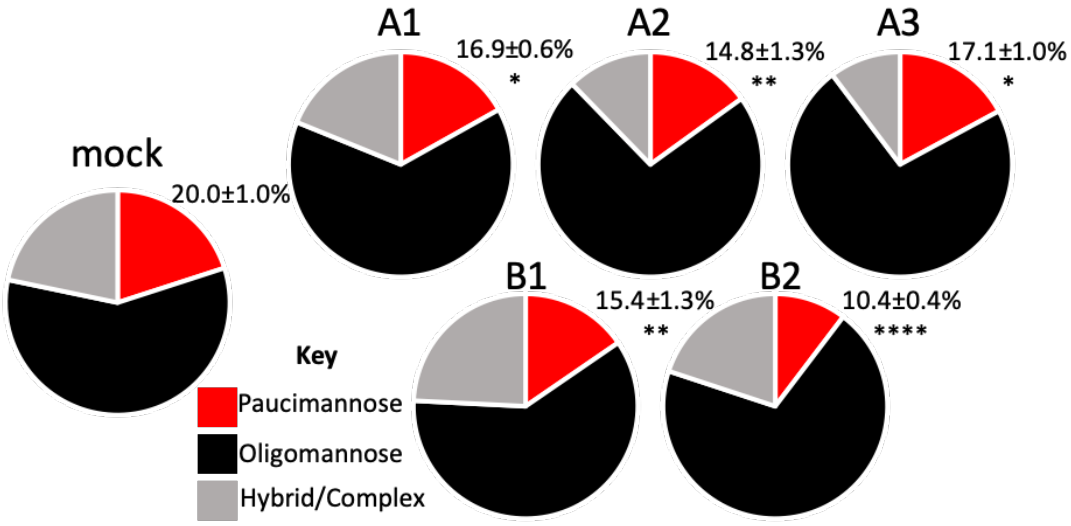

Figure 14. N-glycan profiling of the HL-60 variants*. The charts plot the distribution of the three observed N-glycan types, n = 3. *p < 0.05, **p < 0.005, ****p < 0.00005 (Student's t-test). Mock is the CRISPR-Cas9-infected but unedited HL-60 cell line. A1-A3 are the HEXA-disrupted HL-60 mutants whilst B1-B2 are the HEXB-disrupted HL-60 mutants.*

To further establish the link between Hex and the formation of paucimannosidic proteins, EIC-based quantitative comparisons of the levels of the putative Hex substrates i.e. two prominent paucimannosidic precursor *N*-glycans $GlcNAc_2Man_3GlcNAc_2Fuc_1$ and $GlcNAc_1Man_3GlcNAc_2Fuc_1$ and the paucimannosidic product *N*-glycans $Man_3GlcNAc_2Fuc_1$ (M3F) were made between mockHL-60 and the A1 (*HEXA*$^{-/-}$) and B2 (*HEXB*$^{-/-}$) HL-60 mutants (**Fig. 15i-iii**). Evidently, the GlcNAc-capped *N*-glycans were significantly higher and M3F was significantly lower in the Hex-disrupted mutants compared to mockHL-60 (all $p < 0.05$, $n = 3$, with the exception of ii-iiiA1 that did not reach significance).

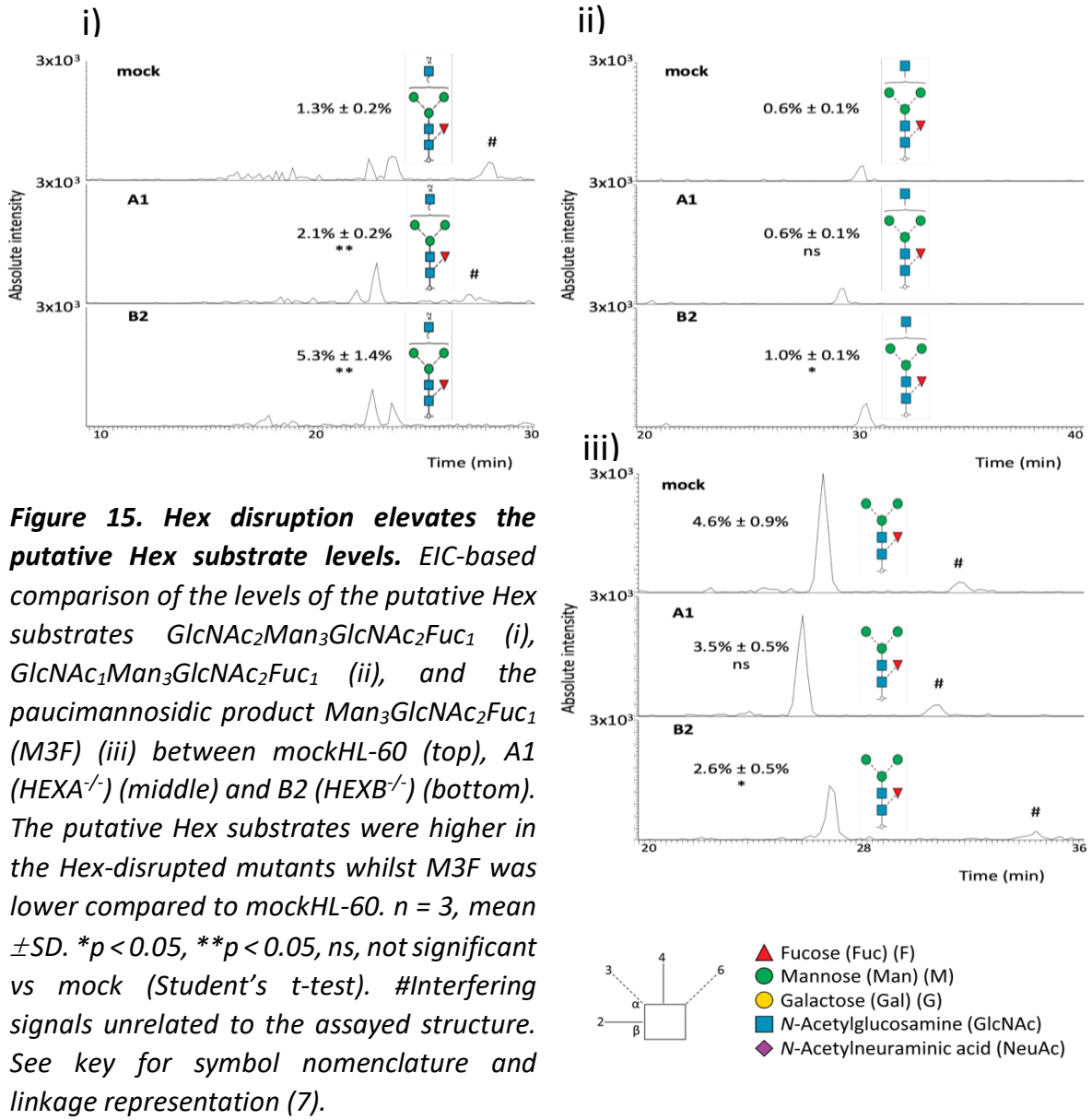

Figure 15. Hex disruption elevates the putative Hex substrate levels. *EIC-based comparison of the levels of the putative Hex substrates* $GlcNAc_2Man_3GlcNAc_2Fuc_1$ *(i),* $GlcNAc_1Man_3GlcNAc_2Fuc_1$ *(ii), and the paucimannosidic product* $Man_3GlcNAc_2Fuc_1$ *(M3F) (iii) between mockHL-60 (top), A1 (HEXA*$^{-/-}$*) (middle) and B2 (HEXB*$^{-/-}$*) (bottom). The putative Hex substrates were higher in the Hex-disrupted mutants whilst M3F was lower compared to mockHL-60. n = 3, mean ±SD. *p < 0.05, **p < 0.05, ns, not significant vs mock (Student's t-test). #Interfering signals unrelated to the assayed structure. See key for symbol nomenclature and linkage representation (7).*

EIC-based quantitation of the PGC-LC-ESI-MS/MS data was also used to assess if the Hex disruption affected the distribution of the paucimannosidic species relative to the mockHL-60 (Fig. 16). The non-core fucosylated paucimannosidic species (e.g. M2, $Man_2GlcNAc_2$) were of particular interest since these structures can potentially be generated directly from truncation of the oligomannosidic-type glycans without the involvement of Hex isoenzymes. The Hex-deficient mutants did neither display significantly altered paucimannose distributions nor a higher M2 level (the only non-core fucosylated paucimannosidic glycan observed) possibly ruling out a significant Hex-independent (i.e. α-mannosidase-driven) formation of afucosylated paucimannosidic glycans, however, more experiments are required to investigate this further.

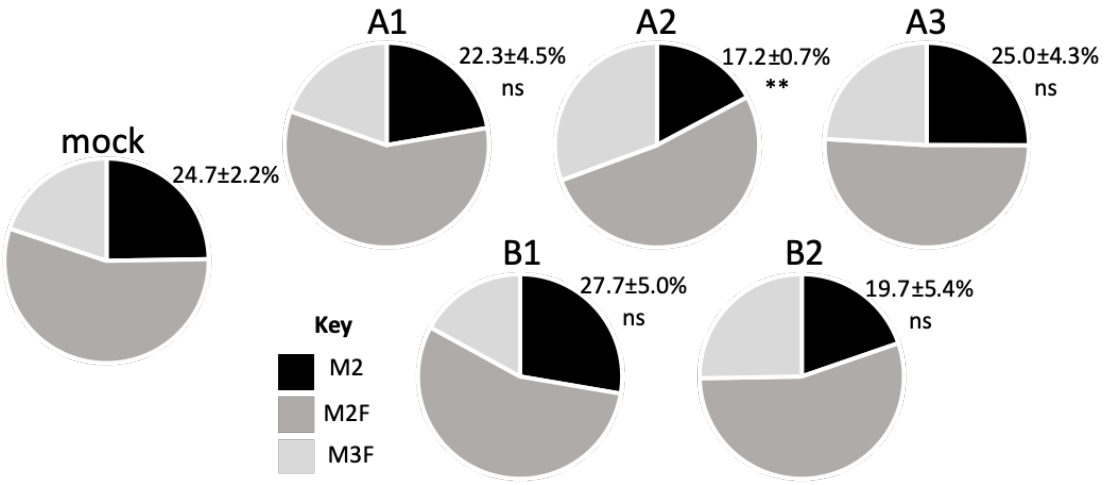

***Figure 16. Paucimannosidic N-glycan distribution of the HL-60 variants**. To investigate if Hex disruption impacted the distribution of paucimannosidic species in the HL-60 mutants, the average relative levels of the main paucimannosidic structures M2 ($Man_2GlcNAc_2$), M2F ($Man_2GlcNAc_2Fuc_1$), and M3F ($Man_3GlcNAc_2Fuc_1$) were plotted. The Hex-disrupted mutants neither displayed a significant increase in the relative abundance of the M2 structure nor a widely altered distribution of the paucimannosidic species relative to mockHL-60, thereby ruling out compensation by the Hex-independent pathway (see Discussion for more). In fact, A2 ($HEXA^{-/-}$) displayed a significant decrease in M2 vs mock. Mean ± SD plotted, n = 3. A1-3, $HEXA^{-/-}$ HL-60 mutants; B1-2, $HEXB^{-/-}$ mutants. Mock, mockHL-60. See key for details.*

3.2. Isolation and subcellular fractionation of resting neutrophils

3.2.1. Characterisation of isolated neutrophils

Resting neutrophils isolated from whole blood using Lymphoprep™ reagent were visualised under a light microscope at 20X magnification (**Appendix Fig. S5**). Significant stacking effects, possibly resulting from the use of high concentrations of the isolated neutrophils via the cytospin technique, made it difficult to accurately visualise and study the morphology and purity of the isolated neutrophils. However, most cells displayed a multi-lobed nuclei, an expected morphological

characteristic of resting neutrophils, indicating high neutrophil purity comparable with the typical purity reached using the Lymphoprep isolation technique (>95%, (127)). The total cell count of the isolated neutrophil fraction was 4.21 x 10^6 cells/mL from a total of 187.5 mL blood, as determined by using an automated cell counter.

3.2.2. Subcellular fractionation of neutrophils

The granules from the isolated neutrophils were released for downstream separation using nitrogen cavitation to gently disrupt the neutrophil plasma membrane via an established protocol (116). The cavitate was then subjected to a high-speed centrifugation step in a four-layered Percoll gradient in order to separate the granule fractions (**Appendix Fig. S6**). Surprisingly, no distinct bands representing the various neutrophil granules were observed after high speed centrifugation (**Fig. S6**). Nonetheless, the samples containing the granular material were carefully fractionated from the bottom of the glass tubes using a Peristaltic pump and a TMB assay was performed to identify the MPO-rich fractions for downstream glycoprotein characterisation.

3.2.3. TMB assay of the neutrophil granule fractions

A TMB assay was employed to identify the MPO-rich fractions after Percoll separation of the neutrophil granules (**Appendix Fig. S7**). TMB is a peroxidase substrate that, once oxidised, changes colour and thereby absorbs light at 450 nm that conveniently can be used to identify the MPO-rich fractions. As expected, high MPO activity was observed in the bottom fractions (fraction 1-12) containing the densest granules, presumably the MPO-rich azurophilic (Az) granules (42). Better resolution of the granule separation was expected based on previous isolations using an identical four-layered Percoll isolation method, see **Appendix Fig. S8**. Due to severe time constraints in this short MRes thesis period, it was decided that a previous granule isolation containing well-isolated specific (Sp), gelatinase (Ge) and secretory vesicles/plasma membrane (Se/Pl) fractions along with an already purified form of human MPO from whole (unfractionated) neutrophils (hereafter called nMPO, Lee BioSolutions, Maryland Heights, US) would be utilised for the subsequent structure-function characterisation of neutrophil MPO.

3.3. Structure-function characterisation of MPO N-glycans

The structure-function investigation of the MPO *N*-glycosylation was carried out as part of a larger study involving several lab members and international collaborators. While I did not directly perform the detailed structural characterisation of the *N*-glycosylation of MPO, I benefitted from having access to this unpublished data (some of which can be found in the Appendix as indicated in

text), in order to explore some important biosynthetic and functional aspects of the peculiar MPO *N*-glycosylation.

3.3.1. 3D structure of MPO, a link between N-glycan processing and solvent accessibility

Deep structural characterisation of the fascinating site- and granule-specific *N*-glycosylation of nMPO was performed by my colleague (Harry C. Tjondro, lead author) and a number of international collaborators as part of a larger research project investigating the peculiar glycobiology of MPO. The manuscript in preparation building in part on data I have generated during this thesis, has been supplied in the **Appendix Fig. S9-12.** My contributions to this manuscript have been clearly indicated (highlighted in yellow in the captions).

The site-specific characterisation of nMPO, elucidated by reverse-phase LC-ESI-MS/MS-based glycopeptide analysis, revealed that Asn323 and Asn483 are predominantly occupied by the paucimannosidic *N*-glycans M2F ($Man_2GlcNAc_2Fuc_1$) and M3F ($Man_3GlcNAc_2Fuc_1$) respectively, whilst Asn355 and Asn391 are predominantly occupied by the oligomannosidic M6 ($Man_6GlcNAc_2$). Asn729 of nMPO is predominantly unoccupied.

With this knowledge in hand, I then set out to explore if there was a link between the observed *N*-glycans at each site and the solvent accessibility of maturely folded MPO. NACCESS, a basic tool to determine solvent accessibility from PDB structures, was applied to five high-resolution x-ray crystal structures of human MPO deposited in the PDB (1D2V, 1CXP, 1DNU, 1DNW, 5FIW) in both the monomeric and dimeric forms. NACCESS provides arbitrary but comparable accessibility values by rolling a probe around on the 3D structure and determining the degree of Van der Waal's interactions to the probe (113). As expected, monomeric MPO (depicted in **Fig. 17Aiv**) demonstrated a strong correlation between the relative solvent accessibilities (**Fig. 17Ai**) to the degree of the *N*-glycan type processing (illustrated as a proportion of *N*-glycans being processed from oligomannosidic to more mature *N*-glycans) (**Fig. 17Aii**) and to the degree of core fucosylation (**Fig. 17Aiii**) at each site.

Most strikingly, Asn355 and Asn391 displayed a significantly lower solvent accessibility relative to the highly accessible Asn323, Asn483 and Asn729 ($p < 0.00005$, $n = 5$), which coincided with a

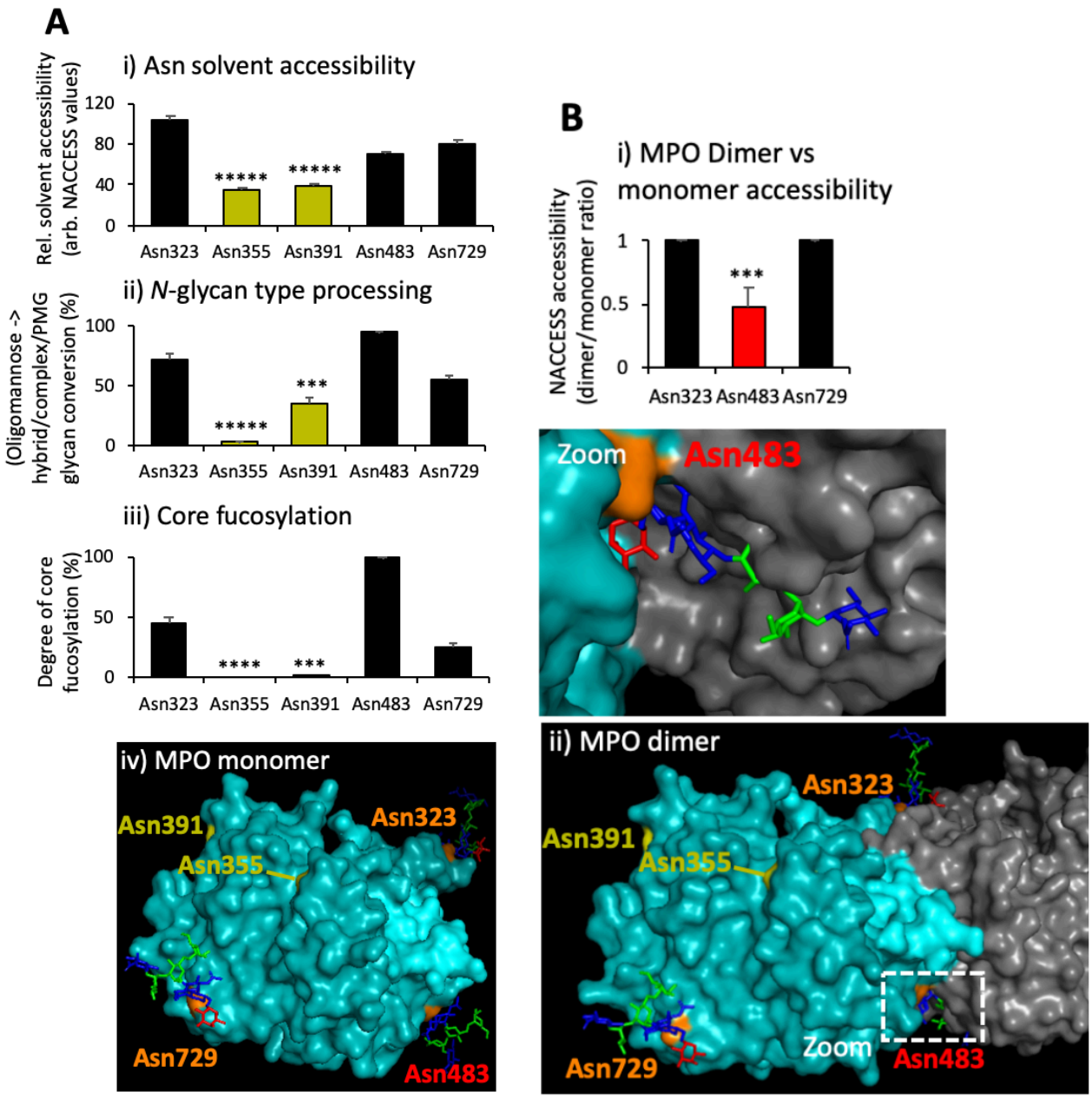

Figure 17. Site-solvent accessibilities of monomeric and dimeric MPO. *(A) Strong correlation was observed between (i) the site-solvent accessibilities, and the degree of (ii) N-glycan processing (calculated as a proportion of the unprocessed oligomannosidic structures vs more processed structures at each site, and (iii) core fucosylation. The lowly accessible sites (Asn355 and Asn391), predominantly decorated with oligomannosidic-type N-glycans, are in light green. iv) Monomeric MPO depicted (α-chain in light blue, β-chain in cyan). (B) i) Asn483 (red) has a lower site solvent accessibility upon MPO dimerisation, as illustrated by a ratio of the monomeric:dimeric solvent accessibility. The two other processed sites Asn323 and Asn729 (orange) remain unaffected by MPO dimerisation. ii) Dimeric MPO (coloured the same as monomeric MPO, opposing monomer in grey). The occlusion of Asn483 is high-lighted, see zoom. PMG, paucimannosidic glycans. Mean $\pm$ SD plotted. ***$p < 0.005$, ****$p < 0.001$, *****$p < 0.0005$.*

dominance of the less processed oligomannosidic structures at Asn355 and Asn391 and with a lack of core fucosylation for the few mature structures at those sites. Taken together, the close correlation between solvent site accessibility of monomeric MPO (as it is expected to appear while trafficking the Golgi) and the type of "early-stage" *N*-glycan processing that would be expected to be occurring in the Golgi on fully folded proteins provides novel insight into the mechanisms facilitating the site-specific *N*-glycosylation of MPO. Interestingly, the solvent accessibility of Asn483 was significantly lower for dimeric vs monomeric MPO (as measured by the ratio of monomeric-to-dimeric accessibilities at each site) (**Fig 17Bi**). The solvent accessibility of the other two accessible (processed) sites (Asn323 and Asn729) was unaffected by MPO dimerisation. Asn483 is situated on the dimerisation interface of MPO. Thus, sterical occlusion may be occurring at this site upon MPO dimerisation (**Fig. 17Bii**), which reportedly occurs in the late Golgi or during granule trafficking (72). Interestingly, this dimerisation-dependent occlusion at Asn483 was found to correlate with a less "late-stage" processing (truncation) at this site including a lower degree of β1,2-GlcNAc and α1,3-Man removal relative to glycans decorating Asn323 and Asn729 (**Appendix Fig. S11Biii-iv**). Collectively, these observations shed new light on how the site-specific glycan processing is affected by MPO surface solvent accessibility and dimerisation during its "early-stage" and "late-stage" biosynthesis in the Golgi and granules, respectively.

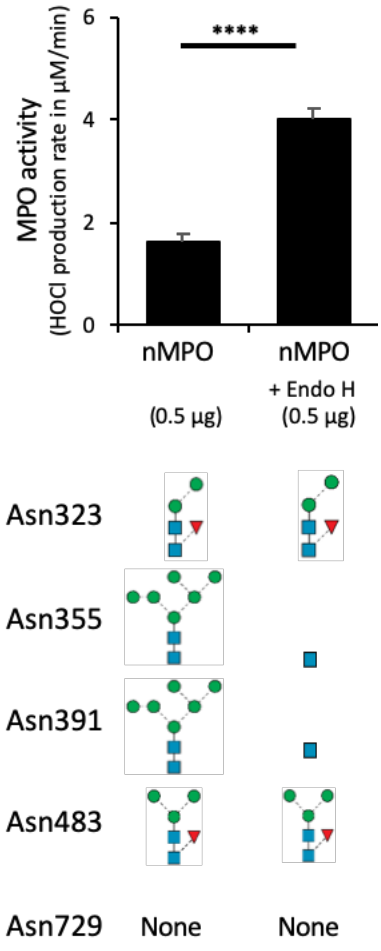

Figure 18. Glycosylation-dependent activity of neutrophil MPO. *Top: An enhancement of activity was observed when treating nMPO with Endo H. Bottom: the most abundant N-glycan at each site across the samples as determined by LC-MS/MS profiling (see **below** for more). n = 3, mean ± SD plotted, **** p < 0.00005, ns not significant.*

3.3.2. Glycoform-dependent MPO activity

The identification of highly unusual glycoforms associated with nMPO and the discovery of granule-specific MPO glycosylation by my colleagues (see **Appendix Fig. S10** and **S12**), prompted me to pose the following research question: *Does MPO display glycoform-dependent activity*?

The hypothesis of glycoform-dependent MPO activity was explored using a chlorination assay, which was used to measure the MPO activity of different MPO glycoforms including i) granule fractionated MPO (displaying different glycosylation, see **Appendix**

Fig. S12) and ii) an *in vitro* generated MPO glycoform that was created to simulate a key granule type of MPO (**Fig. 18**).

For ii) intact nMPO was treated with endoglycosidase H (Endo H) to generate highly truncated GlcNAcβ-Asn residues on the two oligomannosidic-rich *N*-glycan sites of nMPO (i.e. Asn355 and Asn391), thereby partially recapitulating an MPO glycoform identified in the Sp and Ge granules. The *in vitro* generated MPO glycoform was biochemically characterised (see below). MPO residing in the Sp and Ge granules intriguingly demonstrated a significantly higher MPO activity per granule protein content than the MPO residing in the secretory vesicles/plasma membrane (Se/PI) granules as measured by the HOCl production rate using a chlorination assay (**Appendix Fig. S12**). MPO

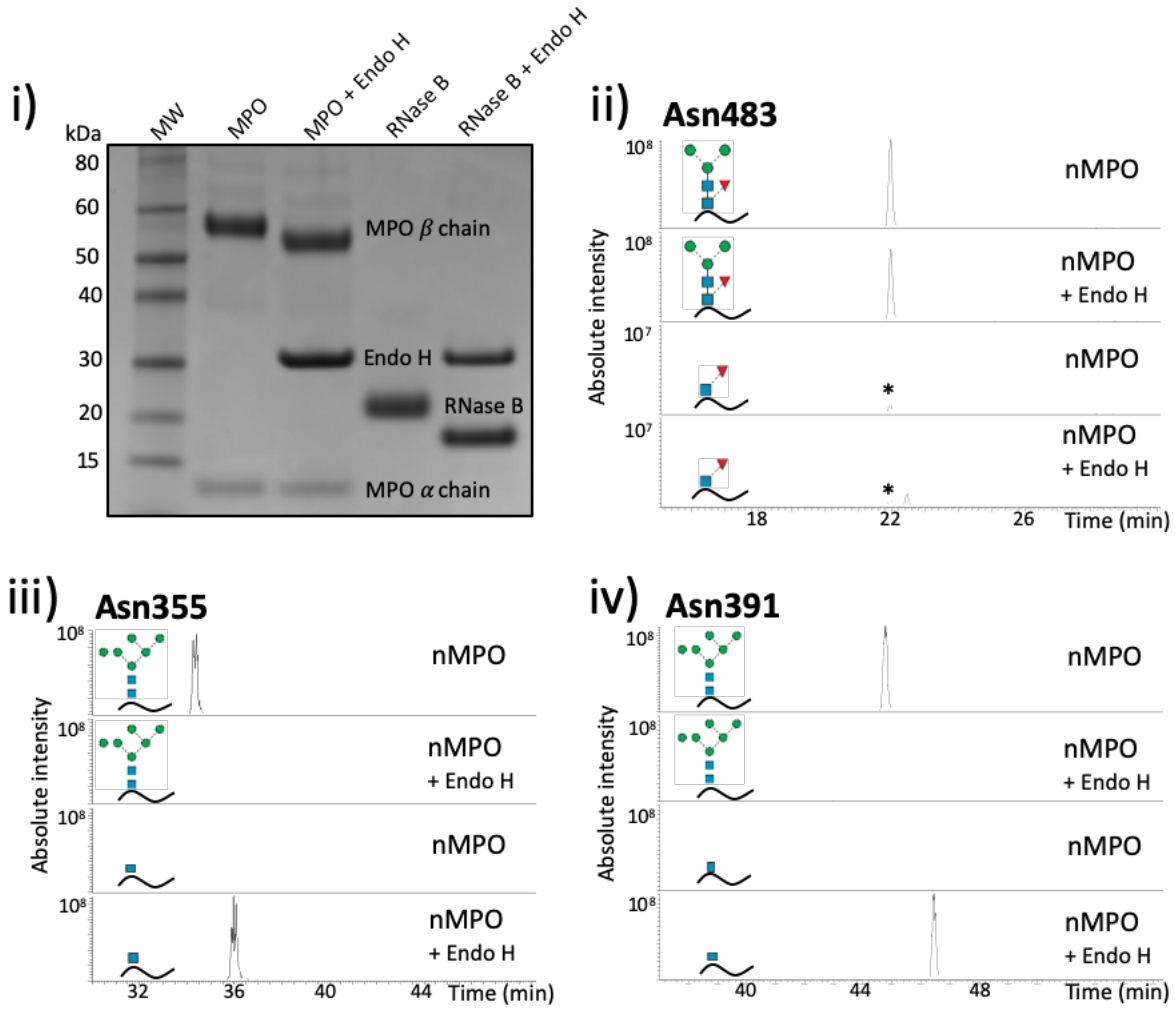

Figure 19. Validation of the Endo H treatment of nMPO*. i) SDS-PAGE demonstrating a shift in the glycosylated β-chain of MPO and RNase B upon Endo H treatment and ii-iv) LC-MS/MS demonstrating that the highly processed sites i.e. Asn483 (ii) remain unaffected whilst the two oligomannosidic sites (Asn355 and Asn391) are affected (iii-iv) by the Endo H treatment. EICs were generated to each of the indicated glycopeptides to follow the extent of the deglycosylation reaction. *Interfering signals arising from in-source fragmentation.*

residing in the Az granules was not included in these activity experiments due to its unavailability, however, AzMPO shares an almost identical glycosylation phenotype with nMPO.

With respect to enzyme activity, the Endo H-treated nMPO glycoform (simulating the MPO glycoform of the Sp/Ge granule-resident MPO) excitingly recapitulated a highly active MPO glycoform when compared to nMPO (**Fig. 18**). In fact, the significant activity gain of the Endo H-treated nMPO was replicated several times in separate assays on separate days to confirm this exciting observation.

To validate that the *in vitro*-generated Endo H-treated nMPO simulated the glycosylation observed for the Sp/Ge granule-resident MPO, detailed biochemical characterisation was performed using SDS-PAGE and LC-ESI-MS/MS-based glycopeptide analysis. Firstly, nMPO and Endo H-treated nMPO were analysed via gel electrophoresis. A model glycoprotein i.e. bovine ribonuclease B, known to carry a single oligomannosidic *N*-glycan, was included as a positive control for the enzymatic activity (128) (**Fig. 19i**). The Endo H-treated nMPO showed a significantly higher mobility of the glycosylated MPO α-chain (55 kDa) than the α-chain of nMPO (58 kDa) while the non-glycosylated β-chains of the two nMPO types displayed similar migration (both 12 kDa). The α-chain bands of Endo H-treated and untreated nMPO were then excised, in-gel digested using trypsin, and subjected to LC-ESI-MS/MS-based *N*-glycopeptide analysis. As expected from the previously defined substrate preference of Endo H (129), the MPO sites containing highly core fucosylated *N*-glycans, and complex- and paucimannosidic-type *N*-glycans at large, such as Asn483, were not affected at any measurable levels by the Endo H-treatment. This conclusion was reached by monitoring (via EIC-based quantitation) key *N*-glycan signatures found at each site and their potential Endo H products (**Fig. 19ii**). As expected, the two sites containing oligomannosidic glycans (Asn355 and Asn391) resulted in the generation of single GlcNAcβ-Asn residues upon the Endo H treatment (**Fig. 19iii-iv**).

3.3.3. Glycoform-dependent inhibition of MPO by ceruloplasmin

The activity of human MPO can be inhibited by an endogenous inhibitor, ceruloplasmin (Cp) (63). In fact, a crystal structure of Cp bound to monomeric MPO is available (PDB: 4EJX, (64)). Interestingly, upon studying this protein complex I noticed that two *N*-glycosylation sites of MPO, Asn391 and, in particular, Asn355, are situated near the Cp binding site (**Fig. 20**). Thus, I hypothesised that the oligomannosidic *N*-glycans conjugated to these MPO sites may impact the binding and inhibition by Cp. To investigate this, I utilised the

previously characterised intact nMPO, Endo H-treated nMPO and the MPO residing in the isolated Se, Ge and Se/Pl fractions, see **Fig. 18** for key glycoforms at each site. These MPO variants were incubated in the presence or absence of Cp at an optimised molar ratio of 1:20 (MPO:Cp) (data from optimisation assay not shown) and their activity profiled by monitoring the HOCl production rate (**Fig. 21**). The addition of Cp unexpectedly increased the activity of nMPO ($p < 0.00005$, $n = 3$) carrying the oligomannosidic-rich (M6) Asn355 and Asn391. It is still unclear how Cp can enhance the activity of nMPO. In contrast, the activity of the Endo H-treated nMPO carrying the highly truncated GlcNAcβ-Asn residues at Asn355 and Asn391 (depicted in **Fig. 20**), was significantly decreased ($p < 0.00005$, $n = 3$) upon Cp incubation indicating an enhanced interaction between Cp and MPO. A high degree of Cp inhibition of the MPO activity was recapitulated in the Sp, Ge and Se/Pl fractions of neutrophil MPO (all $p < 0.005$, $n = 3$) carrying very short Asn355 and Asn391 glycosylation similar to the Endo H-treated nMPO. These interesting observations suggest a glycoform-dependent binding and inhibition of MPO by Cp, a relationship not previously reported for MPO. While the glycoforms of MPO displaying highly truncated glycans at Asn355 and Asn391 are able to bind and thus be inhibited by Cp, the MPO glycoforms carrying elongated oligomannosidic glycans (e.g. M6) at these sites may not be inhibited. This putative enzyme-inhibitor molecular relationship will be discussed further below.

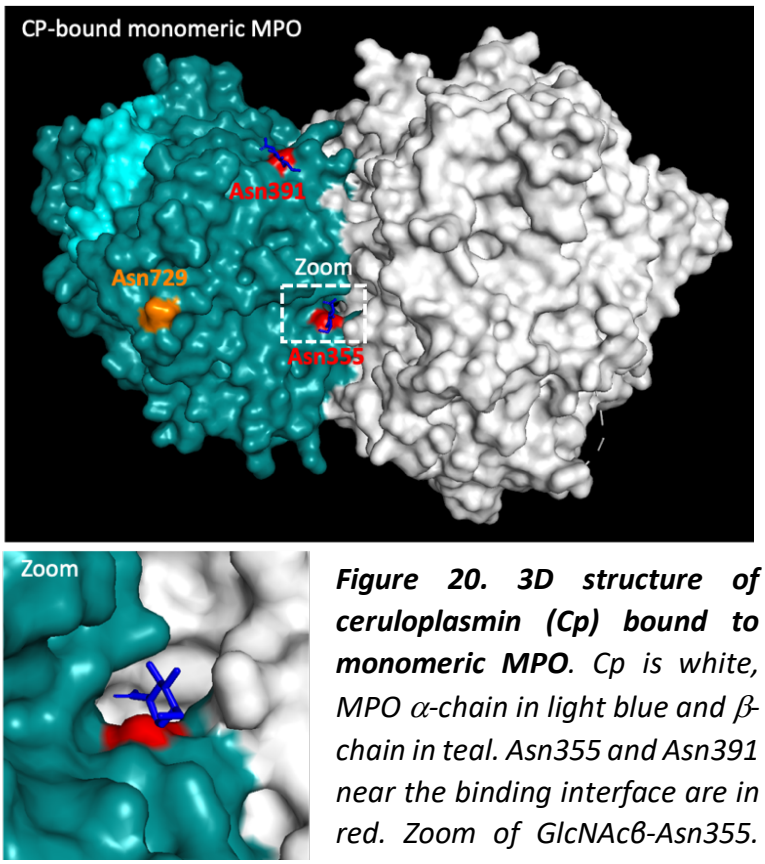

***Figure 20. 3D structure of ceruloplasmin (Cp) bound to monomeric MPO**. Cp is white, MPO α-chain in light blue and β-chain in teal. Asn355 and Asn391 near the binding interface are in red. Zoom of GlcNAcβ-Asn355. PDB 4EJX visualised in Pymol.*

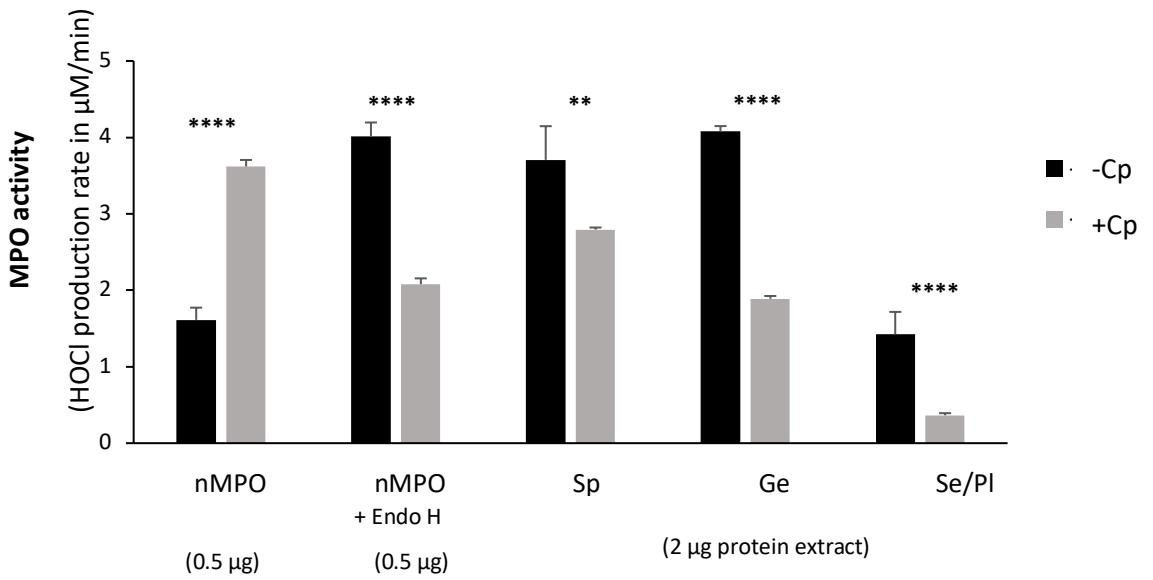

Figure 21. Glycoform-dependent inhibition of MPO by ceruloplasmin (Cp). *The glycoforms of MPO carrying truncated glycans at Asn355 and Asn391 (i.e. nMPO + Endo H, specific (Sp), gelatinase (Ge) and secretory vesicles/plasma membrane (Se/Pl)) fractions were significantly inhibited by Cp, which was not achieved with the nMPO carrying oligomannosidic N-glycans at Asn355 and Asn391. All MPO variants were incubated in the presence or absence of Cp at a molar ratio of 1:20 (MPO:Cp). The quantities of granule protein extracts were normalised across the measurements (see legend). **p < 0.005, ****p < 0.00005. Student's t-tests based on n = 3, data plotted as mean ± SD.*

Chapter 4: Discussion

Only just recently it was discovered that MPO and several other neutrophilic granule proteins are decorated with paucimannosidic (and the further truncated chitobiose core) *N*-glycans, a still under-explored class of *N*-glycans in human glycobiology (8, 94). In fact, neutrophils are increasingly being recognised to abundantly express functional paucimannosidic proteins (94, 95, 98). Whilst taking cues from paucimannose-rich organisms within the eukaryotic kingdom (i.e. worm, flies and plants), the generation of human paucimannosidic proteins was in those papers speculated to be driven by the *N*-acetyl-β-hexosaminidase (Hex), which in human exists as various isoenzymes (localised in the lysosomes as opposed to the fused lobed or Golgi-resident forms of insects and plants) formed by the *HEXA* and *HEXB* gene products, the α- and β-subunits, respectively. Despite the tempting inference from other eukaryotic organisms, the Hex-dependent paucimannosidic protein formation in human still requires validation, which formed one of the aims of this thesis.

As part of a larger research project with several team members and international collaborators, this thesis also aimed to advance our glycobiological knowledge of the biosynthesis and function of

MPO, a key paucimannose-rich glycoprotein in the neutrophil-driven innate immunity, surprisingly still severely understudied with respect to its glycan decorations.

Through biochemical characterisation of multiple CRISPR-Cas9-edited *HEXA*$^{-/-}$ and *HEXB*$^{-/-}$ HL-60 cell lines relative to unaffected wtHL-60 and mockHL-60 variants using Hex-specific enzyme assays and powerful glycomics strategies (see **Fig. 10** and **Table 1** for experimental overview), this thesis is the first to provide direct *in vitro* evidence for the involvement of the *HEXA* and *HEXB* gene products in the generation of paucimannosidic proteins in immature human neutrophils.

Furthermore, MPO-specific enzyme activity assays and other biochemical experiments were performed to gain novel insight into the biosynthesis and functional aspects of the peculiar *N*-glycans decorating MPO. In this thesis I have provided data to suggest that MPO displays a fascinating glycoform-dependent enzyme activity and an equally intriguing glycoform-dependent inhibition by its endogenous inhibitor ceruloplasmin (Cp). Limitations and opportunities of the applied methodologies and the data generated within this thesis are discussed in the context of the available literature in this section.

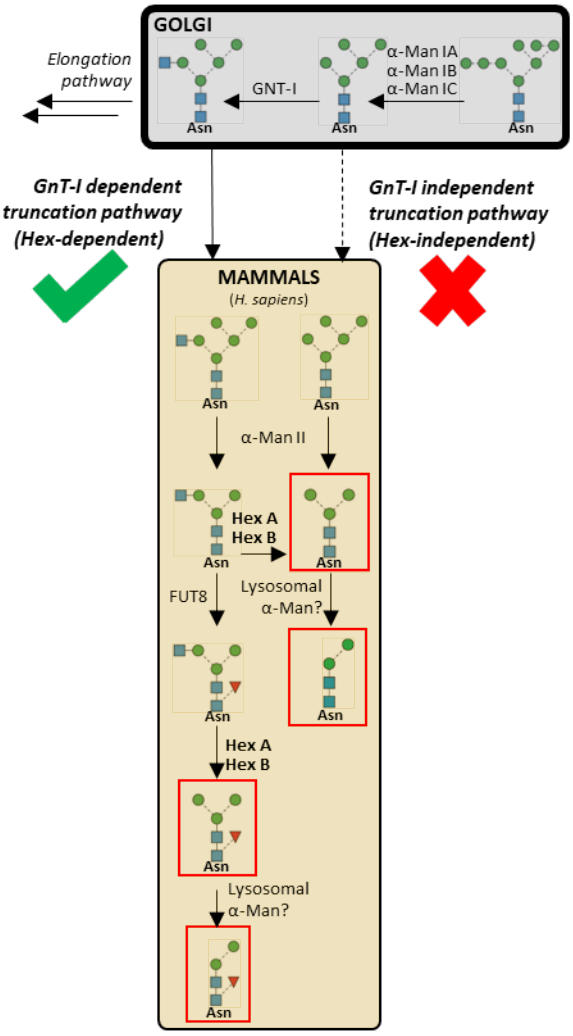

Figure 22. Truncation pathways underpinning paucimannosidic protein formation in human neutrophils. *This thesis has provided in vitro evidence supporting a Hex-mediated generation of paucimannosidic proteins in immature neutrophil-like cells via the GnT-I-dependent pathway. Negligible paucimannosidic glycans (red boxes) seems to be formed via the GnT-I-independent pathway directly from oligomannosidic intermediates via α-mannosidase action, but requires more exploration. Modified from (8).*

4.1. Hex-mediated formation of pauci-mannosidic proteins in human neutrophils

The formation of paucimannosidic proteins across the eukaryotic kingdoms was recently reviewed (8). Contrasting the lower paucimannose-rich species in which the paucimannosidic proteins are known to be constitutively expressed, the

formation of paucimannosidic proteins in humans were suggested to be instigated outside the conventional biosynthetic machinery by the concerted action of two key glycoside hydrolases i.e. Hex and an α-mannosidase demonstrating a linkage preference for α1,3-mannose epitopes in a tissue-specific and physiology-dependent manner (94, 130). Two putative truncation pathways explaining the highly processed (truncated) *N*-glycan features observed on neutrophil proteins were proposed to exist in humans: the *N*-acetylglucosaminyltransferase (GnT-I)-dependent and GnT-I-independent pathways (**Fig. 22**). The GnT-I-dependent pathway, as the name suggests, depends on the action of the key glycosyltransferase GnT-I (*MGAT1*) to add a β1,2-GlcNAc-cap on maturing oligomannosidic structures in order to form putative substrates for the Hex enzymes. This pathway is supposedly the main paucimannose-generating route since abundant core fucosylation, which is known to be driven by the Fut8 glycosyltransferase requiring β1,2-GlcNAc-cap intermediates, are prominent paucimannosidic features (e.g. M2F, M3F). In contrast, the putative GnT-I-independent pathway form paucimannosidic structures directly from oligomannosidic glycan intermediates due to the action of α-mannosidases. These two suggested pathways, which, in effect, can be considered as either Hex-dependent or Hex-independent, respectively, were explored in this thesis using a set of neutrophil-like (HL-60) mutants.

Concerted genetical, morphological, and biochemical characterisation efforts of the Hex disrupted HL-60 mutants were used to generate evidence for a Hex-mediated formation of paucimannosidic proteins via the GnT-I-dependent (Hex-dependent) pathway. Unchanged level of M2 ($Man_2GlcNAc_2$, a structure that may have been formed via the Hex-independent pathway) in the Hex-deficient mutants indicate a lack of compensation by the Hex-independent pathway. However, GnT-I-deficient mutants would provide more informative data when assessing the contribution of the Hex-independent pathway. Compensation mechanisms by other Hex isoenzyme variants could not be ruled out for the investigated Hex disrupted HL-60 mutants. In fact, Hex compensation is possible given the residual Hex activity and paucimannosidic levels observed. Additionally, in humans, two additional nucleocytoplasmic enzymes with glycosidic activity against *N*-acetylhexosamine residues have been identified, known as Hex C and Hex D (encoded by the *MGEA5* and *HEXDC* genes, respectively) (131-134). It is possible that these forms of Hex are present in the HL-60 lysates and may contribute to the residual activity observed in the assays, despite Hex C and Hex D having different substrate preferences and optimal pH ranges. Nonetheless, a proteomics profiling of the mutants would be useful in determining if these forms of Hex are present in the cells.

Attempting to build *in vivo* support for these *in vitro* observations, my colleague recently reported significantly reduced paucimannosylation of neutrophils from a homozygous *HEXB*$^{-/-}$ patient suffering from Sandhoff disease (20.7%) relative to an aged-matched healthy control (40.5%) (unpublished data, personal communication with Dr Ian Loke). Taken together, these observations confirm that the neutrophilic paucimannosidic proteins are formed by the Hex isoenzymes in the Hex-dependent pathway, and, importantly, have demonstrated that both the *HEXA* and *HEXB* gene products contribute to this formation.

In this project, I only had access to single Hex KOs i.e. *HEXA*$^{-/-}$- or *HEXB*$^{-/-}$-disrupted HL-60 mutants. Consequently, these mutants were still actively expressing Hex isoforms (i.e. Hex B ($\beta\beta$) in the *HEXA*$^{-/-}$ and Hex S ($\alpha\alpha$) in the *HEXB*$^{-/-}$-disrupted mutants, see **Table 1** in **Section 3.1.**). Thus, it is difficult to determine the exact contribution of each Hex gene in the formation of paucimannosidic proteins. However, my data indicates that *HEXB*$^{-/-}$ disruption more profoundly impacts the formation of paucimannosidic proteins, possibly due to less contribution from or a lack of compensation by Hex S (125). This unresolved aspect should be delineated by the study of a *HEXA*$^{-/-}$/*HEXB*$^{-/-}$ double HL-60 mutant, which is currently being developed in Prof Neelamegham's Lab, Buffalo Univ, NY. This would allow me to test whether the Hex-free mutants are completely devoid of paucimannosidic glycans in their *N*-glycome. Only from such experiments can the exact truncation pathways be fully delineated.

It is important to mention that the Hex-disrupted HL-60 mutants utilised in these studies were characterised in their undifferentiated (promyelocytic) state since this is the maturation time-point when the paucimannosidic machinery is supposedly being formed (94). It would be interesting to differentiate the HL-60 into mature neutrophil-like cells (135) to test if the differentiation would show a larger difference between the level of paucimannosylation of the Hex-disrupted mutants and the unedited HL-60 cells, in effect, recapitulate the dramatic reduction of paucimannose observed for the Sandhoff disease patient (see above). Further, genetic editing of isolated primary neutrophils is another avenue to complement my observations, but may be challenging given the short life-span of mature resting neutrophils (2).

Whilst the SDS-PAGE gel of the Hex-disrupted HL-60 mutants showed a largely unaffected proteome in comparison to wtHL-60 and mockHL-60, it would be relevant to use (glyco)proteomics to perform a deep characterisation of the (glyco)proteome of these Hex-disrupted mutants to study the exact

impact of Hex-disruption on the (glyco)proteome. Due to severe time restraints this could not be performed within the period of this thesis.

Sandhoff disease (*HEXB*$^{-/-}$) and Tay-Sachs disease (*HEXA*$^{-/-}$) are severe genetic lysosomal storage diseases that are characterised by GM2-gangliosidosis, the accumulation of the ganglioside GM2 in neuronal cells, due to the absence of Hex activity (136). This results in progressive degradation of the neuronal cells, and, ultimately, leads to the early death of affected individuals (4-6 years old). Transcriptional profiling of SD and TSD patients relative to healthy controls, demonstrated an elevated expression of many genes, and attributed these changes to activated macrophages, microglia and astrocytes, important immune cell types, pointing to a link between Hex and compromised innate immunity (137). As a result, whilst the pathological link between Hex-disruption to lysosomal GM2 build-up has been proven beyond doubt in Sandhoff and Tay-Sachs disease, it can be hypothesised that the aberrations in the paucimannose machinery may also contribute to the compromised immunity displayed by affected patients. The Hex-disrupted HL-60 mutants characterised in this thesis is a valuable tool to further investigate this hypothesis.

The "targeting-by-timing" hypothesis proposed by Borregaard and colleagues is widely recognised as the likely mechanism driving the intriguing protein sorting during granule formation in human neutrophils (41). In brief, this hypothesis proposes that the neutrophil granules, and thus their protein content, form sequentially during the stages of neutrophil maturation (detailed in Section 1.1.3). A large proportion of paucimannosidic proteins expressed in neutrophils, and thereby Hex, are localised in the Az granules (42, 94), the first granule to be generated in the early promyelocytic stage of neutrophil maturation (138). Despite this hypothesis, at present the most accurate model for the temporal granule formation, it remains unclear exactly where and when Hex facilitates the formation of paucimannosidic proteins in human neutrophils. Is the formation of paucimannosidic proteins happening during trafficking to the granules or, perhaps more likely, once the glycoprotein intermediates and Hex enzymes reach the granules where a more optimal pH for Hex exists (pH 4-6) (125). These and many other aspects of the paucimannosidic truncation pathway still require validation and further investigation.

4.2. Site-specific processing of MPO N-glycans reveals interesting facets of MPO biosynthesis

An intriguing correlation between the degree of *N*-glycan processing and the solvent accessibility has previously been observed (98, 139). Sites dominated by oligomannosidic glycan generally

display a poor solvent accessibility. To investigate whether this relationship exists for MPO, I used data from a deep site-specific characterisation of MPO isolated from whole neutrophil lysates (nMPO) performed by my colleague Harry C. Tjondro and a solvent accessibility software (NACCESS) to probe the 3D structure of MPO. The solvent accessibilities of the glycosylation sites of monomeric MPO (representative of its form in the 'early' stages of processing i.e. the early Golgi) showed a strong correlation to the degree of *N*-glycan type processing and the degree of core fucosylation. Interestingly, when investigating the solvent accessibility of dimeric MPO (representative of its form in the 'late' stages of processing i.e. late Golgi or in the granules), the accessibility of Asn483 (a highly processed site situated in the MPO dimerisation interface) was significantly lower for dimeric MPO compared to Asn483 of monomeric MPO. The solvent accessibility of the two other highly processed sites, Asn323 and Asn729, were unaffected by MPO dimerisation. Additionally, this dimerisation-dependent occlusion at Asn483 was found to correlate with less "late-stage" processing (truncation) at this site including a lower degree of β1,2-GlcNAc and α1,3-Man removal relative to the Asn323 and Asn729 glycans. Taken together, these observations suggest a previously unreported dimerisation-dependent processing of the Asn483 *N*-glycan of MPO.

To further investigate this putative relationship, site-specific *N*-glycan characterisation of monomeric MPO could be performed and compared to the characterisation of mature dimeric MPO. It is expected that monomeric MPO would demonstrate a high degree of β1,2-GlcNAc and α1,3-Man removal at Asn483 and consequently more processed glycans at this site compared to dimeric MPO. The point of MPO dimerisation is speculated to occur in the granules of human neutrophils (72), but is still debated. The dimerisation-dependent processing at Asn483 proposed herein may shed light on such yet-to-be-fully-confirmed aspects of the complex MPO biosynthesis.

To date, the *N*-glycans decorating MPO have been implicated in microbial binding (140), uptake by macrophages (141), and binding to the extracellular matrix (142) and lipids (143). Additionally, the functional advantages of dimerisation are not well characterised, particularly because the activity of hemi-MPO, a monomeric-like form generated by mild reductive cleavage, demonstrates chlorination activities that are similar to mature dimeric MPO (86). Interestingly, as per the 3D structure of MPO, mature dimeric MPO has six out of its ten *N*-glycosylation sites occupying an exposed planar surface (Asn323, Asn355 and Asn391), a feature not recapitulated in monomeric MPO. Hence, one could hypothesis that the functional advantage of MPO dimerisation is to form this planar surface of multivalently exposed *N*-glycans available for the binding to various interaction partners. This enticing hypothesis naturally requires further investigation.

4.3. Glycoform-dependent features of MPO

Glycoprofiling of granule-isolated MPO (as performed by my colleague, Harry C. Tjondro) demonstrated that Asn355 and Asn391 exhibit strong granule-specific *N*-glycosylation. The *N*-glycosylation of the more processed (and accessible) sites i.e. Asn323, Asn483 and Asn729 were surprisingly similar across the granules. Utilising this valuable insight, I hypothesised that MPO may display glycoform-dependent chlorination activity and Cp-mediated inhibition characteristics.

4.3.1. Glycoform-dependent activity of MPO

Surprisingly, MPO residing in the Sp/Ge granules, containing the highly truncated non-core fucosylated *N*-glycans M2 ($Man_2GlcNAc_2$) and βGlcNAc-Asn in Asn355 and Asn391, respectively, demonstrated a higher activity compared to the Se/Pl-resident MPO carrying M3 ($Man_3GlcNAc_2$) at Asn391. However, these samples were normalised per total granule protein extract, rather than being normalised to the amount of MPO in the sample (and thus profiling specific activity). Additionally, the Az-residing MPO, although being glycosylated highly similarly to nMPO, was not profiled for activity alongside the other granule isolates. I am currently waiting a new batch of isolated granule fractions to investigate this intriguing granule-specific activity of MPO. For these upcoming experiments alternative techniques including ELISA, western blotting and/or targeted proteomics will be utilised to normalise the samples to total MPO content rather than total protein content. Most importantly, when treating nMPO with Endo H, which specifically converts the oligomannose-rich Asn355 and Asn391 to sites carrying ultra-truncated βGlcNAc-Asn residues (while not affecting the more processed sites e.g. Asn483, in effect, creating an artificial glycoform simulating the Sp-/Ge-resident MPO), an increased chlorination activity was observed compared to the activity of nMPO. Thus, this provides evidence for the putative glycoform-dependent activity of MPO.

A study investigating the function of MPO *N*-glycans proposed that glycosylation is required for the optimal activity of MPO (91). Here, the activity of a deglycosylated form of recombinantly-expressed MPO was profiled and demonstrated a significant reduction in activity compared to an untreated form. The reduced activity may be explained by a reduced solubility of MPO due to the removal of the *N*-glycans. In support of this hypothesis, I observed a pronounced loss of solubility when treating isolated nMPO with PNGase F during this thesis (data not shown), but this observation was not further explored. Glycans are known to influence the physicochemical properties of glycoproteins such as their solubilities (144).

Additionally, glycans are known to impact the dynamics, stability and functional activity of glycosylated proteins (145-148). Thus, the glycoform-dependent activity of MPO reported herein may be explained by such mechanisms. Asn355 and Asn391 are situated close to the active site of MPO. Asn391 is in fact positioned on a loop that connects directly to the catalytic residues of the active site (**Fig. 23**). Thus, one could speculate that the glycoform-dependent MPO activity involving exactly the Asn391 and Asn355 glycans is caused by glycan-driven changes to the conformation of the active site of MPO. To investigate this, molecular dynamic simulations of differentially glycosylated MPO have just recently been initiated together with expert collaborators in the field (Prof. Woods, University of Georgia, U.S.). These exciting simulations may provide some mechanistic insight into how the Asn355 and Asn391 glycans affect the MPO active site as experimentally demonstrated by this thesis.

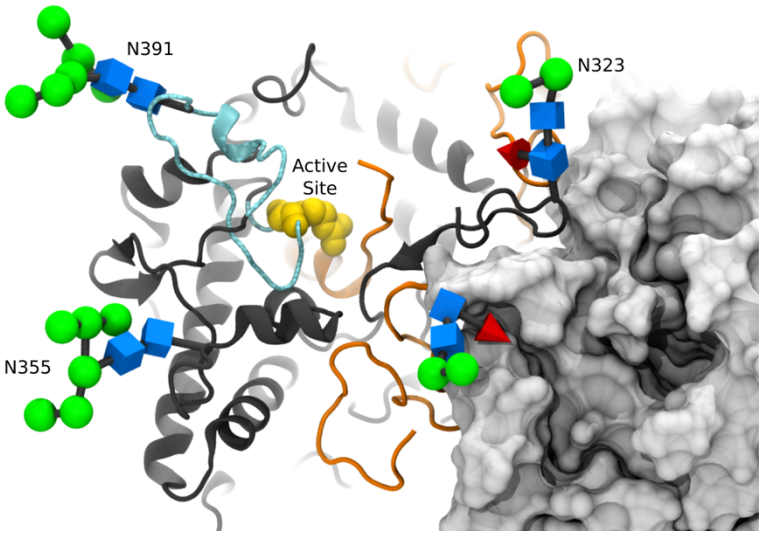

Figure 23. The oligomannosidic glycans at Asn355 and Asn391 are close to the active site of MPO. *Asn391 is positioned on a loop (cyan) that connects to the active site (yellow). MPO α-chain (orange), β-chain (dark grey). Key glycans (see* ***Appendix Fig. S10****) are depicted at Asn323, Asn355 and Asn391. Opposing MPO monomer in surface orientation. Image courtesy of Prof. Woods.*

4.3.2. Glycoform-dependent inhibition of MPO by Cp

Cp is a known endogenous inhibitor capable of strongly inhibiting the production of hypochlorous acid by MPO (63). Excitingly, the chlorination activity of Endo H-treated nMPO carrying βGlcNAc at Asn355 and Asn391 was significantly inhibited by Cp whereas nMPO carrying elongated oligomannosidic glycans (M6) at Asn355 and Asn391 could not be inhibited by Cp. This intriguing observation was recapitulated for Sp-, Ge- and Se/Pl-resident MPO all exhibiting truncated Asn355 and Asn391 glycosylation. This relationship strongly points to a glycoform-dependent inhibition profile of MPO, a relationship that perhaps best is viewed in concert with the glycoform-dependent activity also demonstrated in this thesis. In short, the glycans at Asn355 and Asn391 seem to be critical for both the activity and inhibition of MPO. The biological relevance of the glycoform-dependent activity and inhibition of MPO is still unknown, but it could be speculated that it may be

beneficial for neutrophils to express MPO in both a “highly-active” and “lowly-active” form depending on where these enzymes are required for action. Naturally the “highly-active” MPO (truncated Asn355 and Asn391-glycosylation) requires the greatest inhibition to avoid damage to the host cell once released upon neutrophil degranulation, and this is exactly what my data indicates. In other words, this thesis is the first to suggest that the highly peculiar and granule-specific glycosylation of Asn355 and Asn391 impacts the activity and inhibition of MPO, an exciting putative relationship that clearly warrant further investigation.

Chapter 5: Conclusions and Future Directions

A principal aim of this thesis was to provide evidence for the involvement of the *N*-acetyl-β-hexosaminidase (Hex) isoenzymes in the formation of paucimannosidic proteins in human neutrophils. To this end, a number of CRISPR-Cas9-edited *HEXA*$^{-/-}$ and *HEXB*$^{-/-}$ HL-60 cell lines were explored using different biochemical techniques and compared to unedited HL-60 cell lines. The Hex-disrupted mutants exhibited, as expected, a lower hexosaminidase activity, and, importantly, displayed reduced paucimannosylation compared to unedited controls. Adding further *in vivo* support to the Hex-mediated paucimannosidic protein formation, the link between Hex deficiency and paucimannosidic depletion was recently recapitulated in a *N*-glycome profiling study of neutrophils isolated from a homozygous *HEXB*$^{-/-}$patient suffering from Sandhoff disease relative to an age-matched healthy control performed by a colleague (unpublished observation, personal communication with Dr. Ian Loke, see Discussion for more).

This thesis therefore provides solid evidence confirming the involvement of Hex in the formation of paucimannosidic proteins in human neutrophils, and points to little, if any, utilisation of a Hex-independent pathways, but leaves open several unanswered questions that would benefit from further investigation including i) *what is the relative contribution of Hex A, B and S in the paucimannosidic machinery of healthy neutrophils?*, ii) *what compensation mechanisms exist in individuals homozygous or heterozygous for a single faulty HEX gene?*, iii) *how does the paucimannosidic glycan level of HEXA*$^{-/-}$ *or HEXB*$^{-/-}$ *HL-60 mutants change relative to unedited HL-60 cells during differentiation to “mature” neutrophil-like cells?*, and iv) *is the double HEXA*$^{-/-}$*/HEXB*$^{-/-}$ *HL-60 KO mutants (currently in development in Prof Neelamegham’s Lab, Buffalo Univ, NY) fully devoid in paucimannose*? These and many more research questions including investigations of the

functional impact of paucimannosylation in neutrophil biology are obvious questions that can be addressed using this collection of now genetically, morphologically, and, in part, biochemically well-characterised HL-60 mutants.

Another key aim of this thesis was to characterise the structure-function of the *N*-glycosylation decorating the paucimannose-rich myeloperoxidase (MPO), an important innate immune-related glycoprotein expressed by human neutrophils. To this end, a deep site- and granule-specific characterisation of the *N*-glycosylation of MPO was performed in collaboration with my colleagues at Macquarie University and an international group of scientists. This large program of research has over the past year created an exciting body of evidence documenting that neutrophilic MPO exhibits a fascinating and highly peculiar site- and granule-specific *N*-glycosylation phenotype, and, further shown, as supported by my own data, that MPO displays both a glycoform-dependent chlorination activity and inhibition by it natural inhibitor in serum, ceruloplasmin. To the best of my knowledge, this is the first example of an innate immune-related protein exhibiting different glycosylation features defining important activity and inhibition characteristics depending on its cellular localisation. Needless to say, the ultra-short duration of this thesis has not allowed for the proper orthogonal validation that are required to confirm the many observations and findings presented herein. Such follow-up experiments that can take several pathways including *in vitro*, *ex vivo* and *in vivo* routes using genetically or enzymatically modified MPO from donor and patients suffering from congenital disorders of glycosylation or other pathologies involving MPO or neutrophil deficiencies are well-suited research questions for a PhD research project.

This MRes thesis, albeit short, has given me a flavour of cutting-edge glycoimmunological research using innovative analytical approaches. Fortunately, I was able to present some of the outcomes generated by this thesis in the form of a poster at the recent 18th HUPO World Congress, Adelaide 2019 (see **Appendix Fig. S13** for poster), an experience I will always remember. I have observed that the field is highly dynamic, multi-disciplinary and works by close collaborations and open exchange of information, tools and samples between labs hosting expertise in various areas. Contributing data to the exciting novel discoveries and conclusions within a larger program of research (Tjondro et al., manuscript in preparation, see **Appendix Fig. S9-12**) has been highly stimulating, rewarding and educational. In conclusion, this thesis has generated novel insight into the fascinating glycobiology of neutrophils that I envisage can be of immediate and future use to fundamental, biomedical and clinical scientists alike.

References

1. B. Amulic, C. Cazalet, G. L. Hayes, K. D. Metzler, A. Zychlinsky, Neutrophil function: from mechanisms to disease. *Annu Rev Immunol* **30**, 459-489 (2012).
2. E. Kolaczkowska, P. Kubes, Neutrophil recruitment and function in health and inflammation. *Nat Rev Immunol* **13**, 159-175 (2013).
3. D. Odobasic, A. R. Kitching, S. R. Holdsworth, Neutrophil-Mediated Regulation of Innate and Adaptive Immunity: The Role of Myeloperoxidase. *J Immunol Res* **2016**, 2349817 (2016).
4. M. Phillipson, P. Kubes, The neutrophil in vascular inflammation. *Nat Med* **17**, 1381-1390 (2011).
5. S. J. Klebanoff, Myeloperoxidase-halide-hydrogen peroxide antibacterial system. *J Bacteriol* **95**, 2131-2138 (1968).
6. S. J. Klebanoff, Myeloperoxidase: friend and foe. *J Leukoc Biol* **77**, 598-625 (2005).
7. S. J. Klebanoff, A. J. Kettle, H. Rosen, C. C. Winterbourn, W. M. Nauseef, Myeloperoxidase: a front-line defender against phagocytosed microorganisms. *J Leukoc Biol* **93**, 185-198 (2013).
8. H. C. Tjondro, I. Loke, S. Chatterjee, M. Thaysen-Andersen, Human protein paucimannosylation: cues from the eukaryotic kingdoms. *Biol Rev Camb Philos Soc* 10.1111/brv.12548 (2019).
9. N. Borregaard, J. B. Cowland, Granules of the human neutrophilic polymorphonuclear leukocyte. *Blood* **89**, 3503-3521 (1997).
10. N. Borregaard, M. Sehested, B. S. Nielsen, H. Sengelov, L. Kjeldsen, Biosynthesis of granule proteins in normal human bone marrow cells. Gelatinase is a marker of terminal neutrophil differentiation. *Blood* **85**, 812-817 (1995).
11. E. Dzierzak, S. Philipsen, Erythropoiesis: development and differentiation. *Cold Spring Harb Perspect Med* **3**, a011601 (2013).
12. I. G. Winkler *et al.*, Positioning of bone marrow hematopoietic and stromal cells relative to blood flow in vivo: serially reconstituting hematopoietic stem cells reside in distinct nonperfused niches. *Blood* **116**, 375-385 (2010).
13. J. Grassinger *et al.*, Thrombin-cleaved osteopontin regulates hemopoietic stem and progenitor cell functions through interactions with alpha9beta1 and alpha4beta1 integrins. *Blood* **114**, 49-59 (2009).
14. H. Qian *et al.*, Distinct roles of integrins alpha6 and alpha4 in homing of fetal liver hematopoietic stem and progenitor cells. *Blood* **110**, 2399-2407 (2007).
15. H. Qian, K. Tryggvason, S. E. Jacobsen, M. Ekblom, Contribution of alpha6 integrins to hematopoietic stem and progenitor cell homing to bone marrow and collaboration with alpha4 integrins. *Blood* **107**, 3503-3510 (2006).
16. T. D. Schreiber *et al.*, The integrin alpha9beta1 on hematopoietic stem and progenitor cells: involvement in cell adhesion, proliferation and differentiation. *Haematologica* **94**, 1493-1501 (2009).
17. S. H. Orkin, Transcription factors and hematopoietic development. *J Biol Chem* **270**, 4955-4958 (1995).
18. N. Borregaard, Neutrophils, from marrow to microbes. *Immunity* **33**, 657-670 (2010).
19. C. Nerlov, T. Graf, PU.1 induces myeloid lineage commitment in multipotent hematopoietic progenitors. *Genes Dev* **12**, 2403-2412 (1998).
20. P. Laslo *et al.*, Multilineage transcriptional priming and determination of alternate hematopoietic cell fates. *Cell* **126**, 755-766 (2006).
21. V. A. Reddy *et al.*, Granulocyte inducer C/EBPalpha inactivates the myeloid master regulator PU.1: possible role in lineage commitment decisions. *Blood* **100**, 483-490 (2002).

22. M. D. Bjerregaard, J. Jurlander, P. Klausen, N. Borregaard, J. B. Cowland, The in vivo profile of transcription factors during neutrophil differentiation in human bone marrow. *Blood* **101**, 4322-4332 (2003).
23. T. Tak, K. Tesselaar, J. Pillay, J. A. Borghans, L. Koenderman, What's your age again? Determination of human neutrophil half-lives revisited. *J Leukoc Biol* **94**, 595-601 (2013).
24. R. Gallagher *et al.*, Characterization of the continuous, differentiating myeloid cell line (HL-60) from a patient with acute promyelocytic leukemia. *Blood* **54**, 713-733 (1979).
25. P. Harris, P. Ralph, Human leukemic models of myelomonocytic development: a review of the HL-60 and U937 cell lines. *J Leukoc Biol* **37**, 407-422 (1985).
26. I. T. Boll, G. Fuchs, A kinetic model of granulocytopoiesis. *Exp Cell Res* **61**, 147-152 (1970).
27. J. T. Dancey, K. A. Deubelbeiss, L. A. Harker, C. A. Finch, Neutrophil kinetics in man. *J Clin Invest* **58**, 705-715 (1976).
28. J. Pillay *et al.*, In vivo labeling with 2H2O reveals a human neutrophil lifespan of 5.4 days. *Blood* **116**, 625-627 (2010).
29. R. C. Furze, S. M. Rankin, Neutrophil mobilization and clearance in the bone marrow. *Immunology* **125**, 281-288 (2008).
30. K. J. Eash, A. M. Greenbaum, P. K. Gopalan, D. C. Link, CXCR2 and CXCR4 antagonistically regulate neutrophil trafficking from murine bone marrow. *J Clin Invest* **120**, 2423-2431 (2010).
31. M. J. Christopher, F. Liu, M. J. Hilton, F. Long, D. C. Link, Suppression of CXCL12 production by bone marrow osteoblasts is a common and critical pathway for cytokine-induced mobilization. *Blood* **114**, 1331-1339 (2009).
32. C. L. Semerad, F. Liu, A. D. Gregory, K. Stumpf, D. C. Link, G-CSF is an essential regulator of neutrophil trafficking from the bone marrow to the blood. *Immunity* **17**, 413-423 (2002).
33. K. Ley, C. Laudanna, M. I. Cybulsky, S. Nourshargh, Getting to the site of inflammation: the leukocyte adhesion cascade updated. *Nat Rev Immunol* **7**, 678-689 (2007).
34. R. E. Bruehl *et al.*, Leukocyte activation induces surface redistribution of P-selectin glycoprotein ligand-1. *J Leukoc Biol* **61**, 489-499 (1997).
35. S. Gordon, Phagocytosis: An Immunobiologic Process. *Immunity* **44**, 463-475 (2016).
36. L. Kjeldsen, O. W. Bjerrum, J. Askaa, N. Borregaard, Subcellular localization and release of human neutrophil gelatinase, confirming the existence of separate gelatinase-containing granules. *Biochem J* **287 (Pt 2)**, 603-610 (1992).
37. H. Sengelov, L. Kjeldsen, N. Borregaard, Control of exocytosis in early neutrophil activation. *J Immunol* **150**, 1535-1543 (1993).
38. V. Brinkmann *et al.*, Neutrophil extracellular traps kill bacteria. *Science* **303**, 1532-1535 (2004).
39. S. Boeltz *et al.*, To NET or not to NET:current opinions and state of the science regarding the formation of neutrophil extracellular traps. *Cell Death Differ* **26**, 395-408 (2019).
40. S. U. Gorr, D. S. Darling, An N-terminal hydrophobic peak is the sorting signal of regulated secretory proteins. *FEBS Lett* **361**, 8-12 (1995).
41. V. Le Cabec, J. B. Cowland, J. Calafat, N. Borregaard, Targeting of proteins to granule subsets is determined by timing and not by sorting: The specific granule protein NGAL is localized to azurophil granules when expressed in HL-60 cells. *Proc Natl Acad Sci U S A* **93**, 6454-6457 (1996).
42. S. Rorvig, O. Ostergaard, N. H. Heegaard, N. Borregaard, Proteome profiling of human neutrophil granule subsets, secretory vesicles, and cell membrane: correlation with transcriptome profiling of neutrophil precursors. *J Leukoc Biol* **94**, 711-721 (2013).
43. M. Faurschou, N. Borregaard, Neutrophil granules and secretory vesicles in inflammation. *Microbes Infect* **5**, 1317-1327 (2003).

44. M. Zamocky, C. Jakopitsch, P. G. Furtmuller, C. Dunand, C. Obinger, The peroxidase-cyclooxygenase superfamily: Reconstructed evolution of critical enzymes of the innate immune system. *Proteins* **72**, 589-605 (2008).
45. W. M. Nauseef, Myeloperoxidase in human neutrophil host defence. *Cell Microbiol* **16**, 1146-1155 (2014).
46. A. W. Segal, The function of the NADPH oxidase of phagocytes and its relationship to other NOXs in plants, invertebrates, and mammals. *Int J Biochem Cell Biol* **40**, 604-618 (2008).
47. T. E. DeCoursey, Voltage-gated proton channels: molecular biology, physiology, and pathophysiology of the H(V) family. *Physiol Rev* **93**, 599-652 (2013).
48. M. L. Aiken, R. G. Painter, Y. Zhou, G. Wang, Chloride transport in functionally active phagosomes isolated from Human neutrophils. *Free Radic Biol Med* **53**, 2308-2317 (2012).
49. J. G. Moreland, A. P. Davis, G. Bailey, W. M. Nauseef, F. S. Lamb, Anion channels, including ClC-3, are required for normal neutrophil oxidative function, phagocytosis, and transendothelial migration. *J Biol Chem* **281**, 12277-12288 (2006).
50. Y. T. Sun, C. C. Shieh, E. Delpire, M. R. Shen, K(+)-Cl(-) cotransport mediates the bactericidal activity of neutrophils by regulating NADPH oxidase activation. *J Physiol* **590**, 3231-3243 (2012).
51. L. A. Marquez, J. T. Huang, H. B. Dunford, Spectral and kinetic studies on the formation of myeloperoxidase compounds I and II: roles of hydrogen peroxide and superoxide. *Biochemistry* **33**, 1447-1454 (1994).
52. M. S. Coker, W. P. Hu, S. T. Senthilmohan, A. J. Kettle, Pathways for the decay of organic dichloramines and liberation of antimicrobial chloramine gases. *Chem Res Toxicol* **21**, 2334-2343 (2008).
53. M. J. Davies, C. L. Hawkins, D. I. Pattison, M. D. Rees, Mammalian heme peroxidases: from molecular mechanisms to health implications. *Antioxid Redox Signal* **10**, 1199-1234 (2008).
54. I. Chevrier, D. A. Tregouet, S. Massonnet-Castel, P. Beaune, M. A. Loriot, Myeloperoxidase genetic polymorphisms modulate human neutrophil enzyme activity: genetic determinants for atherosclerosis? *Atherosclerosis* **188**, 150-154 (2006).
55. B. Pulli *et al.*, Measuring myeloperoxidase activity in biological samples. *PLoS One* **8**, e67976 (2013).
56. K. Setsukinai, Y. Urano, K. Kakinuma, H. J. Majima, T. Nagano, Development of novel fluorescence probes that can reliably detect reactive oxygen species and distinguish specific species. *J Biol Chem* **278**, 3170-3175 (2003).
57. Y. Xia, J. L. Zweier, Measurement of myeloperoxidase in leukocyte-containing tissues. *Anal Biochem* **245**, 93-96 (1997).
58. S. Gross *et al.*, Bioluminescence imaging of myeloperoxidase activity in vivo. *Nat Med* **15**, 455-461 (2009).
59. Y. Aratani, Myeloperoxidase: Its role for host defense, inflammation, and neutrophil function. *Arch Biochem Biophys* **640**, 47-52 (2018).
60. N. E. Hellman, J. D. Gitlin, Ceruloplasmin metabolism and function. *Annu Rev Nutr* **22**, 439-458 (2002).
61. M. Segelmark, B. Persson, T. Hellmark, J. Wieslander, Binding and inhibition of myeloperoxidase (MPO): a major function of ceruloplasmin? *Clin Exp Immunol* **108**, 167-174 (1997).
62. A. V. Sokolov *et al.*, Interaction of ceruloplasmin, lactoferrin, and myeloperoxidase. *Biochemistry (Mosc)* **72**, 409-415 (2007).
63. A. L. Chapman *et al.*, Ceruloplasmin is an endogenous inhibitor of myeloperoxidase. *J Biol Chem* **288**, 6465-6477 (2013).

64. V. R. Samygina *et al.*, Ceruloplasmin: macromolecular assemblies with iron-containing acute phase proteins. *PLoS One* **8**, e67145 (2013).
65. T. J. Fiedler, C. A. Davey, R. E. Fenna, X-ray crystal structure and characterization of halide-binding sites of human myeloperoxidase at 1.8 A resolution. *J Biol Chem* **275**, 11964-11971 (2000).
66. M. Blair-Johnson, T. Fiedler, R. Fenna, Human myeloperoxidase: structure of a cyanide complex and its interaction with bromide and thiocyanate substrates at 1.9 A resolution. *Biochemistry* **40**, 13990-13997 (2001).
67. T. Ueda, K. Sakamaki, T. Kuroki, I. Yano, S. Nagata, Molecular cloning and characterization of the chromosomal gene for human lactoperoxidase. *Eur J Biochem* **243**, 32-41 (1997).
68. A. Taurog, Molecular evolution of thyroid peroxidase. *Biochimie* **81**, 557-562 (1999).
69. J. R. Baker, P. Arscott, J. Johnson, An analysis of the structure and antigenicity of different forms of human thyroid peroxidase. *Thyroid* **4**, 173-178 (1994).
70. S. N. Le *et al.*, Modelling of Thyroid Peroxidase Reveals Insights into Its Enzyme Function and Autoantigenicity. *PLoS One* **10**, e0142615 (2015).
71. P. G. Furtmuller *et al.*, Active site structure and catalytic mechanisms of human peroxidases. *Arch Biochem Biophys* **445**, 199-213 (2006).
72. W. M. Nauseef, Biosynthesis of human myeloperoxidase. *Arch Biochem Biophys* **642**, 1-9 (2018).
73. W. M. Nauseef, S. J. McCormick, R. A. Clark, Calreticulin functions as a molecular chaperone in the biosynthesis of myeloperoxidase. *J Biol Chem* **270**, 4741-4747 (1995).
74. W. M. Nauseef, S. J. McCormick, M. Goedken, Coordinated participation of calreticulin and calnexin in the biosynthesis of myeloperoxidase. *J Biol Chem* **273**, 7107-7111 (1998).
75. V. L. Castaneda *et al.*, Ultrastructural, immunochemical, and cytochemical study of myeloperoxidase in myeloid leukemia HL-60 cells following treatment with succinylacetone, an inhibitor of heme biosynthesis. *Exp Hematol* **20**, 916-924 (1992).
76. I. B. Pinnix, G. S. Guzman, H. L. Bonkovsky, S. R. Zaki, J. M. Kinkade, Jr., The post-translational processing of myeloperoxidase is regulated by the availability of heme. *Arch Biochem Biophys* **312**, 447-458 (1994).
77. W. M. Nauseef, S. McCormick, H. Yi, Roles of heme insertion and the mannose-6-phosphate receptor in processing of the human myeloid lysosomal enzyme, myeloperoxidase. *Blood* **80**, 2622-2633 (1992).
78. S. McCormick, A. Nelson, W. M. Nauseef, Proconvertase proteolytic processing of an enzymatically active myeloperoxidase precursor. *Arch Biochem Biophys* **527**, 31-36 (2012).
79. I. Olsson, A. M. Persson, K. Stromberg, Biosynthesis, transport and processing of myeloperoxidase in the human leukaemic promyelocytic cell line HL-60 and normal marrow cells. *Biochem J* **223**, 911-920 (1984).
80. D. T. Akin, J. M. Kinkade, Jr., Processing of a newly identified intermediate of human myeloperoxidase in isolated granules occurs at neutral pH. *J Biol Chem* **261**, 8370-8375 (1986).
81. M. Yamada, S. J. Hur, H. Toda, Isolation and characterization of extracellular myeloperoxidase precursor in HL-60 cell cultures. *Biochem Biophys Res Commun* **166**, 852-859 (1990).
82. N. Moguilevsky *et al.*, Structural and biological properties of human recombinant myeloperoxidase produced by Chinese hamster ovary cell lines. *Eur J Biochem* **197**, 605-614 (1991).
83. P. G. Furtmuller *et al.*, A transient kinetic study on the reactivity of recombinant unprocessed monomeric myeloperoxidase. *FEBS Lett* **503**, 147-150 (2001).

84. I. Grishkovskaya *et al.*, Structure of human promyeloperoxidase (proMPO) and the role of the propeptide in processing and maturation. *J Biol Chem* **292**, 8244-8261 (2017).
85. K. L. Taylor, G. S. Guzman, C. A. Burgess, J. M. Kinkade, Jr., Assembly of dimeric myeloperoxidase during posttranslational maturation in human leukemic HL-60 cells. *Biochemistry* **29**, 1533-1539 (1990).
86. P. C. Andrews, C. Parnes, N. I. Krinsky, Comparison of myeloperoxidase and hemi-myeloperoxidase with respect to catalysis, regulation, and bactericidal activity. *Arch Biochem Biophys* **228**, 439-442 (1984).
87. K. W. Moremen, M. Tiemeyer, A. V. Nairn, Vertebrate protein glycosylation: diversity, synthesis and function. *Nat Rev Mol Cell Biol* **13**, 448-462 (2012).
88. A. Varki, Biological roles of glycans. *Glycobiology* **27**, 3-49 (2017).
89. E. Weerapana, B. Imperiali, Asparagine-linked protein glycosylation: from eukaryotic to prokaryotic systems. *Glycobiology* **16**, 91R-101R (2006).
90. W. M. Nauseef, Posttranslational processing of a human myeloid lysosomal protein, myeloperoxidase. *Blood* **70**, 1143-1150 (1987).
91. P. Van Antwerpen *et al.*, Glycosylation pattern of mature dimeric leukocyte and recombinant monomeric myeloperoxidase: glycosylation is required for optimal enzymatic activity. *J Biol Chem* **285**, 16351-16359 (2010).
92. T. Ravnsborg, G. Houen, P. Hojrup, The glycosylation of myeloperoxidase. *Biochim Biophys Acta* **1804**, 2046-2053 (2010).
93. V. Venkatakrishnan, M. Thaysen-Andersen, S. C. Chen, H. Nevalainen, N. H. Packer, Cystic fibrosis and bacterial colonization define the sputum N-glycosylation phenotype. *Glycobiology* **25**, 88-100 (2015).
94. M. Thaysen-Andersen *et al.*, Human neutrophils secrete bioactive paucimannosidic proteins from azurophilic granules into pathogen-infected sputum. *J Biol Chem* **290**, 8789-8802 (2015).
95. I. Loke, N. H. Packer, M. Thaysen-Andersen, Complementary LC-MS/MS-Based N-Glycan, N-Glycopeptide, and Intact N-Glycoprotein Profiling Reveals Unconventional Asn71-Glycosylation of Human Neutrophil Cathepsin G. *Biomolecules* **5**, 1832-1854 (2015).
96. N. T. Mortimer, B. Z. Kacsoh, E. S. Keebaugh, T. A. Schlenke, Mgat1-dependent N-glycosylation of membrane components primes Drosophila melanogaster blood cells for the cellular encapsulation response. *PLoS Pathog* **8**, e1002819 (2012).
97. S. Dam *et al.*, Combined N-glycome and N-glycoproteome analysis of the Lotus japonicus seed globulin fraction shows conservation of protein structure and glycosylation in legumes. *J Proteome Res* **12**, 3383-3392 (2013).
98. I. Loke, O. Ostergaard, N. H. H. Heegaard, N. H. Packer, M. Thaysen-Andersen, Paucimannose-Rich N-glycosylation of Spatiotemporally Regulated Human Neutrophil Elastase Modulates Its Immune Functions. *Mol Cell Proteomics* **16**, 1507-1527 (2017).
99. K. Tzelepis *et al.*, A CRISPR Dropout Screen Identifies Genetic Vulnerabilities and Therapeutic Targets in Acute Myeloid Leukemia. *Cell Rep* **17**, 1193-1205 (2016).
100. M. C. Gundry *et al.*, Highly Efficient Genome Editing of Murine and Human Hematopoietic Progenitor Cells by CRISPR/Cas9. *Cell Rep* **17**, 1453-1461 (2016).
101. J. M. Walker, The bicinchoninic acid (BCA) assay for protein quantitation. *Methods Mol Biol* **32**, 5-8 (1994).
102. B. D. Zehr, T. J. Savin, R. E. Hall, A one-step, low background coomassie staining procedure for polyacrylamide gels. *Anal Biochem* **182**, 157-159 (1989).
103. M. Wendeler, K. Sandhoff, Hexosaminidase assays. *Glycoconj J* **26**, 945-952 (2009).
104. P. H. Jensen, N. G. Karlsson, D. Kolarich, N. H. Packer, Structural analysis of N- and O-glycans released from glycoproteins. *Nat Protoc* **7**, 1299-1310 (2012).

105. H. Hinneburg *et al.*, Post-Column Make-Up Flow (PCMF) Enhances the Performance of Capillary-Flow PGC-LC-MS/MS-Based Glycomics. *Anal Chem* **91**, 4559-4567 (2019).
106. A. V. Everest-Dass, J. L. Abrahams, D. Kolarich, N. H. Packer, M. P. Campbell, Structural feature ions for distinguishing N- and O-linked glycan isomers by LC-ESI-IT MS/MS. *J Am Soc Mass Spectrom* **24**, 895-906 (2013).
107. B. Domon, C. E. Costello, A systematic nomenclature for carbohydrate fragmentations in FAB-MS/MS spectra of glycoconjugates. *Glycoconjugate Journal* **5**, 397-409 (1988).
108. J. L. Abrahams, M. P. Campbell, N. H. Packer, Building a PGC-LC-MS N-glycan retention library and elution mapping resource. *Glycoconj J* **35**, 15-29 (2018).
109. M. Pabst, J. S. Bondili, J. Stadlmann, L. Mach, F. Altmann, Mass + retention time = structure: a strategy for the analysis of N-glycans by carbon LC-ESI-MS and its application to fibrin N-glycans. *Anal Chem* **79**, 5051-5057 (2007).
110. A. Varki *et al.*, Symbol Nomenclature for Graphical Representations of Glycans. *Glycobiology* **25**, 1323-1324 (2015).
111. C. A. Cooper, E. Gasteiger, N. H. Packer, GlycoMod--a software tool for determining glycosylation compositions from mass spectrometric data. *Proteomics* **1**, 340-349 (2001).
112. A. Ceroni *et al.*, GlycoWorkbench: a tool for the computer-assisted annotation of mass spectra of glycans. *J Proteome Res* **7**, 1650-1659 (2008).
113. T. J. Hubbard SJ (1993) NACCESS. Computer Program. (University College London, Department of Biochemistry and Molecular Biology).
114. F. H. Seeger, T. Tonn, N. Krzossok, A. M. Zeiher, S. Dimmeler, Cell isolation procedures matter: a comparison of different isolation protocols of bone marrow mononuclear cells used for cell therapy in patients with acute myocardial infarction. *Eur Heart J* **28**, 766-772 (2007).
115. K. Dunning, A. O. Safo, The ultimate Wright-Giemsa stain: 60 years in the making. *Biotech Histochem* **86**, 69-75 (2011).
116. L. Udby, N. Borregaard, Subcellular fractionation of human neutrophils and analysis of subcellular markers. *Methods Mol Biol* **412**, 35-56 (2007).
117. P. D. Josephy, T. Eling, R. P. Mason, The horseradish peroxidase-catalyzed oxidation of 3,5,3',5'-tetramethylbenzidine. Free radical and charge-transfer complex intermediates. *J Biol Chem* **257**, 3669-3675 (1982).
118. J. M. Dypbukt *et al.*, A sensitive and selective assay for chloramine production by myeloperoxidase. *Free Radic Biol Med* **39**, 1468-1477 (2005).
119. D. Kolarich, P. H. Jensen, F. Altmann, N. H. Packer, Determination of site-specific glycan heterogeneity on glycoproteins. *Nat Protoc* **7**, 1285-1298 (2012).
120. A. Shevchenko, H. Tomas, J. Havlis, J. V. Olsen, M. Mann, In-gel digestion for mass spectrometric characterization of proteins and proteomes. *Nat Protoc* **1**, 2856-2860 (2006).
121. M. Bern, Y. J. Kil, C. Becker, Byonic: advanced peptide and protein identification software. *Curr Protoc Bioinformatics* **Chapter 13**, Unit13 20 (2012).
122. S. Peri, H. Steen, A. Pandey, GPMAW--a software tool for analyzing proteins and peptides. *Trends Biochem Sci* **26**, 687-689 (2001).
123. Y. Liu *et al.*, A genetic model of substrate deprivation therapy for a glycosphingolipid storage disorder. *J Clin Invest* **103**, 497-505 (1999).
124. H. J. Kytzia, K. Sandhoff, Evidence for two different active sites on human beta-hexosaminidase A. Interaction of GM2 activator protein with beta-hexosaminidase A. *J Biol Chem* **260**, 7568-7572 (1985).
125. S. T. Hepbildikler, R. Sandhoff, M. Kolzer, R. L. Proia, K. Sandhoff, Physiological substrates for human lysosomal beta -hexosaminidase S. *J Biol Chem* **277**, 2562-2572 (2002).

126. A. Varki *et al.*, Symbol nomenclature for glycan representation. *Proteomics* **9**, 5398-5399 (2009).
127. H. Oh, B. Siano, S. Diamond, Neutrophil isolation protocol. *J Vis Exp* 10.3791/745 (2008).
128. J. M. Prien, D. J. Ashline, A. J. Lapadula, H. Zhang, V. N. Reinhold, The high mannose glycans from bovine ribonuclease B isomer characterization by ion trap MS. *J Am Soc Mass Spectrom* **20**, 539-556 (2009).
129. A. L. Tarentino, T. H. Plummer, Jr., F. Maley, The release of intact oligosaccharides from specific glycoproteins by endo-beta-N-acetylglucosaminidase H. *J Biol Chem* **249**, 818-824 (1974).
130. A. I. Lin, G. A. Philipsberg, R. S. Haltiwanger, Core fucosylation of high-mannose-type oligosaccharides in GlcNAc transferase I-deficient (Lec1) CHO cells. *Glycobiology* **4**, 895-901 (1994).
131. M. G. Alteen *et al.*, Mechanism of Human Nucleocytoplasmic Hexosaminidase D. *Biochemistry* **55**, 2735-2747 (2016).
132. G. T. Besley, D. M. Broadhead, Studies on human N-acetyl-Beta-d-hexosaminidase C separated from neonatal brain. *Biochem J* **155**, 205-208 (1976).
133. M. Gutternigg, D. Rendic, R. Voglauer, T. Iskratsch, I. B. Wilson, Mammalian cells contain a second nucleocytoplasmic hexosaminidase. *Biochem J* **419**, 83-90 (2009).
134. L. Wells *et al.*, Dynamic O-glycosylation of nuclear and cytosolic proteins: further characterization of the nucleocytoplasmic beta-N-acetylglucosaminidase, O-GlcNAcase. *J Biol Chem* **277**, 1755-1761 (2002).
135. A. B. Hauert, S. Martinelli, C. Marone, V. Niggli, Differentiated HL-60 cells are a valid model system for the analysis of human neutrophil migration and chemotaxis. *Int J Biochem Cell Biol* **34**, 838-854 (2002).
136. P. Karimzadeh *et al.*, GM2-Gangliosidosis (Sandhoff and Tay Sachs disease): Diagnosis and Neuroimaging Findings (An Iranian Pediatric Case Series). *Iran J Child Neurol* **8**, 55-60 (2014).
137. R. Myerowitz *et al.*, Molecular pathophysiology in Tay-Sachs and Sandhoff diseases as revealed by gene expression profiling. *Hum Mol Genet* **11**, 1343-1350 (2002).
138. J. B. Cowland, N. Borregaard, Granulopoiesis and granules of human neutrophils. *Immunol Rev* **273**, 11-28 (2016).
139. L. Y. Lee, C. H. Lin, S. Fanayan, N. H. Packer, M. Thaysen-Andersen, Differential site accessibility mechanistically explains subcellular-specific N-glycosylation determinants. *Front Immunol* **5**, 404 (2014).
140. R. C. Allen, J. T. Stephens, Jr., Myeloperoxidase selectively binds and selectively kills microbes. *Infect Immun* **79**, 474-485 (2011).
141. S. S. Lefkowitz, M. P. Gelderman, D. L. Lefkowitz, N. Moguilevsky, A. Bollen, Phagocytosis and intracellular killing of Candida albicans by macrophages exposed to myeloperoxidase. *J Infect Dis* **173**, 1202-1207 (1996).
142. L. Kubala *et al.*, The potentiation of myeloperoxidase activity by the glycosaminoglycan-dependent binding of myeloperoxidase to proteins of the extracellular matrix. *Biochim Biophys Acta* **1830**, 4524-4536 (2013).
143. A. V. Sokolov *et al.*, Revealing binding sites for myeloperoxidase on the surface of human low density lipoproteins. *Chem Phys Lipids* **164**, 49-53 (2011).
144. A. Varki, Biological roles of oligosaccharides: all of the theories are correct. *Glycobiology* **3**, 97-130 (1993).
145. V. Gervais, A. Zerial, H. Oschkinat, NMR investigations of the role of the sugar moiety in glycosylated recombinant human granulocyte-colony-stimulating factor. *Eur J Biochem* **247**, 386-395 (1997).

146. H. C. Joao, I. G. Scragg, R. A. Dwek, Effects of glycosylation on protein conformation and amide proton exchange rates in RNase B. *FEBS Lett* **307**, 343-346 (1992).
147. H. S. Lee, Y. Qi, W. Im, Effects of N-glycosylation on protein conformation and dynamics: Protein Data Bank analysis and molecular dynamics simulation study. *Sci Rep* **5**, 8926 (2015).
148. P. M. Rudd *et al.*, Glycoforms modify the dynamic stability and functional activity of an enzyme. *Biochemistry* **33**, 17-22 (1994).

Appendices

Figure S1. NGS of HEXA and HEXB in the investigated CRISPR-Cas9-edited HL-60 mutants. *The three HEXA$^{-/-}$ (A1-A3) and two HEXB$^{-/-}$ (B1-B2) HL-60 mutants produced by our collaborators (Prof. Neelamegham, Buffalo Univ, NY) were differently edited around the PAM sequence as a result of the genetic editing. NGS confirmed that all mutants contained no wild-type genomic DNA in the target region. HL-60 cells are diploid cells and, hence, contain two alleles of the respective HEX genes. A1 was the only mutant to have two different combinations of edits (in a 1:1 ratio of sequences with each combination of edits) and thus we assume that each allele is mutated differently. All other mutants demonstrated that both alleles are mutated the same (as 100% of the sequences identified by NGS demonstrated the same combination of edits). For each clone, the wild-type (wt) and knockout (KO) sequences of the target regions are given. The 20 bp guide region (red), the PAM sequence required for CRISPR recognition (brown), insertions (green), mutations (blue) and deletions (yellow asterisks).*

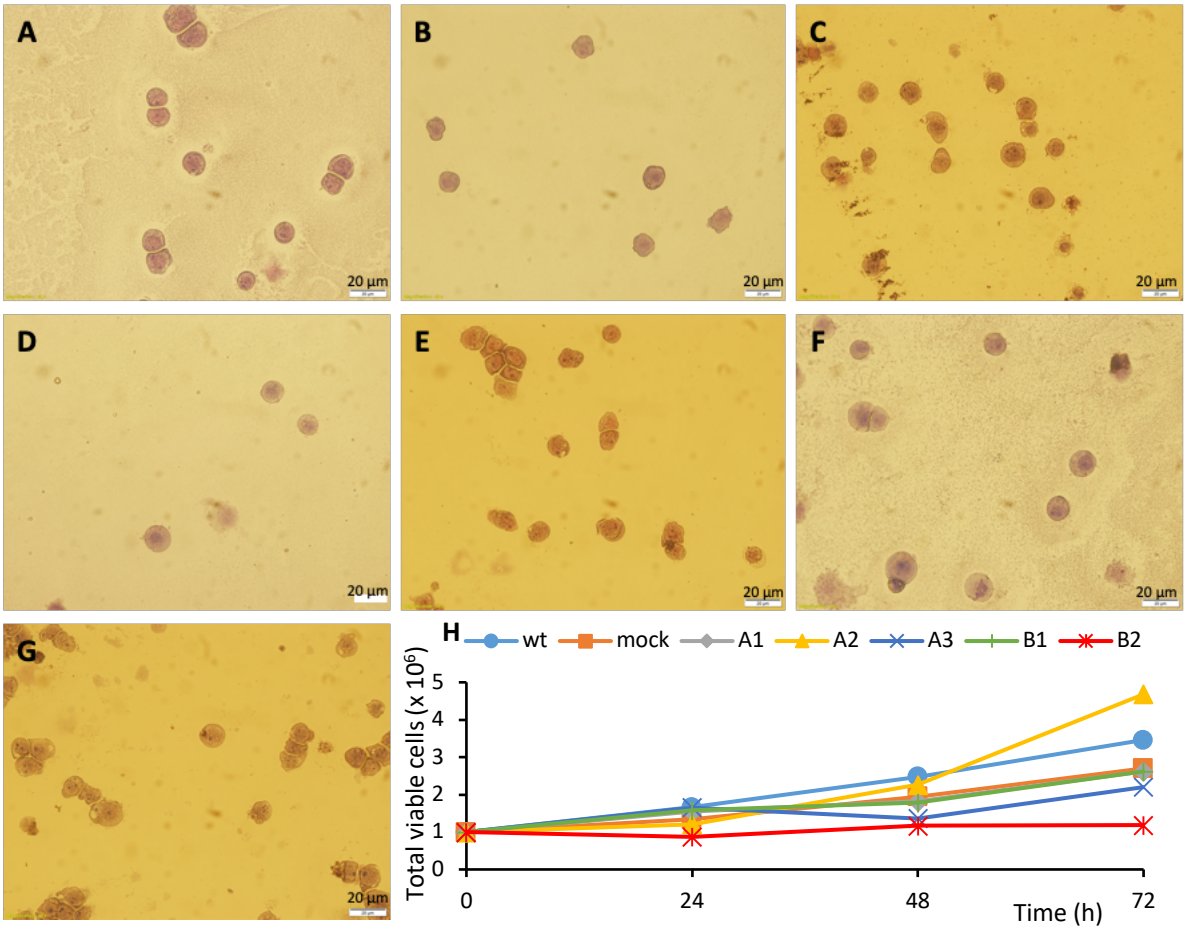

Figure S2. The morphology and growth profiles of Hex-deficient, mock and wtHL-60. *The HEXA$^{-/-}$ (A1 (**C**), A2 (**D**) and A3 (**E**)) and HEXB$^{-/-}$ (B1 (**F**) and B2 (**G**)) clones appeared morphologically similar to wtHL-60 (**A**) and mockHL-60 (**B**). All images were taken at 40X magnification. White scale bars (20 µm). (**H**) Growth/viability profiles of the HL-60 cells.*

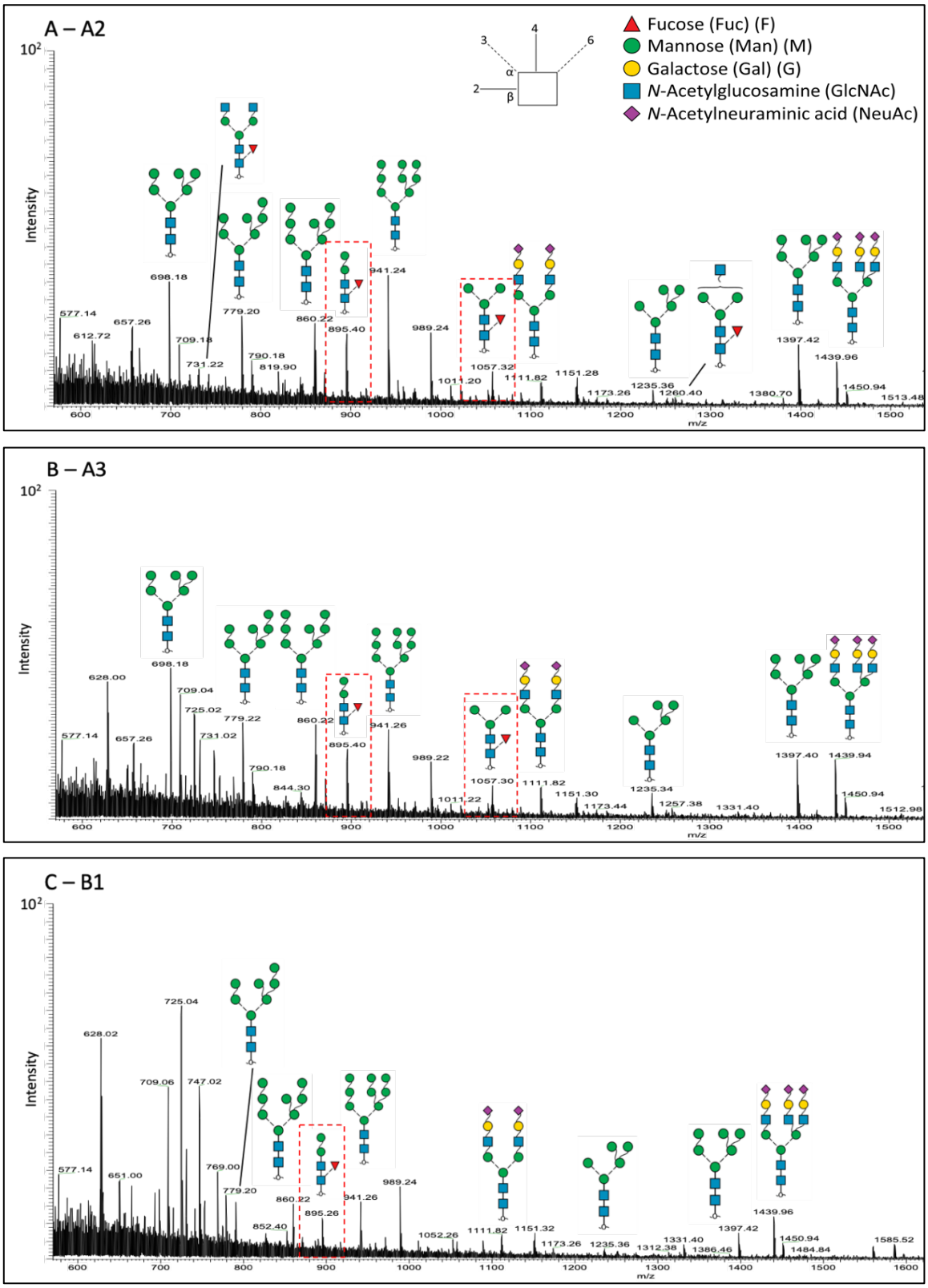

Figure S3. Remaining PGC-LC-MS profiles of N-glycans expressed by HL-60 mutants. *$HEXA^{-/-}$ A1 (A) and A2 (B), $HEXB^{-/-}$ B1 (C). The MS profiles were summed from 18-65 min to allow for visual comparison of the most abundant N-glycans expressed by the HL-60 variants. Structures as solved by manual annotation are depicted. The two paucimannosidic species $Man_2GlcNAc_2Fuc_1$ (M2F, m/z 895.3) and $Man_3GlcNAc_2Fuc_1$ (M3F, m/z 1057.3) are boxed in red. See key for glycan symbol nomenclature and the utilised linkage representation (7).*

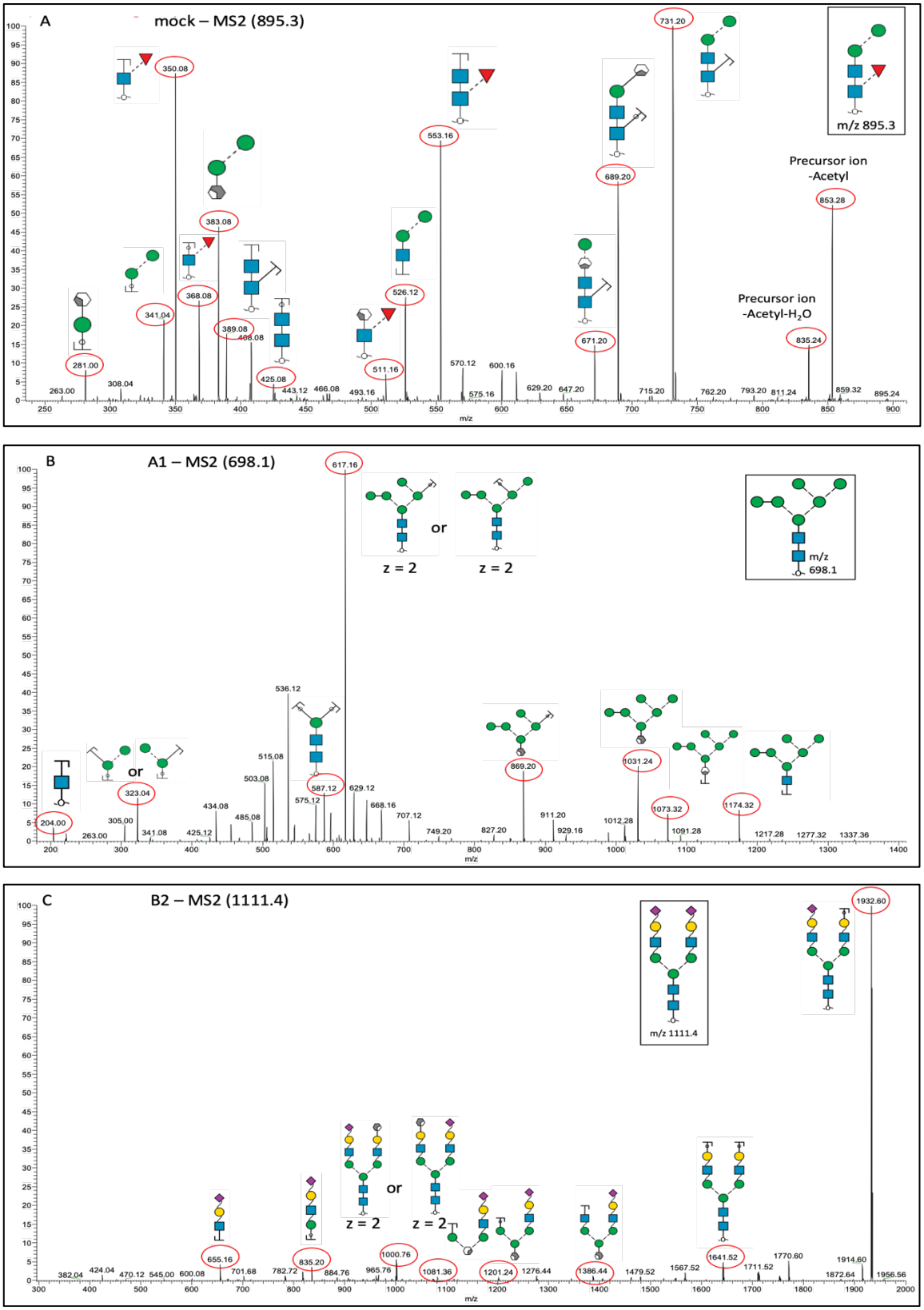

Figure S4. Ion trap CID-MS/MS (-) spectra. *(A) a key paucimannosidic N-glycan M2F (m/z 895.3, $Man_2GlcNAc_2Fuc_1$) from mockHL-60. (B) an oligomannosidic N-glycan M6 (m/z 698.1, $Man_6GlcNAc_2$) from HEXA$^{-/-}$ A1. (C) a biantennary sialyated complex N-glycan (m/z 1111.4). The CID-MS/MS data was manually annotated with characteristic fragments circled in red.*

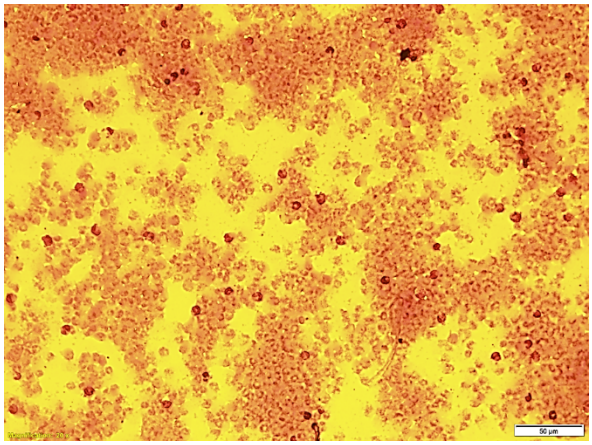

Figure S5. Light microscopy-based visualisation of resiting neutrophils isolated via Lymphoprep™. *20X magnification. The white scale bar equates to 50 μm.*

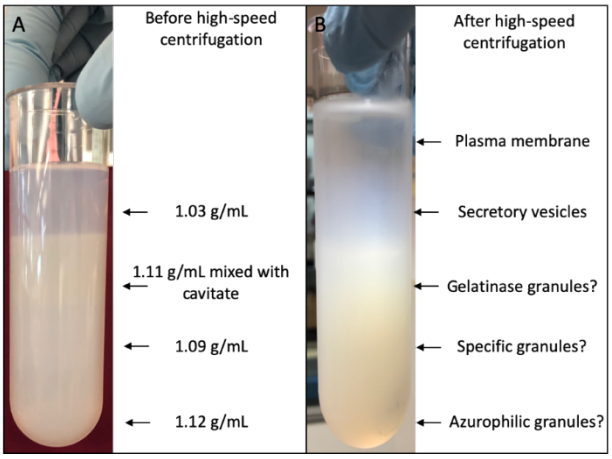

Figure S6. Four-layered Percoll gradient (A) before and (B) after high speed centrifugation. *The Percoll densities are indicated as are the individual neutrophil fractions after separation.*

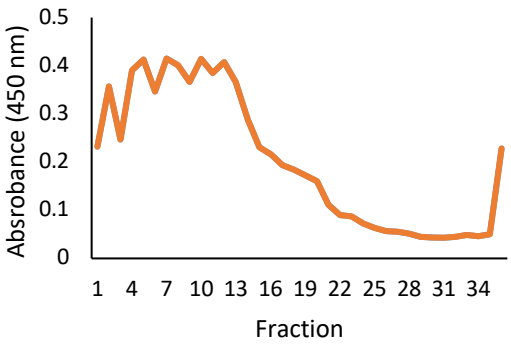

Figure S7. Identification of the MPO-rich fractions of separated neutrophil granule material (approximately fraction 1-12) using a TMB assay.

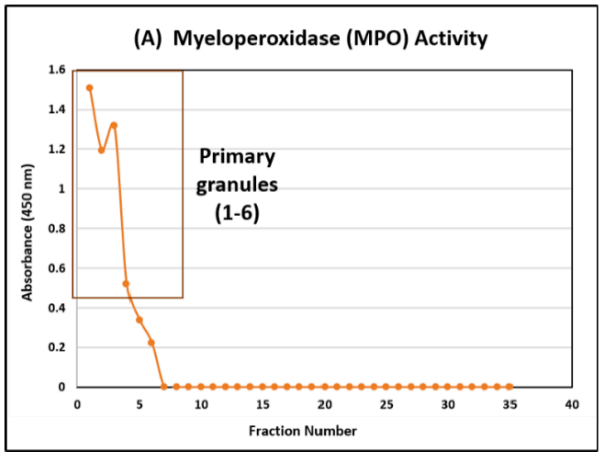

Figure S8. Previous identification of the MPO-rich (primary granules) fractions of separated neutrophil granule material (approximately fraction 1-6) using a TMB assay of MPO activity.

Appendix Fig. S9-12. Manuscript in preparation (title, abstract, figures) All contributions from this thesis highlighted in yellow

Granule-Specific *N*-Glycosylation and Chlorination Activity of Neutrophilic Myeloperoxidase

Harry Tjondro[1], **Julian Ugonotti**[1], Sayantani Chatterjee[1], Ian Loke[2], Si-Yun Chen[3], Hannes Hinneburg[1], Benjamin L. Parker[4], Vignesh Venkatakrishnan[5], Regis Dieckmann[5], Rebeca Kawahara[1], Oliver C. Grant[6], Robert J. Woods[6], Weston Struwe[3], Anna Karlsson[5], Morten Thaysen-Andersen[1#]

[1]Department of Molecular Sciences, Macquarie University, Sydney, NSW, Australia
[2]Department of Biological Sciences, National University of Singapore, Singapore, Singapore
[3]Department of Chemistry, University of Oxford, Oxford, United Kingdom
[4]Department of Physiology, University of Melbourne, Melbourne, VIC, Australia
[5]Department of Rheumatology & Inflammation Research, Institute of Medicine, Sahlgrenska Academy, University of Gothenburg, Gothenburg, Sweden
[6]Complex Carbohydrate Research Center, University of Georgia, Athens, United States

Running title: Granule-specific Features of Human Myeloperoxidase

Abstract

The heavily glycosylated myeloperoxidase (MPO), a key component of neutrophil-mediated innate immunity, produces anti-microbial hypochlorous acid to combat pathogens, but the functional importance of MPO glycosylation remains unexplored. Herein, we first structurally characterised the *N*-glycosylation of MPO of unfractionated human neutrophils (nMPO) using mass spectrometry-based glycomics, glycopeptide, and glycoprotein profiling. Unusual site-specific signatures were observed including paucimannosylation of Asn323 (47%) and Asn483 (56%), oligomannosylation of Asn355 (97%) and Asn391 (64%) while Asn729 was unoccupied (44%) or carried chitobiose core-type *N*-glycans (33%). Native mass spectrometry revealed extreme glycoform heterogeneity of dimeric (142-146 kDa) and monomeric (70-73 kDa) nMPO. Native gel electrophoresis and glycopeptide profiling demonstrated that monomeric and dimeric nMPO displayed key glycan differences of Asn323/Asn483 located in the dimerisation interface. The solvent accessibility of the glycosylation sites of monomeric/dimeric MPO correlated with the observed early- (Golgi) and late-stage (granule) *N*-glycan processing providing support for an oligomerisation-dependent processing of the Asn483-glycans. Further, glycoprofiling of granule-fractionated MPO demonstrated a granule-specific Asn355- and Asn391-glycosylation across the neutrophil compartments. Notably, the specific/gelatinase granule-resident MPO displayed extreme glycan truncation to GlcNAcβ-Asn at Asn355 and Asn391. Interestingly, this unusual MPO glycoform exhibited a comparably higher chlorination activity than MPO from other granules, an observation that could be recapitulated for endoglycosidase H-treated nMPO. Molecular dynamics simulations of granule-relevant MPO glycoforms confirmed that Asn355- and Asn391-glycans perturb the conformation of the active site.

In conclusion, we are the first to report on the granule-specific *N*-glycosylation and chlorination activity of neutrophilic MPO revealing a novel feature of neutrophil glycobiology.

Preliminary Figure 1 of manuscript

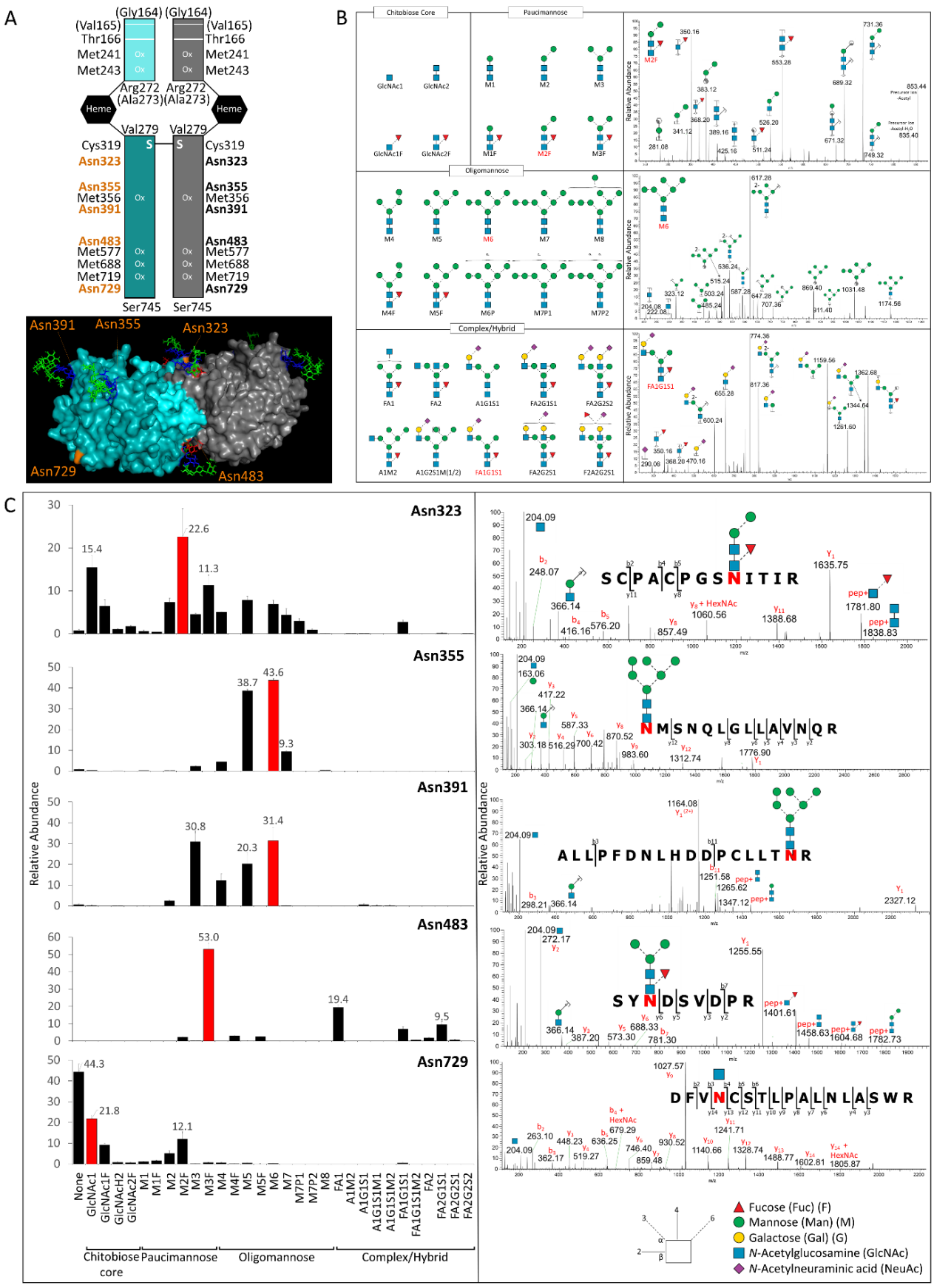

Figure S10. Site-specific N-glycosylation map of human neutrophil-derived myeloperoxidase (nMPO). A) *Top: Schematics of the protein architecture and the common modifications including oxidation and polypeptide processing variants (truncation variants in parenthesis) of the heme-containing (in black) dimeric nMPO. Bottom: 3D structure of nMPO (PDB: 1D2V). The light chain (light blue) and heavy chain (dark blue) are coloured and the N-glycosylation sites labelled in orange of one of the MPO monomers. The most abundant N-glycan identified at each site (see panel C) have been conjugated to the protein using Glycam. Asn729 was left unoccupied.* ***B)*** *Left: Overview of the fine structure and short-hand nomenclature of the N-glycans decorating nMPO as elucidated using PGC-LC-MS/MS-based glycomics. Right: Examples of CID-MS/MS (-) spectra of key N-glycans representing different N-glycan types of nMPO.* ***C)*** *Left: Site-specific N-glycosylation of nMPO as elucidated using reversed-phase LC-MS/MS-based glycopeptide analysis. The relative abundance of each N-glycan at each site is indicated (n = 3, mean ± SD). The most abundant N-glycan at each site is highlighted in red. Right: HCD-MS/MS (+) of the most abundant N-glycan at each site. See key for glycan symbol nomenclature and the utilised linkage representation.*

Preliminary Figure 2 of manuscript

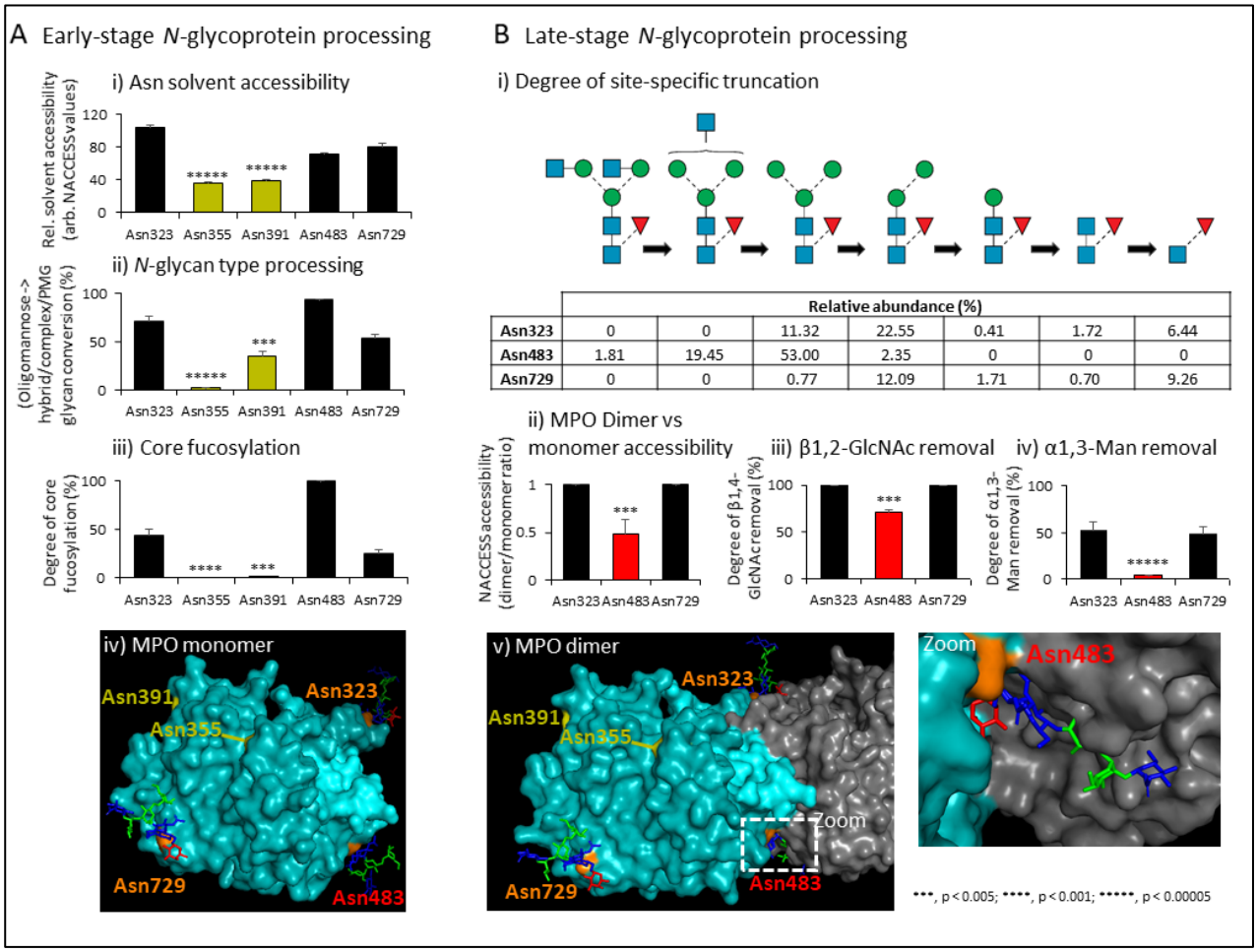

Figure S11. The early and late-stage biosynthetic processing steps of nMPO N-glycans are heavily impacted by the solvent accessibility at each N-glycosylation site. A) *The early stage processing of maturely folded monomeric nMPO in the cis-Golgi demonstrates a strong correlation between the i)*

Asn solvent accessibility and the degree of ii) N-glycan type processing and iii) core fucosylation. The relatively inaccessible sites i.e. Asn355 and Asn391 (light green) were found to carry largely unprocessed oligomannosidic N-glycans (illustrated as the proportion of N-glycans being converted from oligomannosidic to more processed N-glycans) while also displaying negligible amount of core fucosylation of their mature glycans (illustrated as the degree of core fucosylation out of the N-glycans that are able to receive core fucosylation). The solvent inaccessible Asn355 and Asn391 and the solvent accessible Asn323, Asn483 and Asn729 are illustrated on the 3D structure of monomeric nMPO (PDB: 1D2V). ***B****) i) The site-specific late-stage processing (truncation) of maturely folded nMPO happening presumably in the respective granules demonstrates a strong correlation between ii) the limited solvent accessibility of Asn483 (red) upon nMPO dimerisation and the degree of iii) β1,2-GlcNAc and iv) α1,3-Man removal from Asn483 N-glycans illustrating that MPO dimerisation takes place before or quickly after arriving in the granule and that this event affects Asn483 processing. The accessibility of the other heavily truncated sites i.e. Asn323 and Asn729 were not impacted by nMPO dimerisation, which, as a result, did show more complete truncation of the N-glycans conjugated to these sites. V) The occlusion of the Asn483 N-glycan upon nMPO dimerisation is indicated on the dimeric nMPO (1D2V). The sterical occlusion is further illustrated in a zoom demonstrating contact between the Asn483 on one nMPO monomer and the protein surface of the other monomer. See Figure 1 for information of the glycan addition and the used colour coding of the PDB structure. n = 3, mean ± SD, *** p < 0.005, **** p < 0.001, ***** p < 0.00005. See Fig 1 for glycan symbol nomenclature and the utilised linkage representation.*

Preliminary Figure 3 of manuscript

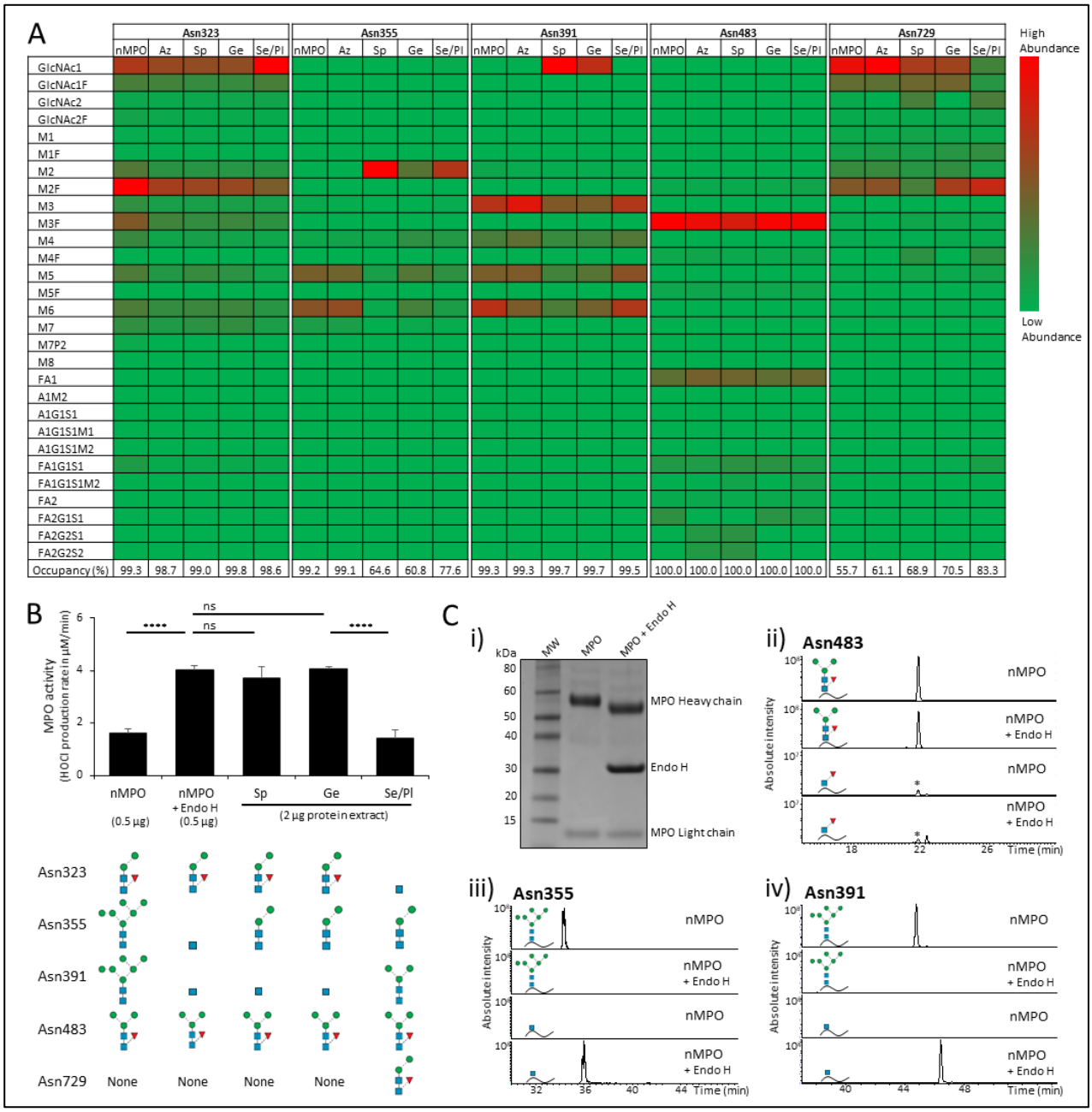

Figure S12. Granule-specific N-glycosylation and activity of MPO from granule fractionated human neutrophils obtained from four healthy donors. ***A)*** *Heat map showing that in particular the N-glycans of Asn355 and Asn391 display strong granule-specific differences in their N-glycosylation of MPO profiled from the specific granules (Sp), gelatinase granules (Ge) and, in part, from the secretory vesicles/plasma membrane fractions (Se/PI) relative to the MPO profiled from the azurophilic granules (Az). The latter profile matched as expected the profile of whole neutrophil-isolated MPO (nMPO) due to the abundance of MPO in the azurophilic granules. The N-glycosylation of the more processed (and accessible) sites i.e. Asn323, Asn483 and Asn729 were surprisingly similar across the granules. The average relative abundance of each N-glycan is plotted (see intensity scales, n = 4 healthy donors),* ***B)*** *Top: The MPO residing in the Sp and Ge granules, which were found to be decorated with highly truncated non-core fucosylated N-glycans i.e. GlcNAc – M2 (or alternatively*

found to be unoccupied) in position Asn355 and Asn391, were found to be significantly more active as measured by the hypochlorous acid (HOCl) production rate (µM/min) than the MPO in the Se/PI fractions when normalised for the amount of protein extract. A similar enhancement of the nMPO activity was observed after treatment with endoglycosidase H (Endo H) that transforms the oligomannose-rich Asn355 and Asn391 to sites carrying ultra-truncated N-glycans while not affecting the more processed sites (e.g. Asn483) (main glycoforms indicated at each site) to mimic the MPO glycoforms of the Sp and Ge granules. ***C****) Validation of the N-glycosylation of Endo H treated nMPO using i) SDS-PAGE and ii-iv) LC-MS/MS demonstrating that only the oligomannosidic sites were affected by the Endo H treatment and not the processed sites as exemplified by monitoring the Asn483 N-glycans. * Artificial in-source fragment ion. n = 3, mean ± SD, *** p < 0.005, **** p < 0.001, ***** p < 0.00005.*

Deciphering the Biosynthesis of Paucimannosidic Proteins in Human Neutrophils

Julian Ugonotti[1], Harry C. Tjondro[1], Sayantani Chatterjee[1], Ian Loke[2], Yuqi Zhu[3], Zeynep Sumer-Bayraktar[4], Meral Topçu[5], Sriram Neelamegham[3], Morten Thaysen-Andersen[1]

[1]Department of Molecular Sciences, Macquarie University, Sydney, Australia, [2]Department of Biological Sciences, National University of Singapore, Singapore, [3]Department of Chemical and Biological Engineering, University at Buffalo, NY, USA, [4]School of Life and Environmental Sciences, Charles Perkins Centre, University of Sydney, Australia, [5]Department of Child Neurology, Hacettepe University, Ankara, Turkey

BACKGROUND

- We recently discovered that human neutrophils express immune-related glycoproteins decorated in paucimannosidic *N*-glycans ($Man_{1-3}GlcNAc_2Fuc_{0-1}$), an under-studied type of *N*-glycosylation in humans[1].
- Inference from the paucimannose-rich lower organisms points to a β-*N*-acetyl-hexosaminidase (Hex)-driven production of paucimannosidic proteins in human neutrophils, however, this remains experimentally unsupported (**Fig. 1**).

AIM: To obtain evidence for a Hex-driven biosynthesis of paucimannosidic *N*-glycoproteins in human neutrophils.

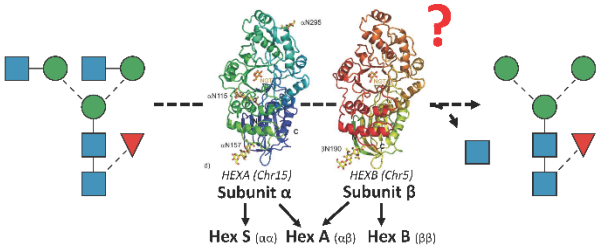

Figure 1. Hypothesised involvement of the Hex isoenzyme in paucimannosidic protein formation.

METHODS

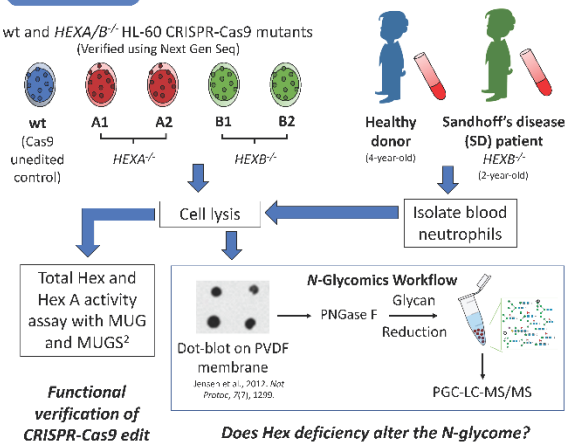

Figure 2. Work flow

RESULTS

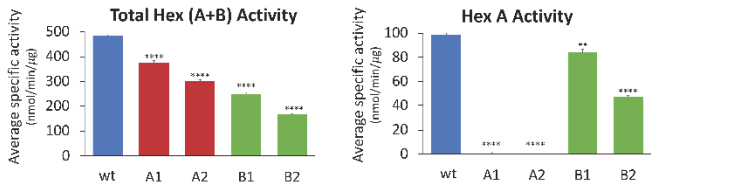

Figure 3. Total Hex and Hex A activity reduced in *HEXA*$^{-/-}$ and *HEXB*$^{-/-}$ HL-60 vs wt HL-60 cells. ****p < 0.00005, **p < 0.005.

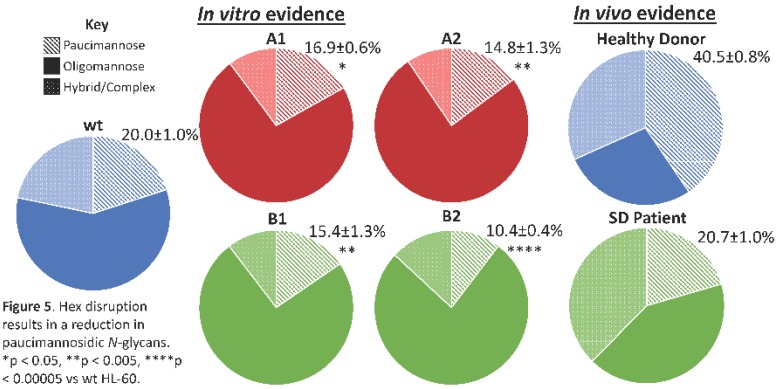

Figure 5. Hex disruption results in a reduction in paucimannosidic *N*-glycans. *p < 0.05, **p < 0.005, ****p < 0.00005 vs wt HL-60.

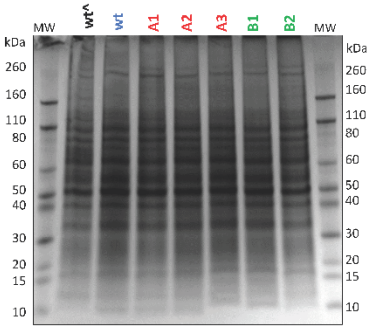

Figure 4. SDS-PAGE of cellular protein extracts demonstrates an unaffected proteome of HL-60 cells upon Hex disruption. ^wtHL-60 cells not undergoing CRISPR-Cas9 infection.

Enzyme activity (nmol/h/mg)	Total Hex (Hex A+B)	Hex A	β-Galac-tosidase
SD patient (2 y) (*HEXB*$^{-/-}$)	41	29	78
Healthy child (4 y)	1223	116	107

Table 1. Hex but not β-Gal activity is reduced in SD patient relative to healthy child.

CONCLUSION

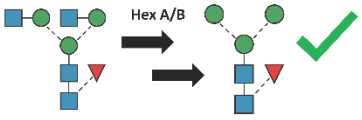

In vitro and *in vivo* evidence for the involvement of Hex in the formation of paucimannosidic proteins in human neutrophils.

FUTURE DIRECTIONS

- Hex-deficient HL-60 mutant are a useful tool to understand the roles of paucimannosidic proteins in neutrophil glycoimmunology.
- Delineate the relative contribution of *HEXA* and *HEXB* in paucimannosidic protein formation in human neutrophils and potential compensation mechanisms.
- Create a *HEXA*$^{-/-}$ and *HEXB*$^{-/-}$ double knock out to obtain a completely paucimannose-deficient neutrophil-like HL-60 cells.

MACQUARIE University

References 1. Thaysen-Andersen M et al. *J Biol Chem.* **290**(14):8789-802 (2015). 2. Wendeler M, Sandhoff K. *Glycoconj J.* **26**(8):945-52 (2009).

Acknowledgements: J.U. thanks Macquarie University for funding this research via the MRES research grant. M.T.-A. is supported by the Macquarie University seeding grant.

Check us out!

Appendix Fig. S13. Poster presented at 18th HUPO World Congress, Adelaide, SA, 2019.